# Izabella Zychor

**Strange particle production
in proton-proton collisions
at intermediate energies**

Summary of Professional Accomplishments

National Centre for Nuclear Research (NCBJ)
Świerk 2013

# Contents

# 1 Personal data

Name and surname      Izabella Zychor

Scientific degrees      MSc, University of Warsaw, Faculty of Physics, 1977

PhD, University of Warsaw, Faculty of Physics, 1983, doctoral thesis *Investigation of the production of hafnium isotopes and isomers in reactions of $^{40}Ar$, $^{84}Kr$ and $^{136}Xe$ ions on tungsten targets* supervisor: Prof. dr hab. W. Kurcewicz

Employment      1977-1987: University of Warsaw, Faculty of Physics

since 1988: National Centre for Nuclear Research (NCBJ), former The Andrzej Sołtan Institute for Nuclear Studies, Świerk

# 2 Description of the achievement for the habilitation qualification

Title of achievement for the habilitation qualification

## Strange particle production in proton-proton collisions at intermediate energies

based on a monothematic series of eight publications:

M1. M.Büscher, H.Junghans, V.Koptev, M.Nekipelov, K.Sistemich, H.Ströher, S.Barsov, G.Borchert, W.Borgs, M.Debowski W.Erven, R.Esser, P.Fedorets, D.Gotta, M.Hartmann, V.Hejny, A.Kacharava, H.R.Koch, V.Komarov, P.Kulessa, A.Kulikov, G.Macharashvili, S.Merzliakov, S.Mikirtychiants, H.Müller, A.Mussgiller, R.Nellen, M.Nioradze, H.Ohm, A.Petrus, F.Rathmann, Z.Rudy, R.Schleichert, C.Schneider, O.W.B.Schult, H.J.Stein, **I.Zychor**, *Identification of $K^+$ mesons from subthreshold pA collisions with ANKE at COSY-Jülich*, Nucl. Instrum. Meth. A481 (2002) 378.

M2. **I.Zychor**, *Monte Carlo simulations for ANKE experiments*, Acta Phys. Pol. B33 (2002) 521.

M3. V.Kleber, M.Büscher, V.Chernyshev, S.Dymov, P.Fedorets, V.Grishina, C.Hanhart, M.Hartmann, V.Hejny, A.Khoukaz, H.R.Koch, V.Komarov, L.Kondratyuk, V.Koptev, N.Lang, S.Merzliakov, S.Mikirtychiants, M.Nekipelov, H.Ohm, A.Petrus, D.Prasuhn, R.Schleichert, A.Sibirtsev, H.J.Stein, H.Ströher, K.H.Watzlawik, P.Wüstner, S.Yaschenko, B.Zalikhanov, **I.Zychor**, *$a_0^+$(980)-Resonance Production in $pp \rightarrow dK^+\bar{K}^0$ Reactions Close to Threshold*, Phys. Rev. Lett. 91 (2003) 172304.

M4. P.Fedorets, M.Büscher, V.Chernyshev, S.Dymov, V.Grishina, C.Hanhart, M.Hartmann, V.Hejny, V.Kleber, H.R.Koch, L.Kondratyuk, V.Koptev, A.Kudryavtsev, P.Kulessa, S.Merzliakov, S.Mikirtychyants, M.Nekipelov, H.Ohm, R.Schleichert, H.Ströher, V.Tarasov, K.H.Watzlawik, **I.Zychor**, $a_0^+$(980)-Resonance Production in the Reaction $pp \rightarrow d\pi^+\eta$ Close to the $K\bar{K}$ Threshold, Phys. Atom. Nucl. 69 (2006) 306.

M5. A.Dzyuba, V.Kleber, M.Büscher, V.Chernyshev, S.Dymov, P.Fedorets, V.Grishina, C.Hanhart, M.Hartmann, V.Hejny, L.Kondratyuk, V.Koptev, P.Kulessa, Y.Maeda, T.Mersmann, S.Mikirtychyants, M.Nekipelov, D.Prasuhn, R.Schleichert, A.Sibirtsev, H.J.Stein, H.Ströher, **I.Zychor**, *Scalar-isovector production close to threshold*, Eur. Phys. J. A29 (2006) 245.

M6. **I.Zychor**, V.Koptev, M.Büscher, A.Dzyuba, I.Keshelashvili, V.Kleber, H.R.Koch, S.Krewald, Y.Maeda, S.Mikirtychiants, M.Nekipelov, H.Ströher, C.Wilkin, *Evidence for an excited hyperon state in $pp \rightarrow pK^+Y^{0*}$*, Phys. Rev. Lett. 96 (2006) 012002.

M7. **I.Zychor**, M.Büscher, M.Hartmann, A.Kacharava, I.Keshelashvili, A.Khoukaz, V.Kleber, V.Koptev, Y.Maeda, T.Mersmann, S.Mikirtychiants, R.Schleichert, H.Ströher, Yu.Valdau, C.Wilkin, *Lineshape of the $\Lambda(1405)$ hyperon measured through its $\Sigma^0\pi^0$ decay*, Phys. Lett. B660 (2008) 167.

M8. **I.Zychor**, *Excited hyperons produced in proton-proton collisions with ANKE at COSY*, Int. J. Mod. Phys. E18 (2009) 241.

All presented results were obtained in the years 1994-2009 within the ANKE Collaboration at the Institute for Nuclear Physics (IKP) at Jülich, Germany. The international ANKE collaboration comprises ∼120 researchers from more than 15 institutes.

As in any high or medium energy physics experiments, many people have been contributing to this work and to all of them I am very grateful. In all these years I was strongly supported by the director of IKP Prof. H. Ströher and by the former director Prof. O. Schult who invited me to be a member of the ANKE Collaboration. I appreciate discussions, meetings and talks, not only on strange particles, with all colleagues from ANKE.

I dedicated this work to the memory of Vladimir Koptev. His great enthusiasm and insightful understanding of physics are behind it.

The description of my contributions to publications forming the basis for the habilitation qualification is given in Chapter 4.1 and publication copies are in Chapter 6.

The statements from co-authors, describing their contribution to publications declared for the habilitation procedure, are included in a separate appendix.

## 2.1 Introduction

Understanding of the origin of hadrons is one of the most important problems to be solved by the quantum chromodynamics as the theory which describes strong interactions. In this theory, hadrons are build from quarks and gluons. Quark and antiquark combine into mesons, whereas baryons are three-quark objects. Quarks interact via the strong force by exchanging gluons. Production of strange particles, containing at least one strange quark, could provide valuable information on both the structure of baryons and the dynamics of the strong interactions because baryonic resonances decay into mesons and a baryon in strong interactions.

The production and properties of hyperons, i.e. baryons composed of three quarks from which one or more are strange quarks, are experimentally investigated for more than 60 years, mostly in hadron-induced reactions, but recently also in photo-production. In addition to searching for missing resonances predicted by quark models, it is important to understand the nature of certain well established states, such as the $\Lambda(1405)$ hyperon resonance located below the $\bar{K}N$ threshold.

The $\Lambda(1405)$ hyperon, known already for more than half a century and being a four-star resonance in The Review of Particle Physics, has still not completely understood structure. The $\Lambda(1405)$ lineshape is not represented satisfactorily by a Breit-Wigner function due to a possible decay on $K^-$ and proton for masses higher than 1435 MeV/c$^2$. In quark-model calculations it is explained as a three-quark baryon. It is also discussed as a candidate for a $\bar{K}N$ molecular state or for a state with a pentaquark structure. The investigation of the $\Lambda(1405)$ lineshape would provide information on the resonance nature: if it is a state described by the quark model or molecular pictures, its lineshape should be independent of the production method.

The $\Sigma(1480)$ hyperon is far from being an established resonance. In The Review of Particle Physics it is described as a "bump", with unknown quantum numbers and given a mere one-star rating. The production of this hyperon was mostly investigated in $K^-$ and proton collisions. In the quark model, in which baryons are interpreted as bound states of three quarks, no excited $\Lambda$ or $\Sigma$ resonances, in addition to the well known states, have been predicted in this mass range. So, the $\Sigma(1480)$ hyperon may be of exotic nature.

In view of these uncertainties we started a program to investigate whether additional information might be obtained from proton-proton interactions at intermediate energies concerning strange particle production and properties.

## 2.2 Synchrotron COSY and magnetic spectrometer ANKE

The presented work is based on data obtained in experiments performed at the **Co**oler **Sy**nchrotron COSY at Jülich.

COSY is a medium energy accelerator and storage ring. COSY provides proton and deuteron beams with a momentum up to 3.7 GeV/c, polarized and unpolarized. Both electron and stochastic cooling are available during measurements.
COSY consists of several ion sources, an isochronous cyclotron, a 100 m long injection beam line, a ring with a circumference equal to 184 m and extraction beam lines to external experiments.
The COSY ring is made up of two 52 m long arc sections with a mirror symmetry and two 40 m long straight sections which act as a telescope with 1:1 imaging.

A magnetic spectrometer ANKE (**A**pparatus for Studies of **N**ucleon and **K**aon **E**jectiles) was built to separate ejectiles from the circulating COSY beam. It is located at an internal position of the COSY ring [J1].
Due to thin targets which could be used at internal positions an influence of background reactions is minimized and a high luminosity is available.
The ANKE spectrometer consists of three dipole magnets guiding the circulating COSY beam through a chicane. The central C-shaped spectrometer dipole separates the reaction products from the primary beam.

The ANKE detection system, comprising fifteen range telescopes, scintillation counters and multiwire proportional chambers, identifies particles of either charge and measures their momenta.
Each of the telescopes is placed in the focal plane of the spectrometer magnet and is suited for the identification of kaons with a certain momentum. A range telescope consists of a stop counter, Cerenkov counter, first passive degrader, energy loss counter, second passive degrader and veto counter [M1]. The thickness of the first passive degraders is chosen such that the $K^+$ loses most of its energy in the energy loss counter. So, it stops either at the edge of it or in the second degrader. The decay products are then registered in the veto counter (Fig. 5 in [M1]). With such a detection system positively charged kaons can be identified at ANKE in a background of pions or protons up to $10^6$ times more intense.

ANKE can register particles in a limited momentum range, i.e. $K^+$ with momenta between 100 and 600 MeV/c$^2$, $\pi^+$ with momenta between 200 and 900 MeV/c, $\pi^-$ with momenta between 400 and 1000 MeV/c$^2$ and protons with momenta higher than 750 MeV/c.

## 2.3 Monte Carlo simulations and data analysis

At the beginning of my participation in the ANKE project I prepared a detailed description of the spectrometer, including magnets, vacuum chambers, targets and detector systems. I used data from technical drawings and direct measurements at the place. The ANKE geometry package defines dimensions and positions of any element.

In the next stage, I prepared a dedicated Monte Carlo program to simulate ANKE experiments, based on the Geant3 code. I regularly updated this program for most of the measurements performed in years 1998-2006 including new experimental conditions, geometrical information and demands from users. It was necessary to include decays of resonances with the width of the order of few tens $MeV/c^2$, observed in the ANKE experiments.

The code was used for preparation of ANKE experiments and simulations of already measured data as well as by several PhD students in their work. Monte Carlo simulations performed with the code, which I wrote, were used for a determination of a detector acceptance, an estimation of the background, an explanation of measured particle spectra.

Simulations allowed one to reconstruct, without free parameters, the momenta of ejectiles using information from scintillation counters and signals from multiwire proportional chambers [M2].

In the analysis of measured data, which are the basis of the presented publications, an identification of negative charged particles was necessary as well as an inclusion of events with three particles in coincidence and later also with four coincident particles. I originally added indispensable programs to the RootSorter used by the ANKE Collaboration. Events obtained in Monte Carlo simulations were analysed under the same conditions as in measurements.

## 2.4 $K^+$ meson production in proton induced collisions

The primarily goal of building ANKE was to provide a device which allows one to study processes leading to $K^+$ meson production in proton interactions with atomic nuclei, in particular at beam energies far below the free nucleon-nucleon threshold ($\sim$1.58 GeV). The determination of an influence of nuclear matter on elementary processes is important for understanding of a possible restoration of a chiral symmetry in a dense hadron matter and properties of the nuclear matter. The $K^+$ production is well suited for this purpose due to a high mass of $K^+$ mesons, a long mean free path in nuclei and only small rescattering in a nuclear matter.

The kaon production in proton collisions with carbon, copper and gold nuclei was investigated in one of the first ANKE experiments. I participated in measurements in

which proton energy was between 1.0 and 2.3 GeV [J2 ÷ J4]. The important conclusion about a high degree of collectivity in the target nucleus was drawn from the momentum spectrum of kaons measured at 1.0 GeV [J5].

One of the next experiments, in which I was involved, was an investigation of the production of a light scalar resonance $a_0^+(980)$ in proton-proton collisions at 2.65 and 2.83 GeV proton energy.
Two decay chains of the $a_0^+(980)$ were analysed: $a_0^+(980) \to K^+ \bar{K}^0$ and $a_0^+(980) \to \pi^+ \eta$. In the $pp \to dK^+ \bar{K}^0$ reaction, measured at 2.65 GeV, about 1000 events were identified with a missing $\bar{K}^0$ particle [M3]. Dominance of the $K\bar{K}$ $s$-wave was deduced based on a joint analysis of invariant-mass and angular distributions. This dominance is a clear evidence for a resonant production of the $a_0^+(980)$. The second decay channel for the $a_0^+(980)$ resonance, $a_0^+(980) \to \pi^+ \eta$, was also observed in proton-proton collisions [M4]. The $pp \to dK^+ \bar{K}^0$ reaction was investigated at a higher beam energy of 2.83 GeV [M5], supporting conclusions from the above mentioned publications.

## 2.5 Hyperon production in proton-proton collisions

In the $pp \to pK^+ Y^0$ reaction at a beam momentum of 3.65 GeV/c hyperons $Y^0$ with masses up to $\sim$1540 MeV/c$^2$ can be produced.

### 2.5.1 Observation of the excited hyperon $Y^{0*}(1480)$

Data obtained in 2002 during the experiment on scalar meson $a_0^+(980)$ studies, described in the previous chapter, were used to investigate a hyperon $Y^{0*}(1480)$ production. During a four-week long measurement the integrated luminosity was determined to be equal to 6 pb$^{-1}$.

A multibody final state, containing a proton, a positively charged kaon, and a charged pion, together with an unidentified residue $X$, was studied in the $pp \to pK^+ Y^0 \to pK^+ \pi^{\pm} X^{\mp}$ reaction [M6].
Events with three identified charged particles $(p, K^+ \pi^+)$ and $(p, K^+ \pi^-)$ were retained for further analysis. For the $pp \to pK^+ \pi^+ X^-$ reaction a clear enhancement corresponding to $X^- = \Sigma^-(1197)$ was observed in the missing-mass distribution $MM(pK^+\pi^+)$. In the $pp \to pK^+ \pi^- X^+$ case, the missing-mass distribution $MM(pK^+\pi^-)$ is more complicated because the $\pi^-$ may originate not only from a reaction with $X^+ = \Sigma^+(1189)$ but also from a secondary decay of $\Lambda \to p\pi^-$, arising from background reactions.
For further analysis events corresponding to the $\Sigma$ production were selected. A double-humped structure with peaks around 1390 and 1480 MeV/c$^2$ is observed in the missing-mass distributions $MM(pK^+)$ for the $(\pi^+ X^-)$ case. In the $(\pi^- X^+)$ case, the distribution peaks at 1480 MeV/c$^2$.

In order to explain the measured missing-mass distributions $MM(pK^+)$ Monte Carlo

simulations were performed for both final states $(\pi^+ X^-)$ and $(\pi^- X^+)$. The production of well established hyperon resonances $(\Sigma(1385)$, $\Lambda(1405)$ and $\Lambda(1520))$ as well as non-resonant reactions, like $pp \rightarrow NK^+X$, $pp \rightarrow NK^+\pi X$ and $pp \rightarrow NK^+\pi\pi X$ (N denotes a nucleon, X - any hyperon which could be produced in the experiment), were included in these simulations.

For both final states $(\pi^+ X^-)$ and $(\pi^- X^+)$ an excess of events in the measured $MM(pK^+)$ distributions is observed around the missing mass of 1480 MeV/c². The production of another excited hyperon $Y^{0*}$ was then taken into account: $pp \rightarrow pK^+Y^{0*} \rightarrow pK^+\pi^\pm X^\mp$. The $Y^{0*}$ mass and width, determined from a comparison of measured and simulated missing-mass distributions for both final states, is equal to $(1480\pm15)$ MeV/c² and $(60\pm15)$ MeV/c², respectively. The statistical significance of the signal, assuming that this is due to the production of the $Y^{0*}$, is at least 4.5 standard deviations. The cross section estimates are consistent for both final states and are of the order of few hundred nanobarns.

On the basis on presented data we cannot decide about a nature of the observed $Y^{0*}(1480)$ hyperon: it could be a one-star $\Sigma(1480)$ resonance described in The Review of Particle Physics or a $\Lambda(1480)$ hyperon. In the quark models barions are interpreted as bound states of three valence quarks where hyperons contain at least one strange quark. No excited $\Lambda$ or $\Sigma$ resonances, in addition to the well known states, have been predicted for masses lower than 1600 MeV/c². Thus, it seems to be difficult to reconcile the low mass of the $Y^{0*}(1480)$ within the existing classification of 3q baryons. There are models, in which a hyperon with the mass around 1480 MeV/c² could have an exotic nature, connected, e.g., with a pentaquark structure (see Refs. [13-19] in [M6]). Since a clear theoretical picture has not yet appeared, any conclusion about the nature of the $Y^{0*}(1480)$ would be premature.

### 2.5.2 Investigation of the $\Lambda(1405)$ hyperon through its $\Sigma^0\pi^0$ decay

The nature of the $\Lambda(1405)$ hyperon is still not fully understood though it is known for more than 60 years. Part of the difficulty in elucidating the nature of the $\Lambda(1405)$ is due to its mass only $\sim$20 MeV/c² higher than the nearby $\Sigma^0(1385)$. In addition, both hyperons have a similar width of the order of several dozen MeV/c² (see Table 1 in [J7] for comparison of resonance properties). So, with an experimental mass resolution of 10-20 MeV/c² the $\Lambda(1405)$ lineshape obtained from $\Sigma^+\pi^-$ and $\Sigma^-\pi^+$ decays is distorted by the $\Sigma^0(1385)$. The cleanest approach to identify the $\Lambda(1405)$ is through the measurement of the $\Sigma^0\pi^0$ channel, since isospin forbids this channel for the decay of the $\Sigma^0(1385)$ (Fig. 1 in [M8]). This method was used in the presented studies of the $\Lambda(1405)$ hyperon [M7].

We used data obtained in the experiment done in 2005. A hydrogen target was irradiated by a proton beam with a momentum of 3.65 GeV/c. In the measurement lasted four weeks the integrated luminosity equal to 69 pb$^{-1}$ was determined from elastic proton-proton scattering.

In the $pp \rightarrow pK^+Y^0 \rightarrow pK^+p\pi^- X^0$ reaction we were searching for four-fold coincidences, comprising two protons, one positively charged kaon and one negatively charged pion.

Such a configuration can correspond to the reaction chains involving the $\Sigma^0(1385)$ and $\Lambda(1405)$ as intermediate states:

$pp \to pK^+\Sigma^0(1385) \to pK^+\Lambda\pi^0 \to pK^+p\pi^- \pi^0$,

$pp \to pK^+\Lambda(1405) \to pK^+\Sigma^0\pi^0 \to pK^+\Lambda\gamma\pi^0 \to pK^+p\pi^- \pi^0\gamma$.

In the $\Sigma^0(1385)$ case, the residue is $X^0 = \pi^0$, while for the $\Lambda(1405)$, $X^0 = \pi^0\gamma$. These conditions were then used to discriminate between both hyperons: for the $\Sigma^0(1385)$ case, the mass of the residue $X^0$ is equal to the pion mass, and for the $\Lambda(1405)$, the $X^0$ mass is higher than the pion mass.

Since the properties of the $\Sigma^0(1385)$ are undisputed, we used this hyperon as a test case for the $\Lambda(1405)$ analysis. Monte Carlo simulations were performed for resonant and non-resonant production with four particles $(p, p, K^+, \pi^-)$ in the exit channel. The calculated missing-mass distribution $MM(pK^+)$ is in agreement with the measured distribution where the $\Sigma^0(1385)$ peak dominates over a small background.

To obtain the $\Lambda(1405)$ lineshape, the simulated distribution being a sum of non-resonant contributions was subtracted from the measured missing-mass distribution $MM(pK^+)$. The background-subtracted data exhibit a prominent structure around 1400 MeV/c$^2$. There is no indication of a second one near 1500 MeV/c$^2$, which might result from production of the $\Lambda(1520)$. There is no evidence either for a significant contribution from the $Y^{0*}(1480)$ hyperon. If this state were the same as the one-star $\Sigma^0(1480)$ of The Review of Particle Physics, the decay into $\Sigma^0\pi^0$ would be forbidden.

Models based on unitary chiral theory find two states in the neighborhood of the $\Lambda(1405)$ with masses of 1390 and 1420 MeV/c$^2$ (Refs. [8, 9] in [M7]). Both states may contribute to the experimental distributions, and it is their relative population, which depends upon the production mechanism, that will determine the observed lineshape. The missing-mass distribution obtained from the $\Sigma^0\pi^0$ decay was then compared with those from $\Sigma^+\pi^-$ and $\Sigma^-\pi^+$ decays (Refs. [11, 13] in [M7]). Our experimental findings show that the properties (mass, width, and shape) of the $\Lambda(1405)$ resonance are essentially identical for these three different production modes. This observation, which contradicts predictions based on the unitary theory, stimulated both theoretical discussions and experimental developments on the nature of the $\Lambda(1405)$. However, there is no yet one theoretical approach explaining all experimental results. In view of relatively small number of events ($156 \pm 23$) identified in the presented studies lasted almost one month, further measurements are needed, also in $\gamma$ induced reactions.

The production cross section for the $\Sigma^0(1385)$ and $\Lambda(1405)$ hyperons in proton-induced collisions at a beam momentum of 3.65 GeV/c, determined in the presented experiment, is of the order of a few $\mu$b.

More details about $\Sigma^0(1385)$ and $\Lambda(1405)$ studies, including a comparison of experimental conditions, can be found in conference proceedings [O2].

### 2.5.3 Bound kaonic nuclear states

For the first time, the hypothesis of a possible existence of deeply bound kaonic nuclear states was formulated in 1986 by S.Wycech [Nucl. Phys. A450 (1986) 399c]. In 2002 Y.Akaishi and T.Yamazaki presented the theoretical predictions for light atomic nuclei [Phys.Rev. C65 (2002) 044005].

In the FINUDA experiment the production of a bound kaonic state was investigated through its decay into a $\Lambda$ hyperon and a proton [M.Agnello et al., Phys. Rev. Lett. 94, 212303 (2005)]. The invariant-mass distribution of the $\Lambda p$ pair showed a significant mass decrease with respect to the mass of the system expected in case of a simple two-nucleon absorption, namely 2370 MeV/c$^2$. The binding energy of 115 MeV and the decay width of 67 MeV was determined for the detected $K^-pp$ system.
The observation of a structure with similar parameters in the DISTO experiment [T.Yamazaki et al., Phys. Rev. Lett. 104, 132502 (2010)] motivated us to check if we could identify events corresponding to the bound kaonic state production in data measured with the ANKE spectrometer [O3]. Data from the $\Lambda(1405)$ studies were used for this purpose (Chapter 2.5.2).

The $pp \rightarrow K^+X^+$ reaction was investigated in collisions induced on a hydrogen target by protons with a momentum of 3.65 GeV/c. Assuming a decay of the $X^+$ into $p\Lambda$, followed by the $\Lambda \rightarrow p\pi^-$ decay, the final state with four particles ($K^+$, two protons and $\pi^-$) could be observed. The experimental missing-mass $MM(K^+)$ distribution showed no events for $MM(K^+) < 2370$ MeV/c$^2$. Since ANKE detectors register particles in a limited momentum range (Chapter 2.2), it was concluded that this restricted acceptance of the ANKE spectrometer is responsible for a non-observation of the nuclear bound kaonic state with a mass of 2250-2350 MeV/c$^2$ and a width of 50-100 MeV/c$^2$, if such a state exists.

Experiments on bound kaonic nuclear states are performed or planned in a few laboratories, e.g, E15 and E17@J-PARC, AMADEUS@Frascati.

## 2.6    Conclusions

The most important conclusions from studies on hyperon production in proton-proton collision at intermediate energies:

1. The obtained results on hyperon production in $pp$ collisions at intermediate energies showed that the ANKE spectrometer operating at the COSY ring at Jülich is a unique device suitable to investigate hyperon properties.
2. However, due to small cross sections for hyperons measured in the investigated reactions (few hundred nanobarns to a few $\mu$b) and high background from non-resonant production, experiments are difficult.
3. For the first time $pp$ collisions were used to produce $Y^{0*}(1480)$ and $\Lambda(1405)$ hyperons.
4. After more than 20 years new data on the $Y^{0*}(1480)$ were obtained. No such a resonance has been predicted by 3q models, so it could have an exotic nature. The measurements planned with the PANDA@FAIR detector build at GSI in Darmstadt can provide more information on the $Y^{0*}(1480)$ nature.
5. The presented measurements showed that the mass, width and shape of the $\Lambda(1405)$ resonance do not depend on the production mechanism. This result, which contradicts predictions based on the unitary theory, stimulated both theoretical discussions and experimental developments (e.g., CLAS, HADES, KLOE) on the $\Lambda(1405)$ nature.

Results on strange particle production in $pp$ collisions were published in fifteen papers, in which I am an author or co-author [M1 ÷ M8, J1 ÷ J7]. They were presented by me at a number of conferences and seminars, as well as they were documented in details in contributions to NCBJ Annual Reports at Świerk and the Institute for Nuclear Physics at Jülich.

# 3    Description of other scientific achievements

After achieving in 1977 a Master of Science diploma at the Faculty of Physics at the University of Warsaw, I started to work there at the Nuclear Spectroscopy Division. During my work I was involved in research and student teaching.
In years 1977-1987 I provided classes on nuclear physics, programming and physics laboratory for students from the Faculty of Physics.
I participated in experiments performed at the Nuclear Spectroscopy Division, e.g., in the investigations of the $\alpha$ decay of thorium [J8].

In 1983 I finished my PhD thesis *Investigation of the production of hafnium isotopes and isomers in reactions of $^{40}Ar$, $^{84}Kr$ and $^{136}Xe$ ions on tungsten targets*. The experiments were done at the Centre for Heavy Ion Research (GSI) in Darmstadt. The data analysis and calculations were performed in Warsaw and Darmstadt. The main conclusions from

these experiments were presented in my PhD thesis and two publications [J9, J10]. The general behaviour of the measured mass distributions of hafnium and lutetium isotopes, especially on the neutron deficient side, was explained in terms of the partial statistical equilibrium model. It was found that the yield of hafnium and lutetium isomeric states increases significantly with increasing projectile mass. In addition, it was shown that hafnium and lutetium isomeric states are produced in multinucleon transfer reactions, including the $K^\pi = 16^+$ yrast trap in the $^{178}$Hf isotope.

After finishing my PhD I was involved in the collaboration with Institut des Sciences Nucléaires in Grenoble. We concentrated on studies of the linear momentum transfer in light and heavy-ion induced reactions. Our data extend the systematics of average linear momentum transfer to lighter target masses, previously known only for highly fissile elements [J11, O4].

In 1985-1987 I was working at GSI in Darmstadt. I was involved in experiments at the velocity separator SHIP (Separator for Heavy Ion Reaction Products). The aims of experiments were the investigation of the fusion reactions induced by heavy ions accelerated by the linear accelerator UNILAC as well as studies of the decay properties of reaction products.
During my stay at GSI, the experiments to search for the heaviest elements were the most important ones for the SHIP group [J12, O5]. I took part in the measurements to search for elements 107, 108 and 110.
Two isotopes with masses 264 and 265 of the element 108, named hassium in 1997, were produced in complete fusion of $^{58}$Fe with $^{208}$Pb [J13, J14].
For the first time, the $\alpha$ decay of element 107, named bohrium in 1997, was identified in the $^{54}$Cr$+^{209}$Bi $\to^{263}$107 reaction [J15]. Two $\alpha$ emitting isotopes with masses 261 and 262 were identified. For the isotope with mass 262 a transition, assigned to an isomeric state, was found.
Attempts to synthesize element 110 in the $^{64}$Nir$+^{208}$Pb and $^{40}$Ar$+^{235}$U reactions were negative. No chains were observed that could be attributed to this element [O6]. The successful experiment to produce element 110 was done in 1995.
I also participated in investigations of the $^{58}$Ni$+^{102}$Pd $\to^{160}$W and $^{58}$Ni$+^{106}$Cd $\to^{164}$Os reactions used for systematic studies of the decay modes of neutron deficient nuclei close to the proton drip line [O7]. The new isotopes $^{162}$Os and $^{156}$Tm were identified in these reactions [J16].
In data already collected during previous SHIP experiments a new 3.2 $\mu$s isomer in $^{76}$Rb was identified [J17]. The isomer decays by the emission of four $\gamma$ rays and an energy of 316.94 keV above the ground state was assigned to this isomer. The properties of this isomeric state resulted in the first indication of shape coexistence in this nucleus at low spins.
In continuation of the analysis, a new isomeric state in $^{142}$Tb was established [O8 and in Nucl. Data Sheets 112 (2011) 1949].

In 1988 I started to work at the National Centre for Nuclear Research (NCBJ) at Świerk.

At the beginning, I simulated interactions between matter and electrons with energies lower than 20 MeV. Beams of such electrons are produced in linear accelerators, e.g., for medical applications.

A detailed information about the distribution of the dose delivered to a patient is required in order to perform an optimal radiotherapy. The collimation of the beam is necessary to limit its size and to protect healthy tissues. The broad uniform electron beam, characterized by a flat radial absorbed dose distribution and a well defined area to be treated, is the most important purpose of the electron beam design for radiotherapy. To flatten the radiation fields of medical electron linear accelerators, scattering foils are inserted into the electron beam.

The complete scattering system influences the shape of depth dose distributions and the maximum absorbed dose rate at a treatment distance. The influence of a beam forming system on absorbed dose distributions could be examined using Monte Carlo simulations. To perform simulations in arbitrary, user-defined, complex geometries made of any material I wrote the SHOWME program based on the Geant3 code [O9 ÷ O11, J18].

I used the same code to investigate bremsstrahlung production, especially to find the best target for such a process [O12].

Another application of the SHOWME code was connected with a design of a high power electron accelerator for industrial technologies since the heating of a beam output window is a result of electron interaction with matter, mainly due to multiple scattering.

The obtained results were published regularly in IPJ Annual Reports between 1989 and 1997 and presented on six international conferences and workshops [P1÷P6] as well as on seminars.

In 1994 I started a long-term collaboration with the Institute for Nuclear Physics at Jülich (Germany). In the beginning my visits there were supported by the TEMPUS mobility and training programme.

During my first stay I was studying details of the ion optics of a circulating beam in the COSY accelerator storage and cooler synchrotron ring operating at Jülich.

At that time conditions for two experiments at internal target positions had to be investigated. One experiment, using the ANKE magnetic spectrometer, was related to the investigation of subthreshold $K^+$ meson production. The other one was the COSY-13 experiment dedicated to the measurements of the lifetime of heavy hypernuclei produced in proton collisions with atomic nuclei. It was essential to operate COSY ion optically in such a way that the machine acceptance remains large. The machine optimization required extensive calculations with the MAD code which describes an accelerator, simulates beam dynamics and optimizes beam optics. In next few years I performed a large number of calculations to find an optimal setting of the COSY accelerator for the two classes of experiments [O13, P7].

While the construction of the ANKE spectrometer was going on, I participated in experiments performed within the COSY-13 Collaboration. I was a member of this collaboration in years 1996-2000.

The hypernucleus lifetime was measured in the $(p, K^+)$ reaction by the observation of delayed fission using the recoil shadow method. This method can be used for very heavy

nuclei, where fission induced by the hyperon decay becomes a significant excitation mode. I participated in investigations in which Bi and U targets were irradiated by protons from the circulating beam in the COSY storage ring, operating in a supercycle. The use of this operation mode eliminates the systematic errors in background subtraction. The proton beam energies were chosen in such a way that at the higher energies (1.5 and 1.9 GeV) hypernuclei could be produced. The background was then determined at a lower beam energy of 1.0 GeV.

Details of physical phenomena, experimental setup, conditions of performed experiments and obtained results are presented in [J19÷J29, O14÷O16].

The measurement performed during irradiation of a Bi target with 1.9 GeV protons resulted in the most precise value of the lifetime of heavy hypernuclei, equal to [161±7(statist)±14(system)] ps [J24].

In December 2000 the experimental setup of COSY-13 was removed from the COSY ring.

In 1998 the ANKE spectrometer was used for the first time for physics experiments at the COSY ring at Jülich. Up tp 2009 I was involved in experiments dedicated to the production of strange particles, described in Chapter 2.

In 2000 I was invited to the Paul Scherrer Institute (PSI) at Villigen (Switzerland) to join the SINDRUM II experiment in its last stage.

The SINDRUM II experiment tests the conservation of lepton-flavour in neutrinoless coherent muon-electron conversion in muonic atoms: $\mu^- + (A, Z) \rightarrow e^- + (A, Z)$, A=mass number, Z=proton number. The observation of the muon-electron conversion would give evidence that the lepton flavour is not conserved and this, in turn, is a sign of new physics beyond the Standard Model of particle physics. Signature of the $\mu$-$e$ conversion is a single electron with characteristic energy. The intrinsic electron background from normal three-body decay of the bound muon has a broad energy distribution vanishing at the $\mu$-$e$ conversion energy.

In the SINDRUM II experiment a high intensive muon beam was stopped in a target and the energy of emitted electrons was measured with a cylindrical magnetic spectrometer around the target. The experimental sensitivity was mainly dependent on the energy resolution and the total number of muons stopped in the target.

The measurement resulted in the branching ratio of $\mu$-$e$ conversion in muonic gold relative to the nuclear capture probability $\Gamma(\mu^- Au \rightarrow e^- Au_{g.s.}/\Gamma_{capture}(\mu^- Au) < 7 \times 10^{-13}$ (90%C.L.) [J30, O17]. This finding is more stringent by two orders of magnitude than the best previous limit and still remains the most precise one. It was the final result of the research program with the SINDRUM II spectrometer - in autumn 2000 it was removed from its place.

In 2004 the proposal for transferring the WASA detector from CELSIUS@Uppsala to Jülich was accepted [O18]. In summer 2006 the WASA detector was installed at an internal target position in the COSY ring.

One of the discussed physics experiments was an investigation of the hadron structure through precise measurements of all possible decay chains. At that time the ANKE Collaboration found evidence for a hyperon with mass 1480 MeV/c$^2$ by simultaneous

investigations of charged decay channels (Chapter 2.5.1). It was expected that measurements done with the WASA detector will allow to study not only charged decay channels but neutral too. Another planned experiment was to investigate the nature of the $\Lambda(1405)$ resonance in proton-proton collisions by measuring its lineshape with a mass resolution and statistics better than in ANKE experiments. Since no efficient way to separate protons and $K^+$ mesons was found, investigations on hyperon production were suspended whereas the program dealing with "$\eta$ physics" is successfully going on WASA@COSY [J31].

During my collaboration with the Institute for Nuclear Physics at Jülich I participated in preparation of six proposals for experiments connected with the COSY [O18 ÷ O23]. Two contributions describing results from investigations done with COSY-13 and ANKE detectors were published in the report "Nuclear Physics in Poland 1996-2006" [O24].

In 2011 I started to use the Geant4 code for applications. Monte Carlo simulations with the Geant4-DNA code can be used for modelling the interactions of very low energy charged particles with biological nanostructures like DNA segments or nucleosomes [O25, P29].

Since 2012 I participate in the EURATOM project *Development of the selected diagnostic techniques (Cerenkov detectors, solid-state nuclear track detectors, scintillation detectors for hard X-ray diagnostics)* as a leader of the task *Monte Carlo simulations of gamma-ray interactions with scintillators.*
We investigate the possibility to use scintillators for X and gamma-ray radiation diagnostics in thermonuclear reactors, including the constructed research reactor ITER. The main task of investigations of the scintillators, like NaI(Tl), $LaBr_3(Ce)$, $CeBr_3$, is to find if such materials could be used in gamma radiation detectors for high-temperature plasma monitoring. The following parameters of scintillators are measured: light output, non-proportionality, energy resolution, detection efficiency, decay time, nuclear radiation resistance. Monte Carlo simulations of gamma-ray interactions with matter are used for designing and optimization of detection systems [O26] as well as for analysis of phenomena taking place in tokamaks.

# 4  List of publications and bibliometric data

## 4.1  List of publications for the habilitation qualification

*with a description and estimate percent of my contribution*

**Achievement title**

### Strange particle production in proton-proton collisions at intermediate energies

based on a monothematic series of eight publications

M1. M.Büscher, H.Junghans, V.Koptev, M.Nekipelov, K.Sistemich, H.Ströher, S.Barsov, G.Borchert, W.Borgs, M.Debowski W.Erven, R.Esser, P.Fedorets, D.Gotta, M.Hartmann, V.Hejny, A.Kacharava, H.R.Koch, V.Komarov, P.Kulessa, A.Kulikov, G.Macharashvili, S.Merzliakov, S.Mikirtychiants, H.Müller, A.Mussgiller, R.Nellen, M.Nioradze, H.Ohm, A.Petrus, F.Rathmann, Z.Rudy, R.Schleichert, C.Schneider, O.W.B.Schult, H.J.Stein, **I.Zychor**, *Identification of $K^+$ mesons from subthreshold pA collisions with ANKE at COSY-Jülich*, Nucl. Instrum. Meth. A481 (2002) 378. contribution: updating description of ANKE geometry according to experimental conditions and implementing into Monte Carlo code, participating in experiments, partial data analysis, 10%

M2. **I.Zychor**, *Monte Carlo simulations for ANKE experiments*, Acta Phys. Pol. B33 (2002) 521. contribution: publication authored only by me, based on experimental results and simulations, participating in experiments, performing data analysis and all Monte Carlo simulations, writing a paper

M3. V.Kleber, M.Büscher, V.Chernyshev, S.Dymov, P.Fedorets, V.Grishina, C.Hanhart, M.Hartmann, V.Hejny, A.Khoukaz, H.R.Koch, V.Komarov, L.Kondratyuk, V.Koptev, N.Lang, S.Merzliakov, S.Mikirtychiants, M.Nekipelov, H.Ohm, A.Petrus, D.Prasuhn, R.Schleichert, A.Sibirtsev, H.J.Stein, H.Ströher, K.H.Watzlawik, P.Wüstner, S.Yaschenko, B.Zalikhanov, **I.Zychor**, *$a_0^+$(980)-Resonance Production in $pp \rightarrow dK^+\bar{K}^0$ Reactions Close to Threshold*, Phys. Rev. Lett. 91 (2003) 172304. contribution: preparing a Monte Carlo code used for simulations, participating in experiments, updating description of ANKE geometry according to experimental conditions, partial data analysis and simulations, 15%

M4. P.Fedorets, M.Büscher, V.Chernyshev, S.Dymov, V.Grishina, C.Hanhart, M.Hartmann, V.Hejny, V.Kleber, H.R.Koch, L.Kondratyuk, V.Koptev, A.Kudryavtsev, P.Kulessa, S.Merzliakov, S.Mikirtychyants, M.Nekipelov, H.Ohm, R.Schleichert, H.Ströher, V.Tarasov, K.H.Watzlawik, **I.Zychor**, *$a_0^+$(980)-Resonance Production in the Reaction $pp \rightarrow d\pi^+\eta$ Close to the $K\bar{K}$ Threshold*, Phys. Atom. Nucl. 69 (2006) 306. contribution: preparing a Monte Carlo code used for simulations, participating in experiments, updating description of ANKE geometry according to experimental conditions, partial data analysis and simulations, 15%

M5. A.Dzyuba, V.Kleber, M.Büscher, V.Chernyshev, S.Dymov, P.Fedorets, V.Grishina, C.Hanhart, M.Hartmann, V.Hejny, L.Kondratyuk, V.Koptev, P.Kulessa, Y.Maeda, T.Mersmann, S.Mikirtychyants, M.Nekipelov, D.Prasuhn, R.Schleichert, A.Sibirtsev, H.J.Stein, H.Ströher, **I.Zychor**, *Scalar-isovector production close to threshold*, Eur. Phys. J. A29 (2006) 245. contribution: preparing a Monte Carlo code used for simulations, participating in experiments, updating description of ANKE geometry according to experimental conditions, partial data analysis and simulations, 15%

M6. **I.Zychor**, V.Koptev, M.Büscher, A.Dzyuba, I.Keshelashvili, V.Kleber, H.R.Koch, S.Krewald, Y.Maeda, S.Mikirtychiants, M.Nekipelov, H.Ströher, C.Wilkin, *Evidence for an excited hyperon state in $pp \rightarrow pK^+Y^{0*}$*, Phys. Rev. Lett. 96 (2006) 012002. contribution: preparing a Monte Carlo code used for simulations, implementing

17

ANKE geometry, inclusion of decays of resonances with the width of the order of few tens MeV/c$^2$, participating in experiments, preparing computer codes for data analysis to identify negative charged particles and events with three particles in coincidence, performing data analysis and all simulations, writing publications, 70%

M7. **I.Zychor**, M.Büscher, M.Hartmann, A.Kacharava, I.Keshelashvili, A.Khoukaz, V.Kleber, V.Koptev, Y.Maeda, T.Mersmann, S.Mikirtychiants, R.Schleichert, H.Ströher, Yu.Valdau, C.Wilkin, *Lineshape of the Λ(1405) hyperon measured through its $\Sigma^0\pi^0$ decay*, Phys. Lett. B660 (2008) 167.

contribution: preparing a Monte Carlo code used for simulations, implementing ANKE geometry, participating in experiments, preparing computer codes for data analysis to identify events with four particles in coincidence, performing data analysis and all simulations, interpretation of results, writing publications, 70%

M8. **I.Zychor**, *Excited hyperons produced in proton-proton collisions with ANKE at COSY*, Int. J. Mod. Phys. E18 (2009) 241.

contribution: publication authored only by me, based on experimental results and Monte Carlo simulations, writing a paper

## 4.2    List of other publications

### 4.2.1    Publications in journals indexed in the JCR base

*with a description and estimate percent of my contribution*

J1. S.Barsov, U.Bechstedt, W.Bothe, N.Bongers, G.Borchert, W.Borgs, W.Brautigam, M.Büscher, W.Cassing, V.Chernyshev, B.Chiladze, J.Dietrich, M.Drochner, S.Dymov, W.Erven, R.Esser, A.Franzen, E.Golubeva, D.Gotta, T.Grande, D.Grzonka, A.Hardt, M.Hartmann, V.Hejny, L.vonHorn, L.Jarczyk, H.Junghans, A.Kacharava, B.Kamys, A.Khoukaz, T.Kirchner, F.Klehr, W.Klein, H.R.Koch, V.Komarov, L.Kondratyuk, V.Koptev, S.Kopyto, R.Krause, P.Kravtsov, V.Kruglov, P.Kulessa, A.Kulikov, N.Lang, N.Langenhagen, A.Lepges, J.Ley, R.Maier, S.Martin, G.Macharashvili, S.Merzliakov, K.Meyer, S.Mikirtychyants, H.Müller, P.Munhofen, A.Mussgiller, M.Nekipelov, V.Nelyubin, M.Nioradze, H.Ohm, A.Petrus, D.Prasuhn, B.Prietzschk, H.J.Probst, K.Pysz, F.Rathmann, B.Rimarzig, Z.Rudy, R.Santo, H.Paetzgen.Schieck, R.Schleichert, A.Schneider, C.Schneider, H.Schneider, U.Schwarz, H.Seyfarth, A.Sibirtsev, U.Sieling, K.Sistemich, A.Selikov, H.Stechemesser, H.J.Stein, A.Strzalkowski, K.H.Watzlawik, P.Wüstner, S.Yaschenko, B.Zalikhanov, N.Zhuravlev, K.Zwoll, **I.Zychor**, O.W.B.Schult, H.Ströher, *ANKE, a new facility for medium energy hadron physics at COSY-Jülich*, Nucl. Instrum. Meth. A462 (2001) 364.

contribution: updating description of ANKE geometry according to experimental conditions and implementing into Monte Carlo code, participating in experiments, partial data analysis, 5%

J2. S.Barsov, V.Koptev, S.Mikirtychiants, U.Bechstedt, G.Borchert, W.Borgs, M.Büscher, W.Erven, D.Gotta, M.Hartmann, H.Junghans, F.Klehr, H.R.Koch,

P.Kulessa, R.Maier, H.Ohm, D.Prasuhn, R.Schleichert, H.Schneider, O.W.B.Schult, H.Seyfarth, K.Sistemich, H.J.Stein, H.Ströher, M.Debowski, H.Müller, B.Rimarzig, C.Schneider, F.Rathmann, A.Mussgiller, B.Kamys, K.Pysz, Z.Rudy, **I.Zychor**, A.Kacharava, V.Komarov, A.Kulikov, V.Kurbatov, G.Macharashvili, S.Merzliakov, A.Petrus, P.Fedorets, M.Nioradze, *Study of medium modifications with the new spectrometer ANKE at COSY- Jülich*, Acta Phys. Pol. B 31 (2000) 357.
contribution: updating description of ANKE geometry according to experimental conditions and implementing into Monte Carlo code, participating in experiments, partial data analysis, 5%

J3. S.Barsov, U.Bechstedt, G.Borchert, W.Borgs, M.Büscher, M.Debowski, W.Erven, R.Esser, P.Fedorets, D.Gotta M.Hartmann, H.Junghans, A.Kacharava, B.Kamys, F.Klehr, H.R.Koch, V.Komarov, V.Koptev, P.Kulessa, A.Kulikov, V.Kurbatov, G.Macharashvili, R.Maier, S.Merzliakov, S.Mikirtychyants, H.Müller, A.Mussgiller, M.Nekipelov, M.Nioradze, H. Ohm, A.Petrus, D.Prasuhn, K.Pysz, F.Rathmann, B.Rimarzig, Z.Rudy, R.Schleichert, C.Schneider, H.Schneider, O.W.B.Schult, H.Seyfarth, K.Sistemich, H.J.Stein, H.Ströher, **I.Zychor**, *Measurement of subthreshold $K^+$ production in pA collisions with ANKE*, Acta Phys. Pol. B31 (2000) 2159.
contribution: updating description of ANKE geometry according to experimental conditions and implementing into Monte Carlo code, participating in experiments, partial data analysis, 5%

J4. S.Barsov, U.Bechstedt, G.Borchert, W.Borgs, M.Büscher, M.Debowski, W.Erven, R.Esser, P.Fedorets, D.Gotta, M.Hartmann, H.Junghans, A.Kacharava, B.Kamys, F.Klehr, H.R.Koch, V.Komarov, V.Koptev, P.Kulessa, A.Kulikov, V.Kurbatov, G.Macharashvili, R.Maier, S.Merzliakov, S.Mikirtychyants, H.Müller, A.Mussgiller, M.Nioradze, H.Ohm, A.Petrus, D.Prasuhn, K.Pysz, F.Rathmann, B.Rimarzig, Z.Rudy, R.Schleichert, C.Schneider, H.Schneider, O.W.B.Schult, H.Seyfarth, K.Sistemich, H.J.Stein, H.Ströher, **I.Zychor**, *Subthreshold $K^+$-production studies with ANKE at COSY- Jülich*, AIP Conf. Proc. 549 (2000) 421.
contribution: updating description of ANKE geometry according to experimental conditions and implementing into Monte Carlo code, participating in experiments, partial data analysis, 5%

J5. V.Koptev, M.Büscher, H.Junghans, M.Nekipelov, K.Sistemich, H.Ströher, V.Abaev, H.H.Adam, R.Baldauf, S.Barsov, U.Bechstedt, N.Bongers, G.Borchert, W.Borgs, W.Brautigam, W.Cassing, V.Chernyshev, B.Chiladze, M.Debowski, J.Dietrich, M.Drochner, S.Dymov, J.Ernst, W.Erven, R.Esser, P.Fedorets, A.Franzen, D.Gotta, T.Grande, D.Grzonka, G.Hansen, M.Hartmann, V.Hejny, L.vonHorn, L.Jarczyk, A.Kacharava, B.Kamys, A.Khoukaz, T.Kirchner, S.Kistryn, F.Klehr, H.R.Koch, V.Komarov, S.Kopyto, R.Krause, P.Kravtsov, V.Kruglov, P.Kulessa, A.Kulikov, V.Kurbatov, N.Lang, N.Langenhagen, I.Lehmann, A.Lepges, J.Ley, B.Lorentz, G.Macharashvili, R.Maier, S.Martin, S.Merzliakov, K.Meyer, S.Mikirtychiants, H.Müller, P.Munhofen, A.Mussgiller, V.Nelyubin, M.Nioradze, H.Ohm, A.Petrus, D.Prasuhn, B.Prietzschk, H.J.Probst, D.Protic, K.Pysz, F.Rathmann, B.Rimarzig, Z.Rudy, R.Santo, H.Paetzgen.Schieck, R.Schleichert, A.Schneider, C.Schneider, H.Schneider, G.Schug, O.W.B.Schult, H.Seyfarth,

A.Sibirtsev, J.Smyrski, H.Stechemesser, E.Steffens, H.J.Stein, A.Strzalkowski, K.H.Watzlawik, C.Wilkin, P.Wüstner, S.Yaschenko, B.Zalikhanov, N.Zhuravlev, P.Zolnierczuk, K.Zwoll, **I.Zychor**, *Forward $K^+$ production in subthreshold pA collisions at 1.0 GeV*, Phys. Rev. Lett. 87 (2001) 022301.

contribution: participating in experiments, partial data analysis, 5%

J6. **I.Zychor**, V.Koptev, M.Büscher, A.Dzyuba, I.Keshelashvili, V.Kleber, R.Koch, S.Krewald, Y.Maeda, S.Mikirtychyants, M.Nekipelov, H.Ströher, C.Wilkin, *Indication of an excited hyperon state in pp collisions with ANKE at COSY- Jülich*, Nucl. Phys. A755 (2005) 403c.

contribution: participating in experiments, preparing a Monte Carlo code used for simulations, implementing ANKE geometry, preparing computer codes for data analysis, performing data analysis and all simulations, writing publications, 70%

J7. **I.Zychor**, *Hyperon production in proton-proton collisions with ANKE at COSY*, Acta Phys. Pol. B36 (2005) 2351.

contribution: publication authored only by me, based on experimental results and Monte Carlo simulations, writing a paper

J8. E.Ruchowska, B.Szweryn, T.Batsch, **I.Zychor**, *Alpha-Decay of $^{232}Th$ to the Excited States of $^{228}Ra$*, Nukleonika 28 (1983) 1.

contribution: preparation and participation in measurements, data analysis, writing publication, 25%

J9. **I.Zychor**, K.Rykaczewski, H.Ahrens, H.Folger, W.Kurcewicz, K.Sümmerer, N.Kaffrell, N.Trautmann, *Hafnium and Lutetium Isomers Produced in Heavy-Ion Collisions of 7.6 MeV/u $^{40}Ar$, 8.5 MeV/u $^{84}Kr$ and 8.5 MeV/u $^{136}Xe$ on $^{nat}W$ Targets*, Radiochimica Acta 33 (1983) 1.

contribution: preparation and participation in measurements, preparation of computer programs, data analysis, writing publication, 70%

J10. **I.Zychor**, K.Rykaczewski, W.Kurcewicz, H.Ahrens, H.Folger, N.Kaffrell, N.Trautmann, *Hafnium and Lutetium Isotopes Produced in Heavy-Ion Collisions of 7.6 MeV/u $^{40}Ar$, 8.5 MeV/u $^{84}Kr$ and 8.5 MeV/u $^{136}Xe$ on Tungsten Targets*, Nucl. Phys. A414 (1984) 301.

contribution: preparation and participation in measurements, preparation of computer programs, data analysis, performing theoretical calculations, result interpretation, writing publication, 70%

J11. T.Batsch, J.Blachot, Q.Chen, J.Crancon, M.Fatyga, A.Gizon, J.Jastrzebski, H.Karwowski, W.Kurcewicz, A.Lleres, T.Mroz, L.Pienkowski, P.P.Singh, S.E.Vigdor, **I.Zychor**, *Target Mass Dependence of the Average Linear Momentum Transfer*, Phys. Lett. B189 (1987) 287.

contribution: participation in measurements, data analysis, preparation of publication, 7%

J12. S.Hofmann, P.Armbruster, G.Münzenberg, W.Reisdorf, K.H.Schmidt, H.G.Burkhard, F.P.Hessberger, H.J.Schött, Y.K.Agarwal, G.Berthes, U.Gollerthan, H.Folger, R.Hingmann, J.G.Keller, M.E.Leino, P.Lemmertz, M.Montoya, K.Poppensieker, A.B.Quint, **I.Zychor**, *The Influence of the Surprising Decay Properties of Element 108 on Search Experiments for New Elements*, Nucl. Phys. A447 (1985) 335c.

contribution: participation in experiments, data analysis, 10%

J13. G.Münzenberg, P.Armbruster, G.Berthes, H.Folger, F.P.Hessberger, S.Hofmann, K.Poppensieker, W.Reisdorf, A.B.Quint, K.H.Schmidt, H.J.Schött, K.Sümmerer, **I.Zychor**, M.E.Leino, U.Gollerthan, E.Hanelt, *Evidence for* $^{264}108$, *the Heaviest Known Even-Even Isotope*, Z. Phys. A324 (1986) 489.
contribution: participation in experiments, data analysis, 15%

J14. G.Münzenberg, P.Armbruster, G.Berthes, H.Folger, F.P.Hessberger, S.Hofmann, J.Keller, K.Poppensieker, A.B.Quint, W.Reisdorf, K.H.Schmidt, H.J.Schött, K.Sümmerer, **I.Zychor**, M.E.Leino, R.Hingmann, U.Gollerthan, E.Hanelt, *Observation of the Isotopes* $^{264}108$ *and* $^{265}108$, Z. Phys. A328 (1987) 49.
contribution: participation in experiments, data analysis, 15%

J15. G.Münzenberg, P.Armbruster, S.Hofmann, F.P.Hessberger, H.Folger, J.G.Keller, V.Ninov, K.Poppensieker, A.B.Quint, W.Reisdorf, K.H.Schmidt, J.R.H.Schneider, H.J.Schött, K.Sümmerer, **I.Zychor**, M.E.Leino, D.Ackermann, U.Gollerthan, E.Hanelt, W.Morawek, D.Vermeulen, Y.Fujita, T.Schwab, *Element 107*, Z. Phys. A333 (1989) 163.
contribution: participation in experiments, data analysis, 12%

J16. S.Hofmann, P.Armbruster, G.Berthes, T.Faestermann, A.Gillitzer, F.P.Hessberger, W.Kurcewicz, G.Münzenberg, K.Poppensieker, H.J.Schött, **I.Zychor**, *The New Nuclei* $^{162}Os$ *and* $^{156}Ta$ *and the N=84 Alpha-Emitting Isomers*, Z. Phys. A333 (1989) 107.
contribution: preparation and participation in experiments, data analysis, 10%

J17. S.Hofmann, **I.Zychor**, F.P.Hessberger, G.Münzenberg, *Identification of a 3.2 µs Isomer in* $^{76}Rb$, Z. Phys. A325 (1986) 37.
contribution: preparation of computer codes, data analysis, interpretation of obtained results based on the Nilsson model, discussion of results, writing publication, 80%

J18. **I.Zychor**, *Computer simulation of beam formation in therapeutic accelerators*, Nukleonika 41(2) (1996) 5.
contribution: preparation of Monte Carlo code based on Geant3, performing simulations, writing publication

J19. Z.Rudy, W.Borgs, W.Cassing, T.Hermes, L.Jarczyk, B.Kamys, H.R.Koch, P.Kulessa, R.Maier, H.Ohm, D.Prasuhn, K.Pysz, O.W.B.Schult, A.Strzalkowski, Y.Uozumi, **I.Zychor**, *Study of the* $U(p,K^+)$ *reaction at* $T_p$=1.0 *GeV and 1.5 GeV*, Acta Phys. Pol. B27 (1996) 3061.
contribution: preparation and participation in experiments, preparation of computer programs, data analysis, discussion of results, writing publication, 10%

J20. K.Pysz, W.Borgs, W.Cassing, T.Hermes, L.Jarczyk, B.Kamys, S.Kistryn, H.R.Koch, P.Kulessa, R.Maier, H.Ohm, D.Prasuhn, Z.Rudy, O.W.B.Schult, H.J.Stein, A.Strzalkowski, Y.Uozumi, **I.Zychor**, *The production cross-section of heavy* Λ-*hypernuclei*, Societa Italiana di Fisica, Conf. Proc. 59 (1997) 354.
contribution: preparation and participation in experiments, preparation of computer programs, data analysis, discussion of results, writing publication, 10%

J21. H.Ohm, T.Hermes, W.Borgs, H.R.Koch, R.Maier, D.Prasuhn, H.J.Stein, O.W.B.Schult, K.Pysz, Z.Rudy, L.Jarczyk, B.Kamys, P.Kulessa, A.Strzalkowski, W.Cassing, Y.Uozumi, **I.Zychor**, Λ-*hyperon lifetime in very heavy hypernuclei*

*produced in the p+U interaction*, Phys. Rev. C55 (1997) 3062.
contribution: preparation and participation in experiments, preparation of computer programs, data analysis, discussion of results, writing publication, 10%

J22. T.Hermes, K.Pysz, Z.Rudy, W.Borgs, W.Cassing, L.Jarczyk, B.Kamys, H.R.Koch, P.Kulessa, R.Maier, H.Ohm, D.Prasuhn, O.W.B.Schult, H.J.Stein, A.Strzalkowski, Y.Uozumi, **I.Zychor**, *Search for heavy hypernuclei produced in the $^{238}U(p,K)_\Lambda A+X$ reaction at COSY-Jülich*, Nucl. Phys. A626 (1997) 279c.
contribution: preparation and participation in experiments, preparation of computer programs, data analysis, discussion of results, writing publication, 10%

J23. H.Ohm, W.Borgs, W.Cassing, M.Hartmann, T.Hermes, L.Jarczyk, B.Kamys, H.R.Koch, P.Kulessa, R.Maier, D.Prasuhn, K.Pysz, Z.Rudy, H.J.Stein, A.Strzalkowski, O.W.B.Schult, Y.Uozumi, **I.Zychor**, *Investigation of production and fission decay of heavy hypernuclei at COSY-Jülich*, Nucl. Phys. A629 (1998) 416c.
contribution: preparation and participation in experiments, preparation of computer programs, data analysis, discussion of results, writing publication, 10%

J24. P.Kulessa, Z.Rudy, M.Hartmann, K.Pysz, B.Kamys, H.Ohm, L.Jarczyk, A.Strzalkowski, W.Borgs, H.R.Koch, R.Maier, D.Prasuhn, O.W.B.Schult, **I.Zychor**, W.Cassing, H.Hodde, M.Matoba, *Production of heavy hypernuclei in the p + Bi reaction and determination of their lifetime for fission induced by $\Lambda$ decay*, Phys. Lett. B427 (1998) 403.
contribution: preparation and participation in experiments, preparation of computer programs, data analysis, discussion of results, writing publication, 10%

J25. W.Borgs, W.Cassing, M.Hartmann, H.Hodde, L.Jarczyk, B.Kamys, H.R.Koch, P.Kulessa, R.Maier, M.Matoba, H.Ohm, D.Prasuhn, K.Pysz, Z.Rudy, O.W.B.Schult, A.Strzalkowski, **I.Zychor**, *K-$\Lambda$ production in p+Bi interaction*, Acta Phys. Pol. B29 (1998) 3169.
contribution: preparation and participation in experiments, preparation of computer programs, data analysis, discussion of results, writing publication, 10%

J26. P.Kulessa, K.Pysz, **I.Zychor**, Z.Rudy, H.Ohm, B.Kamys, M.Hartmann, W.Cassing, H.R.Koch, A.Strzalkowski, H.Hodde, W.Borgs, R.Maier, D.Prasuhn, M.Matoba, O.W.B.Schult, *Measurement of the lifetime of heavy hypernuclei produced in the bombardment of Bi with protons*, Nucl. Phys. A639 (1998) 283c, Erratum-ibid. A645 (1999) 606.
contribution: preparation and participation in experiments, preparation of computer programs, data analysis, discussion of results, writing publication, 10%

J27. K.Pysz, **I.Zychor**, T.Hermes, M.Hartmann, H.Ohm, P.Kulessa, W.Borgs, H.R.Koch, R.Maier, D.Prasuhn Z.Rudy, B.Kamys, W.Cassing, J.Pfeiffer, Y.Uozumi, L.Jarczyk, A.Strzalkowski, O.W.B.Schult, *Measurement of the lifetime of heavy $\Lambda$ hypernuclei with the recoil shadow method and internal targets in the storage ring COSY- Jülich*, Nucl. Instrum. Meth. A420 (1999) 356.
contribution: preparation and participation in experiments, preparation of computer programs, data analysis, discussion of results, writing publication, 10%

J28. H.Ohm, W.Borgs, W.Cassing, M.Hartmann, L.Jarczyk, B.Kamys, H.R.Koch, P.Kulessa, H.J.Maier, R.Maier, M.Matoba, D.Prasuhn, K.Pysz, Z.Rudy,

O.W.B.Schult, H.Ströher, A.Strzalkowski, Y.Uozumi, **I.Zychor**, *Determination of the lifetime of heavy $\Lambda$ hypernuclei at COSY-Jülich*, AIP Conf. Proc. 512 (2000) 157. contribution: preparation and participation in experiments, preparation of computer programs, data analysis, discussion of results, writing publication, 10%

J29. **I.Zychor**, W.Borgs, W.Cassing, M.Hartmann, L.Jarczyk, B.Kamys, H.R.Koch, P.Kulessa, R.Maier, M.Matoba, H.Ohm, D.Prasuhn, K.Pysz, Z.Rudy, O.W.B.Schult, H.J.Stein, H.Ströher, A.Strzalkowski, Y.Uozumi, *Measurements of the $\Lambda$ hyperon lifetime in heavy hypernuclei at COSY-Jülich*, Acta Phys. Pol. B31 (2000) 405. contribution: preparation and participation in experiments, preparation of computer programs, data analysis, discussion of results, writing publication, 10%

J30. W.H.Bertl, F.Rosenbaum, N.M.Ryskulov, R.Engfer, E.A.Hermes, G.Kurz, A.van der Schaaf, T.Kozlowski, **I.Zychor**, J.Kuth, G.Otter, P.Wintz, *A Search for $\mu$-e Conversion in Muonic Gold*, Eur. Phys. J. C47 (2006) 337. contribution: participation in measurements, data analysis, performing simulations, preparation of publication, 8%

J31. C.Adolph, ..., **I.Zychor** (<u>139 authors</u>), *Measurement of the $\eta \rightarrow 3\pi^0$ Dalitz plot distribution with the WASA detector at COSY*, Phys. Lett. B677 (2009) 24. contribution: participation in measurements, 1%

### 4.2.2   Other publications not indexed in the JCR base

O1. O.W.B.Schult, ..., **I.Zychor** (247 authors), *The physics research program at COSY-Jülich*, Proc. 14th RCNP Osaka International Symposium on Nuclear Reaction Dynamics of Nucleon - Hadron Many Body System: From Nucleon Spins and Meson in Nuclei to Quark Lepton (1995), ed. by H.Ejiri, T.Noro, K.Takahisa and H.Toki (World Scientific Publishing Co., 1996), p.460.

O2. **I.Zychor**, *Studies of the $\Lambda$(1405)  in Proton-Proton Collisions with ANKE at COSY-Jülich*, Proc. of the 11th International Conference on Meson-Nucleon Physics and Structure of the Nucleon; MENU 2007, 10-14 September, FZJ, Jülich (2007) SLAC eConf C070910 (2007) 310.

O3. **I.Zychor**, *Deeply Bound $K^-pp$ States*, IPJ Annual Report 2009, p.115, ISSN 1232-5309 (2010); more details in *Bound kaonic nuclear states with ANKE@COSY*, IKP Annual Report 2008, Jul-4282, p.8 (2009).

O4. T.Batsch, J.Blachot, Q.Chen, J.Crancon, M.Fatyga, A.Gizon, J.Jastrzebski, W.Kurcewicz, L.Pienkowski, P.P.Singh, T.Ward, **I.Zychor**, *Linear momentum and energy deposition deduced from the investigation of the radioactive reaction products*, Proc. 4th International Conference on Nuclear Reaction Mechanisms, Varenna, Italy, ed. E. Gadioli, Ricerca Scientifica ed Educazione Permanente, Suppl. N. 46 (1985) p.87.

O5. S.Hofmann, P.Armbruster, G.Berthes, H.Folger, U.Gollerthan, E.Hanelt, F.P.Hessberger, M.E.Leino, G.Münzenberg, K.Poppensieker, B.Quint, W.Reisdorf, K.H.Schmidt, H.J.Schött, K.Sümmerer, **I.Zychor**, *Heavy Elements - Experiments on Synthesis and Decay*, Proc. International Symposium on Weak and Electromagnetic Interactions in Nuclei, Heidelberg, Germany (1986), ed. by H.V.Klapdor, Springer-Verlag Berlin (1986) p.179.

O6. G.Münzenberg, F.P.Hessberger, P.Armbruster, S.Hofmann, K.H.Schmidt, G.Berthes,

H.Folger, H.Geissel, J.G.Keller, P.Lemmertz, M.Montoya, K.Poppensieker, B.Quint, H.J.Schött, **I.Zychor**, M.E.Leino, U.Gollerthan, *Attempt to synthesize element 110 by fusion of* $^{64}Ni + ^{208}Pb$, GSI Scientific Report 1985 (1986) p.29; G.Münzenberg, P.Armbruster, G.Berthes, H.Folger, F.P.Hessberger, S.Hofmann, K.Poppensieker, B.Quint, W.Reisdorf, K.H.Schmidt, H.J.Schött, K.Sümmerer, **I.Zychor**, M.E.Leino, U.Gollerthan, E.Hanelt, *An attempt to synthesize element 110 in the reaction* $^{40}Ar + ^{235}U$, GSI Scientific Report 1986 (1987) p.14.

O7. S.Hofmann, P.Armbruster, F.P.Hessberger, G.Münzenberg, H.J.Schött, **I.Zychor**, *Experiments for the Investigation of Proton Radioactivity*, Proc. International School-Seminar on Heavy Ion Physics, Dubna, USSR, 1986, ed. by Yu.P.Gangrsky, Dubna D7-87-68 (1987) p.378.

O8. **I.Zychor**, S.Hofmann, F.P.Hessberger, G.Münzenberg, *The New 15 μs Isomer in* $^{142}Tb$, GSI Annual Report 1988 GSI 89-1 (1989) p.31.

O9. **I.Zychor**, *Computer simulation of* $e^-$ *and X beam transport and formation for therapy*, Report 3/ZDAJ/90, Świerk (1989), in Polish.

O10. **I.Zychor**, *Collimation and formation of e- and X beams for use in radiotherapy methodology and computer codes*, Report 18/P-X/91, Świerk (1991), in Polish.

O11. **I.Zychor**, *The application of Monte Carlo Method to Electron and Photon Beams Transport*, SINS Report 3/X, ISSN 1232-5309, Świerk (1994), in Polish.

O12. **I.Zychor**, *Electron to bremsstrahlung conversion - physics and calculations*, Report O-32/ZDAJ/88, Świerk (1988), in Polish.

O13. **I.Zychor**, *Beam parameters at internal target positions for experiments in COSY-Jülich*, SINS Report 15/X, ISSN 1232-5309, Świerk (1996).

O14. L.Jarczyk, O.W.B.Schult, K.Pysz, W.Borgs, W.Cassing, T.Hermes, B.Kamys, S.Kistryn, H.R.Koch, P.Kulessa, R.Maier, H.Ohm, D.Prasuhn, Z.Rudy, A.Strzalkowski, Y.Uozumi, B.Zipper, **I.Zychor**, *Lifetime of* $\Lambda$ *Hyperons in Heavy Nuclei*, Proc. 8th International Conference on Nuclear Reaction Mechanisms, Varenna, Italy, ed. by E.Gadioli, Ricera Scientifica ed Educazione Permanente, Suppl. N. 111 (1997) p.152.

O15. O.W.B.Schult, K.Pysz, S.Kistryn, W.Borgs, W.Cassing, T.Hermes, L.Jarczyk, B.Kamys, H.R.Koch, P.Kulessa, R.Maier, H.Ohm, D.Prasuhn, Z.Rudy, A.Strzalkowski, Y.Uozumi, **I.Zychor**, *The lifetime of hyperactinides*, Proc. XXXV International Winter Meeting on Nuclear Physics, Bormio, Italy, ed. by I. Iori, Ricerca Scientifica ed Educazione Permanente, Suppl. N. 110 (1997) p.90.

O16. **I.Zychor**, K.Pysz, P.Kulessa, T.Hermes, Z.Rudy, W.Cassing, M.Hartmann, H.Ohm, S.Kistryn, W.Borgs, B.Kamys, H.R.Koch, R.Maier, D.Prasuhn, J.Pfeiffer, Y.Uozumi, L.Jarczyk, A.Strzalkowski, M.Matoba, H.Ströher, O.W.B.Schult, *Lifetime Measurements of Hypernuclei at COSY*, Proc. International Symposium on Nuclear Electro-Weak Spectroscopy for Symmetries in Electro-Weak Nuclear-Processes NEWS 99, World Scientific Publishing Co. Pte. Ltd. (2002) p.207.

O17. W.H.Bertl, F.Rosenbaum, N.M.Ryskulov, R.Engfer, E.A.Hermes, G.Kurz, A.van der Schaaf, P.Wintz, J.Kuth, G.Otter, T.Kozlowski, **I.Zychor**, *Search for muon-electron conversion on gold*, Proc. International Europhysics Conference on High-Energy Physics (HEP 2001), Budapest, Hungary, PoS(hep2001)155.

O18. H.-H.Adam, ..., **I.Zychor** (138 authors), COSY proposal No. 136 *WASA at COSY*,

nucl-ex/0411038.

O19. W.Borgs, W.Cassing, M.Hartmann, L.Jarczyk, B.Kamys, H.R.Koch, P.Kulessa, R.Maier, M.Matoba, H.Ohm, D.Prasuhn, K.Pysz, Z.Rudy, H.J.Stein, H.Ströher, A.Strzakowski, Y.Uozumi, **I.Zychor**, COSY proposal No. 44 for the COSY-13 Collaboration *Determination of the $\Lambda$ Lifetime in Hypernuclei Produced in p+Au and p+U Reactions* (1998-2000).

O20. M.Büscher, H.Junghans, V.Kleber, R.Koch, R.Schleichert, K.Sistemich, H.Ströher, V.P.Chernyshev, P.Fedorets, L.A.Kondratyuk, Ye.S.Golubeva, V.Grishina, V.Koptev, S.Mikirtychiants, A.Khoukaz, A.Kacharava, G.Macharashvili, B.Chiladze, M.Nioradze, **I.Zychor**, COSY proposal No. 55 for the ANKE Collaboration *Study of $a_0^+(980)$ Mesons at ANKE* (2000-2001).

O21. M.Büscher, M.Hartmann, V.Kleber, R.Koch, R.Schleichert, H.Ströher, V.P.Chernyshev, P.Fedorets, L.A.Kondratyuk, Ye.S.Golubeva, V.Grishina, V.Koptev, S.Mikirtychiants, M.Nekipelov, A.Khoukaz, N.Lang, S.Dymov, V.Komarov, G.Macharashvili, **I.Zychor**, E.L.Bratkovskaya, W.Cassing, COSY proposal No. 97 for the ANKE Collaboration *Investigation of Neutral Scalar Mesons $a_0/f_0$ with ANKE* (2001-2003).

O22. V.Koptev, S.Mikirtychiants, M.Nekipelov, M.Büscher, M.Hartmann, V.Hejny, H.Ohm, R.Schleichert, A.Sibirtsev, H.J.Stein, H.Ströher, Z.Rudy, **I.Zychor**, S.Dymov, V.Komarov, G.Macharashvili, S.Merzliakov, B.Zalykhanov, COSY proposal No. 112 for the ANKE Collaboration *Investigation of Subthreshold $K^+$-Production Processes by Measuring $K^+p$ and $K^+d$ Correlations* (2002).

O23. A.Kacharava, F.Rathmann, C.Wilkin, S.Barsov, ..., **I.Zychor** (83 authors), COSY proposal No. 152 *Spin physics from COSY to FAIR*, nucl-ex/0511028.

O24. Report of Polish Nuclear Physics Network "Nuclear Physics in Poland 1996-2006", **I.Zychor**, P. Kulessa, K. Pysz, *Hyperon resonances produced in proton-proton collisions*; L.Jarczyk, B.Kamys, P.Kulessa, K.Pysz, Z.Rudy, A.Strzalkowski, **I.Zychor**, *Nonmesonic decay of $\Lambda$ hyperon in heavy hypernuclei*, ed. by Heavy Ion Laboratory, Warsaw University (2007) ISBN 978-83-926674-0-7.

O25. **I.Zychor**, *Monte Carlo Simulations for DNA-size Nanostructures*, NCBJ Annual Report 2011, p.196, ISSN 1232-5309 (2012).

O26. **I.Zychor** et al., *Monte Carlo Simulations of Gamma-ray Interactions with Scintillators*; P.Sibczyski, ..., **I.Zychor**, *Characterization of $CeBr_3$ Scintillator in Gamma Spectrometry*, NCBJ Annual Report 2012 (2013).

### 4.3 Bibliometric data, June 2013

1. Total impact factor
   (according to the Journal Citation Report(JCR) list)      77

2. Total number of cited references (according to Web of Science)      687
   therein without self-citations      641

3. Hirsch index (according to Web of Science)      15

# 5 Other professional activities

## 5.1 Participation in research projects

1991-1994: Investigator in the grant 2293/2/91 supported by the State Committee for Scientific Research *800 keV, 0.4 ÷ 1 MW accelerator prototype for $SO_2$ and $NO_x$ removal from flue gases*

1993-1997: Participant in the EU TEMPUS Joint European Programme (JEP 4329-PL)

2000-2001: Group leader in the EU project LIFE-COSY supported under the 5th Framework Programme ,,Access to Research Infrastructures", project title: *Measurement of the $a_0(980)$ Meson Production*

2001-2003: Project leader from Polish side in the bilateral project POL 01/015 *Study of mesons at ANKE* supported by the State Committee for Scientific Research (Poland) and Federal Ministry of Education and Research (Germany)

2004-2008: The only investigator in projects financed by the Forschungszentrum Jülich (Germany) under the COSY-FFE programme (COSY-78, Contract No. 41553602)
   1. *Strange Baryon Production at ANKE* (2004-2007)
   2. *Excited Hyperon Production at ANKE and WASA* (2007-2008)

2010-2011: Investigator in the project *Computing Centre in Świerk: infrastructure and services for power industry* (POIG.02.03.00-00-013/09)

since 2012: Group leader in the ,,EURATOM fussion" project (FU07-CT-2007-00061): *Development of the selected diagnostic techniques (Cerenkov detectors, solid-state nuclear track detectors, scintillation detectors for hard X-ray diagnostics)*, task title: *Monte Carlo simulations of gamma-ray interactions with scintillators*

## 5.2 Awards

2005 the yearly internal award of the Director of the Andrzej Sołtan Institute for Nuclear Studies in the basic research category was won by my work on the evidence for the excited hyperon $Y^{0*}(1480)$

## 5.3   Participation in conferences and workshops

P1. **I.Zychor**, *Theory and practice of electron beam to X-ray converters* (oral), IAEA/ICGFI Workshop on Use of Electron Accelerators for Food Irradiation, Warsaw, Poland (1991)

P2. **I.Zychor**, *Computer codes of accelerator physics and Monte Carlo simulation of accelerated particle transport and interaction with matter* (oral), TEMPUS Workshop on accelerator applications, Warsaw, Poland (1993)

P3. **I.Zychor**, *Monte Carlo simulation of absorbed dose distribution for application in radiotherapy of cancer* (oral), TEMPUS Workshop on accelerator applications in medicine, 1993, Uppsala, Sweden (1993)

P4. **I.Zychor**, *Applications of the Monte Carlo Code for Radiation Transport Simulation for Use in Radiotherapy* (poster), 4th European Particle Accelerator Conference, London, UK (1994)

P5. **I.Zychor**, *Computer simulation of beam formation in therapeutic accelerators* (poster), 10th Congress of the Polish Society of Medical Physics, Cracow, Poland (1995)

P6. S.Kulinski, W.Maciszewski, M.Pachan, E.Plawski, **I.Zychor**, *Computer simulation of $e^-$ / X converter for high power electron accelerator dedicated to irradiation technology* (poster), 5th European Conference on Accelerators in Applied Research and Technology, Eindhoven, The Netherlands (1997)

P7. **I.Zychor**, R.Maier, S.Martin, D.Prasuhn, O.W.B.Schult, *Beam Parameters at the Internal Target Positions for Experiments in COSY-Jülich* (poster), European Particle Accelerator Conference, Sitges, Spain (1996)

P8. **I.Zychor**, *Investigations of Heavy Hypernuclei at COSY* (oral), Workshop on Perspectives of Strangeness and Hypernuclear Physics, Darmstadt, Germany (1998)

P9. **I.Zychor** for the COSY-13 Collaboration, *Measurements of the $\Lambda$ hyperon lifetime in heavy hypernuclei at COSY-Jülich* (poster), XXVI Mazurian Lakes School of Physics, Krzyże, Poland (1999)

P10. **I.Zychor**, *Proton Induced Reactions at Internal Targets at COSY-Jülich* (oral), XXVI Mazurian Lakes School of Physics, Krzyże, Poland (1999)

P11. **I.Zychor**, *Monte Carlo simulations for ANKE experiments* (poster), XXVII Mazurian Lakes School, Krzyże, Poland (2001)

P12. V.Koptev, P.Kravchenko, M.Nekipelov, **I.Zychor**, *Strange Baryon Production at ANKE* (oral), Hadron Physics at COSY, Bad Honnef, Germany (2003)

P13. V.Koptev, P.Kravchenko, M.Nekipelov, **I.Zychor**, *Heavy hyperons: ANKE data* (oral), 5th ANKE Workshop on Strangeness Production on Nucleons and Nuclei, Krzyże, Poland (2003)

P14. **I.Zychor**, *Heavy Hyperon Production at ANKE* (oral), 6th ANKE Workshop on Strangeness Production on Nucleons and Nuclei, Gatchina, Russia (2004)

P15. **I.Zychor**, *Evidence for a new $Y^{0*}$ hyperon in pp collisions at ANKE* (oral), Caucasian-German School and Workshop on Hadron Physics, Tbilisi, Georgia (2004)

P16. **I.Zychor**, *Evidence for an excited hyperon state in pp collisions with ANKE at COSY-Jülich* (oral), 10th International Conference on the Structure of Baryons, Palaiseau, France (2004)

P17. **I.Zychor**, *Hyperon production in pp collisions with ANKE at COSY* (oral), Cracow

Epiphany Conference on Hadron Spectroscopy, Cracow, Poland (2005)

P18. **I.Zychor**, *Observation of an excited hyperon state in pp collisions with ANKE at COSY Jülich* (oral), DPG-Spring Meeting, Berlin, Germany (2005)

P19. **I.Zychor**, *Hyperon Production in pp collisions at ANKE* (oral), COSY-FFE Workshop, Jülich, Germany (2005)

P20. **I.Zychor**, *Hyperon production at ANKE* (oral), 2nd Caucasian-German School/Workshop on Hadron Physics, Tbilisi, Georgia (2006)

P21. **I.Zychor**, *Studies of Λ(1405) from ANKE to WASA* (oral), WASA Collaboration Meeting, Jülich, Germany (2007)

P22. **I.Zychor**, *Hyperon production in hadronic collisions with ANKE@COSY* (oral), DPG-Spring Meeting, Giessen, Germany (2007)

P23. **I.Zychor**, *Studies of Λ(1405) in pp Collisions with ANKE at COSY-Jülich* (oral), 11th International Conference on Meson-Nucleon Physics and the Structure of the Nucleon, Jülich, Germany (2007)

P24. **I.Zychor**, *Λ(1405) produced in pp collisions with ANKE* (oral), COSY-FFE Workshop, Bad Honnef, Germany (2007)

P25. **I.Zychor**, *Excited hyperons produced in pp collisions with ANKE at COSY* (oral), 7th International Conference on Nuclear Physics at Storage Rings, Lanzhou, China (2008)

P26. **I.Zychor**, *Hyperon production* (oral), ANKE Physics Workshop, Jülich, Germany (2009)

P27. **I.Zychor**, *Świerk Computing Centre* (oral), Workshop on Essential Safety Assessment Knowledge, Trieste, Italy (2010)

P28. K.Gomulski, J.Malesa, R.Możdżonek, K.Różycki, K.Samul, **I.Zychor**, *Safety of Nuclear Power Plants* (poster), Conference *Polish science and technology for nuclear power plants in Poland*, Mądralin, Polska (2011)

P29. **I.Zychor**, A.Bantsar, B.Grosswendt, S.Pszona, *Monte Carlo Simulations for Nanodosimetry* (poster), 1st Nano-IBCT Conference, Caen, France (2011)

## 5.4   Selected seminars

1. *Monte Carlo Calculations of Electron Pencil Beams*, Cyfronet, Świerk, Poland (1992)
2. *Applications of the Monte Carlo Code for Radiation Transport Simulation for Use in Radiotherapy*, Institute for Nuclear Physics, Jülich, Germany (1994)
3. *Physical Parameters at the Internal Target Positions in the COSY ring*, Institute for Nuclear Physics, Jülich, Germany (1995)
4. *Characteristics of the COSY Beam for ANKE Experiments*, Institute for Nuclear Physics, Jülich, Germany (1995)
5. *The application of Monte Carlo method to electron and photon beam transport*, Institute for Nuclear Chemistry and Technology, Warsaw, Poland (1997)
6. *Network at Accelerator Physics of SINS*, Free University, Amsterdam, The Netherlands (1997)
7. *COSY-13: Latest Analysis*, Institute for Nuclear Physics Jülich, Germany (1998)
8. *Particle production at near threshold energies*, Warsaw University of Technology, Warsaw, Poland (2000)

9. *Momentum reconstruction of particles in side and forward detectors in ANKE*, Institute for Nuclear Physics, Jülich, Germany (2002)
10. *Observation of an excited hyperon state in pp $\rightarrow$ pK$^+$Y$^{0*}$*, COSY Programme Advisory Committee Meeting, Jülich, Germany (2004)
11. *Observation of the excited neutral resonance in the pp $\rightarrow$ pK$^+$Y$^{0*}$ reaction*, The Andrzej Sołtan Institute for Nuclear Studies, Świerk, Poland (2005)
12. *Excited hyperon production in pp reactions with the ANKE detector: programme summary*, The Andrzej Sołtan Institute for Nuclear Studies, Świerk, Poland (2007)
13. *Some conclusions and remarks after the Trieste Workshop*, The Andrzej Sołtan Institute for Nuclear Studies, Świerk, Poland (2010)

## 5.5  Organizational activities

1. Organisation of international workshops
    1. TEMPUS Workshop on Accelerator Applications, Świerk, Poland (1993), co-organizer
    2. 3rd ANKE Workshop on Scalar Meson Production at ANKE/COSY, Świerk, Poland (2002), organizer
    3. 5th ANKE Workshop on Strangeness Production on Nucleons and Nuclei, Krzyże, Poland (2003), organizer
2. Co-editor of proceedings
    1. 3rd ANKE Workshop on Scalar Meson Production at ANKE/COSY, Berichte des Forschungszentrums Jülich. Jül-4000, ISSN 0944-2952
    2. 5th ANKE Workshop on Strangeness Production on Nucleons and Nuclei, Berichte des Forschungszentrums Jülich, Jül-4109, ISSN 0944-2952

## 5.6  Visits to foreign institutes

| | |
|---|---|
| 1979 | Joint Institute for Nuclear Research, Dubna, USSR (3 weeks) |
| 1980 | Centre for Heavy Ion Research (GSI), Darmstadt, Germany (10 days) |
| 1981 | Centre for Heavy Ion Research (GSI), Darmstadt, Germany (1 month) |
| 1984 | Institut des Sciences Nucléaires, Grenoble, France (1 month) |
| 1985-1987 | Centre for Heavy Ion Research (GSI), Darmstadt, Germany (scientific position for 2 years) |
| 1987 | Centre for Heavy Ion Research (GSI), Darmstadt, Germany (3 weeks) |
| 1998 | Kernfysisch Versneller Instituut (KVI), Groningen, The Netherlands (1 week) |
| 2000-2001 | Paul Scherer Institute (PSI), Villigen, Switzerland (scientific position for 5 months) |
| 1994-2009 | Institute for Nuclear Physics (IKP), Jülich, Germany, in total ∼6.5 years |

# 6 Copies of publications for the habilitation qualification

# Identification of $K^+$-mesons from subthreshold pA collisions with ANKE at COSY-Jülich

M. Büscher[a],*, H. Junghans[a], V. Koptev[b], M. Nekipelov[a,b], K. Sistemich[a],
H. Ströher[a], S. Barsov[b], G. Borchert[a], W. Borgs[a], M. Debowski[c], W. Erven[d],
R. Esser[e,1], P. Fedorets[f], D. Gotta[a], M. Hartmann[a], V. Hejny[a], A. Kacharava[g,h],
H.R. Koch[a], V. Komarov[g], P. Kulessa[a,i], A. Kulikov[g], G. Macharashvili[g,h],
S. Merzliakov[g], S. Mikirtychiants[b], H. Müller[c], A. Mussgiller[a], R. Nellen[a],
M. Nioradze[h], H. Ohm[a], A. Petrus[g], F. Rathmann[a], Z. Rudy[j], R. Schleichert[a],
Chr. Schneider[c], O.W.B. Schult[a], H.J. Stein[a], I. Zychor[k]

[a] Institut für Kernphysik, Forschungszentrum Jülich, 52425 Jülich, Germany
[b] High Energy Physics Department, Petersburg Nuclear Physics Institute, 188350 Gatchina, Russia
[c] Institut für Kern- und Hadronenphysik, Forschungszentrum Rossendorf, D-01474 Dresden, Germany
[d] Zentralinstitut für Elektronik, Forschungszentrum Jülich, 52425 Jülich, Germany
[e] Institut für Kernphysik, Universität zu Köln, Zülpicher Str. 77, 50937 Köln, Germany
[f] Institute for Theoretical and Experimental Physics, Cheremushkinskaya 25, 117259 Moscow, Russia
[g] Laboratory of Nuclear Problems, Joint Institute for Nuclear Research, 141980 Dubna, Russia
[h] High Energy Physics Institute, Tbilisi State University, University Street 9, 380086 Tbilisi, Georgia
[i] The Henryk Niewodniczanski Institute of Nuclear Physics, Radzikowskiego 152, PL-31342, Cracow, Poland
[j] Institute of Physics, Jagellonian University, Reymonta 4,30059 Cracow, Poland
[k] The Andrzej Soltan Institute for Nuclear Studies, 05400 Swierk, Poland

## Abstract

The spectrometer ANKE has been put into operation at the accelerator COSY of the Forschungszentrum Jülich in spring 1998. An initial scientific goal is to study $K^+$-production in pA collisions at subthreshold energies far below the free NN-threshold at $T_p = 1.58$ GeV. This requires the identification of $K^+$-mesons in a background of pions and protons, about $10^6$ times more intense. In this paper the sophisticated detection system and the software procedures for kaon identification are described. With the help of TOF, energy-loss and range measurements as well as the track information from wire chambers, it is possible to measure $d^2\sigma/d\Omega\,dp$ for deep subthreshold $K^+$ production at beam energies down to $T_p = 1.0$ GeV. © 2002 Elsevier Science B.V. All rights reserved.

*Corresponding author.
E-mail address: m.buescher@fz-juelich.de (M. Büscher).
[1] Now working at: Saint-Gobain Crystals & Detectors GmbH, 42929 Wermelskirchen, Germany.

## 1. Introduction

The production of $K^+$-mesons in proton–nucleus reactions at beam energies below the free nucleon–nucleon threshold ($T_p = 1.58\,\text{GeV}$), so-called subthreshold production presently is a topic of strong interest [1–4]. Since $K^+$-mesons have a long mean free path in the nuclear medium it is expected that valuable information about short-range correlations in nuclei can be extracted from these studies. Further research goals are insights into the reaction dynamics, different production mechanisms and the properties of the produced kaons inside the nuclear environment. In a recent theoretical paper [3] it has been pointed out that the existing data still do not allow to draw unambiguous conclusions about the above mentioned issues. Differential spectra are needed in a wide momentum range for different target nuclei and beam energies. This is particularly the case at beam energies below 1.2 GeV since so far only total cross-sections have been measured there [1].

The great challenge of kaon studies at beam energies far below the NN-threshold is the fact that the production cross sections are extremely small. Furthermore, the produced $K^+$-mesons have a short lifetime and, thus, a very compact detection system is mandatory, in particular at low kaon momenta. The magnetic spectrometer ANKE [5–10] and its detectors have been built and optimized for such measurements.

In order to get realistic estimates on the $K^+$ and background rates at ANKE, calculations were performed using the Rossendorf-Collision (ROC) model [11]. Fig. 1 shows the result of these model calculations for proton–carbon collisions. The production cross-sections shown in the figure are integrated over the angular range $\vartheta = 0$–$10°$—roughly corresponding to the angular acceptance of ANKE [6,10]. It can be seen that the background of protons and pions stays nearly constant whereas the kaon cross-section dramatically decreases as the energy approaches the absolute threshold ($T_p = 0.75\,\text{GeV}$ for carbon); at $T_p = 1.0\,\text{GeV}$, the lowest energy of our measurements up to now, the $K^+/\pi^+$ ratio is as small as $\sim 10^{-6}$. Note that the cross-sections presented in Fig. 1 are momentum integrated. Most of the
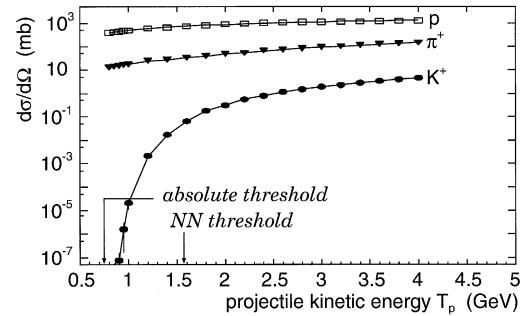


Fig. 1. Predicted momentum-integrated cross sections for the production of $K^+$ mesons and background particles in proton-carbon collisions into emission angles $\vartheta < 10°$. The calculations were made using the Rossendorf-Collision (ROC) model [11].

produced protons are above the momentum range measured at ANKE. Thus, in the spectra presented in Section 3.1, the number of pions and protons is approximately equal. However, high-momentum protons can hit structure material, e.g., the pole shoes of the spectrometer magnet and produce secondary particles. In fact, those turned out to be the most severe source of background, see Section 3.2.

The spectrometer ANKE has been described in detail in Ref. [9]. Therefore, in this paper only a brief overview of the setup and its detection systems for $K^+$-mesons is given. The procedures for data analysis are described and it is shown how momentum distributions of kaons from proton–nucleus collisions at beam energies as low as 1.0 GeV are obtained.

## 2. Description of the experimental setup

### 2.1. Principles of $K^+$-identification with ANKE

For the identification of $K^+$-mesons the following criteria are used at ANKE:

- ANKE provides a momentum focusing of the ejectiles (Section 2.2). This is used to define the $K^+$-momenta and serves as an important means to suppress the background of pions and protons in range telescopes (Section 2.3.2).

- A fast on-line trigger system based on start- and stop detectors of a time-of-flight setup allows the selection of particles with certain momenta and emission angles at the target. Narrow time-of-flight (TOF) gates can be defined for the identification of pions, kaons and protons, respectively (Section 2.3).

- Range telescopes in the focal surface of the spectrometer dipole discriminate pions, kaons and protons with the same momenta due to their different energy losses. Passive degraders in the telescopes between the scintillation counters enhance the discrimination efficiency (Sections 2.3.2 and 3.1).

- The $K^+$-mesons are stopped in the range telescopes. Their decay with a lifetime of $\tau = 12.4$ ns provides an effective criterion for the identification of these mesons via the detection of delayed signals (Sections 2.3.2 and 3.1).

- The tracks of the ejectiles are measured with multi-wire proportional chambers (MWPCs) (Section 2.3.1). From this information the emission angles at the target are deduced and a suppression of background not originating from the target is possible (Section 3.2).

## 2.2. The ANKE spectrometer

The ANKE spectrometer [7–10] is located at the internal target position TPA of the cooler synchrotron COSY-Jülich. It consists of three dipole magnets—two smaller ones (D1 and D3, see Fig. 2) to guide the circulating COSY beam and a C-shaped spectrometer magnet (D2) with a large gap height of 20 cm. Between D1 and D2, space for the installation of various internal targets is available. For the measurements described here, triangular-shaped foil targets made of carbon (polycrystalline diamond), copper and gold were suspended from frames [9]. The target dimensions typically are 2 mm (width at base glued to the frame), 20 mm (length) and 0.04–15 mg/cm$^2$ (thickness). D2 has an angular acceptance of $\Delta\Omega \approx 50$ msr for ejectiles emitted under forward angles $\vartheta \approx 0°$. Furthermore, the flight path of the ejectiles between target and the focal-surface detectors is short ($l \approx 150 \ldots 400$ cm) so that kaons
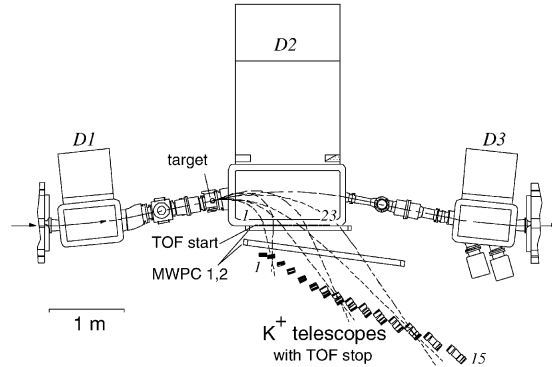


Fig. 2. Top view of the ANKE spectrometer and detectors used for $K^+$ identification. The dashed lines show trajectories of ejectiles with different momenta and horizontal emission angles of $\vartheta = \pm 10°$. The numbers indicate the positions of the 23 start counters and the 15 telescopes.

reach the detectors with a probability of $\sim 30\%$ in spite of their short lifetime.

Each of the range telescopes located at the focal-surface was optimized for a certain kaon-momentum range, see Section 2.3.2. Therefore, when changing the beam energy to measure the $K^+$-momentum spectra for different projectile energies, one must keep constant (i) the field in the ANKE magnets and (ii) the relative locations of target and D2 so that the momenta of the ejectiles hitting a certain telescope remain constant. Consequently, the radius of curvature and the deflection angle of the circulating COSY beam changes in all three dipoles with varying beam energy. This can be compensated by a movement of the spectrometer dipole D2 perpendicular to the direction of the undisturbed COSY beam [9]. For the measurements described in this paper, all three magnets were operated at a fixed field strength of $B = 1.30$ T (measurement of the $K^+$-production cross-sections) or at the maximum achievable field strength in D2 of $B = 1.57$ T (calibration measurements for the time-of-flight detectors). The lower field strength used for the cross-section measurements was chosen in order to avoid too large deflection angles of the COSY beam at low beam energies. The resulting deflection angles in D1, $\alpha = 10.1–5.5°$ at $T_p = 1.0 \ldots 2.3$ GeV, are in any case smaller than the maximum value of $10.6°$

permitted by the bellows of the vacuum system, see Ref. [9] for details.

Ray-tracing calculations [10] show that at $B = 1.30\,T$ the $K^+$ telescopes cover a momentum range of $p \approx 110$–$525\,MeV/c$. The horizontal angular acceptance of D2 for which the focusing properties are still sufficient to allow kaon identification in the telescopes is $\vartheta \approx -15°\ldots + 15°$, cf. Section 2.3. The vertical acceptance is given by the gap height of D2 and varies between $\phi \approx \pm 7°$ for the lowest momenta and $\pm 3.5°$ (highest). The heights of all detectors were chosen such that they cover the full vertical acceptance of the spectrometer dipole.

### 2.3. $K^+$-detection system

The schematic layout of the $K^+$-detection system at ANKE is sketched in Fig. 3. It is rigidly connected to the spectrometer dipole D2 and consists of three major components: (i) 23 TOF-start counters (*PILOT-U, Nuclear Enterprises*) close to the vacuum window (made of $500\,\mu m$ Al) at the right-hand side of D2. The counters are positioned as close as possible to the exit window in order to maximize the distance to the TOF-stop counters. Each start counter has a horizontal angular acceptance of $2°$–$6°$ depending on the ejectile momenta. All scintillators are $27\,cm$ high and $5\,cm$ wide. Their thickness has been chosen as a compromise between sufficient light output and little small-angle scattering. It increases from
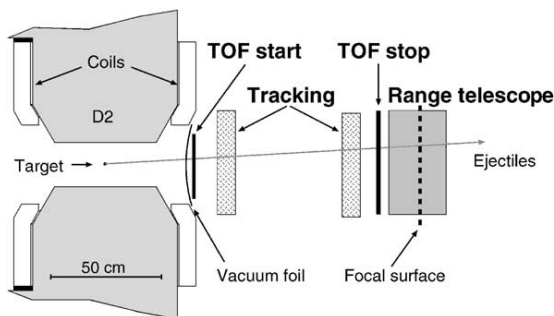


Fig. 3. Simplified layout of the detection system used for the subthreshold $K^+$-studies at ANKE (looking in the direction of the circulating COSY beam).

$0.5\,mm$ (counters 1, 2) for the low momentum detectors to $1.0\,mm$ (counters 3–5) and $2.0\,mm$ for higher momenta. Each scintillator is read out on both ends by a photomultiplier. (ii) The tracking system to reconstruct ejectile trajectories consisting of two multi-wire proportional chambers (MWPC 1, 2). They are located in front of all detector components except the TOF-start counters in order to minimize distortions of the ejectile trajectories due to small-angle scattering. (iii) 15 range telescopes which are placed along the focal surface of D2. The horizontal angular acceptance of each telescope varies from $\pm 1°$ to $\pm 15°$ depending on the on- or off-line coincidences with the corresponding start counters. Each telescope is composed of TOF-stop, $\Delta E$, veto scintillation counters (*BC408, Bicron*), which are read out by photomultipliers on both sides, and two passive degraders made of copper. Telescopes 9–15 also contain lucite Cherenkov counters. For a detailed description of the telescopes see Section 2.3.2.

The precise time information from the start, stop, $\Delta E$ and veto counters (see Section 3.1 for values of the time resolution) is achieved by constant-fraction discriminators and mean timers both specifically developed for this purpose [12]. In addition, the vertical spatial information in each scintillator is obtained from the time difference of both phototubes. The resolution for the stop detectors is better than $30\,mm$ (FWHM). With one specially built VME-module for each stop counter it is possible to set a common TOF gate (length variable between 3 and $23\,ns$) in coincidence with up to 16 individually adjustable start-stop combinations [12]. In this way corridors of acceptable start-stop combinations can be defined through which the $K^+$-mesons from the target should pass. A total of 16 VME modules is needed for the ANKE on-line TOF trigger which allows to select pions, kaons or protons already during data taking.

#### 2.3.1. Multi-wire proportional chambers

The two MWPCs [13,14] of the ANKE $K^+$-detection system have been built in a modular design at the Forschungszentrum Rossendorf and differ only in the dimension of the sensitive planes and the diameter of the anode wires (see Table 1).

Table 1
Properties of MWPC 1 and MWPC 2

|  | MWPC1 | MWPC2 |
| --- | --- | --- |
| Gas mixture | 70% Ar : 30% $CO_2$ | 70% Ar : 30% $CO_2$ |
| No. of anode planes | 3 | 3 |
| Arrangement of anode wires | Vertical and $+30°$ and $-30°$ inclined | Vertical and $+30°$ and $-30°$ inclined |
| HV anodes | 0 V | 0 V |
| max. HV cathodes | $-3000$ V | $-3000$ V |
| Wire spacing | 2.54 mm | 2.54 mm |
| Distance anode–cathode | 5 mm | 5 mm |
| No. of wires per plane | 512 | 768 |
| Anode wires | 20 μm tungsten | 25 μm tungsten |
| Cathode material | 18 μm mylar foil | 23 μm mylar foil |
| Sensitive area | $35 \times 130$ cm$^2$ | $60 \times 196$ cm$^2$ |

The arrangement of the sensitive wires in the planes, vertical and inclined by $+30°$ and $-30°$, respectively, allows to determine the space co-ordinates of the particle track in the wire chamber. Together with the knowledge of the magnetic field of the D2 magnet one can reconstruct the momentum and emission angle of the particle at the target position. The necessary accuracy of the reconstructed momentum $\Delta p/p$ is 2–3% for pions. This can be achieved with a wire spacing of 2.54 mm. An intrinsic resolution $\sim 0.7$ mm between the inclined and vertical planes has been determined in test measurements [13].

The readout of the chambers is performed using a highly integrated front-end system based on two chips which were developed at the Rutherford Appleton Laboratory (RAL) [15]. The analog chip RAL 118 amplifies and discriminates the signal. The digital chip RAL 111 on the one hand provides the proper delay of the signal using a digital shift register. This is necessary since the signal of the MWPCs must be stored until the system trigger has been generated. On the other hand, RAL 111 digitizes the signals and performs zero suppression. The latter leads to a huge data reduction since in a typical event only around 2% of the wires have a signal and only the numbers of those wires are sent to the subsequent data-aquisition system. Thus during the $K^+$-measurements particle fluxes of about 5000 s$^{-1}$ per wire could be handled by the readout system. A more detailed description of the complete readout system can be found in Ref. [16].

The drift time of electrons in the used gas mixture is 80 ns at most [17]. Therefore no restrictions are expected when the chamber is operated at a maximal particle flux of $10^6$ s$^{-1}$. To minimize the number of multiple hits the width of the readout gate is set to 110 ns.

### 2.3.2. The $K^+$ range telescopes

The $K^+$-telescopes are positioned along the focal surface of D2 perpendicular to the trajectories of ejectiles which leave the target in the forward direction, $\vartheta = 0°$. Each detector covers a limited momentum range given by its width of 10 cm and the dispersion of D2. The values for the momentum acceptances which are shown in the right column of Table 2 were calculated for ejectiles emitted at $0°$ from the target and neglecting small angle scattering in the vacuum foils and the detector components.

Fig. 4a shows momentum distributions for three telescopes which were obtained from data on $\pi^+$-production in proton–carbon collisions and from corresponding GEANT simulations. For the reconstruction of the pion momenta from the wire-chamber information, a simple box-field approach has been applied in which the trajectories in front of and behind the effective field of D2 are described by straight lines. The ejectile momenta are determined by calculating a circular arc with a constant radius of curvature connecting these straight lines. The fact that each of the telescopes is hit by ejectiles within a rather limited momentum range of $\Delta p/p =$ 7–24%, provided they

Table 2
Dimensions of the telescope components used for the measurements at $B = 1.30$ T. In addition, telescopes #9–15 contain 5 cm thick lucite Cherenkov counters between stop and degrader I. The momentum ranges covered by each telescope are given in the last column

| Telescope | Height (cm) | Thickness (cm) | | | | | Momentum range (MeV/$c$) |
| --- | --- | --- | --- | --- | --- | --- | --- |
| | | Stop | Degr.I | $\Delta E$ | Degr.II | Veto | |
| 1 | 52 | 0.3 | — | 0.5 | 0.2 | 1.0 | 110–140 |
| 2 | 57 | 0.5 | — | 0.5 | 0.2 | 1.0 | 140–160 |
| 3 | 62 | 1.0 | — | 1.0 | 0.2 | 1.0 | 160–182 |
| 4 | 67 | 1.0 | — | 1.0 | 0.8 | 1.0 | 182–205 |
| 5 | 77 | 1.0 | 0.1 | 1.5 | 0.8 | 1.0 | 205–227 |
| 6 | 82 | 1.0 | 0.11–0.37 | 2.0 | 0.8 | 1.0 | 227–252 |
| 7 | 88 | 1.0 | 0.26–0.58 | 2.0 | 1.6 | 1.0 | 252–280 |
| 8 | 94 | 1.0 | 0.43–0.82 | 3.0 | 1.3 | 1.0 | 280–310 |
| 9 | 100 | 1.0 | 0.11–0.57 | 3.0 | 1.0 | 1.0 | 310–340 |
| 10 | 100 | 1.0 | 0.49–1.08 | 3.0 | 1.5 | 1.0 | 340–370 |
| 11 | 100 | 1.0 | 1.06–1.78 | 3.0 | 1.7 | 1.0 | 370–400 |
| 12 | 100 | 1.0 | 1.70–2.57 | 4.0 | 1.0 | 1.0 | 400–430 |
| 13 | 100 | 1.0 | 2.56–3.49 | 4.0 | 1.0 | 1.0 | 430–460 |
| 14 | 100 | 1.0 | 3.23–4.34 | 5.0 | 2.0 | 1.0 | 460–490 |
| 15 | 100 | 1.0 | 4.20–5.37 | 5.0 | 2.0 | 1.0 | 490–525 |
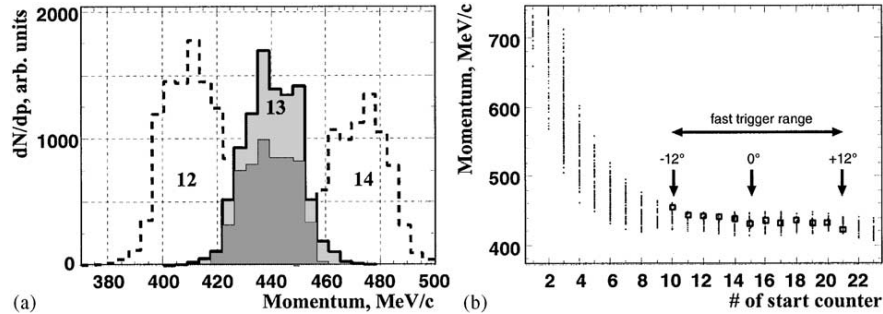


Fig. 4. (a) Momentum distribution of pions from p(2.3 GeV)C → $\pi^+$X reactions emitted at angles $\leqslant 10°$ and detected in telescopes #13 (light shaded histogram), 12 and 14 (dashed). For comparison the result of a GEANT simulation is given (dark shaded, scaled down by an arbitrary factor). (b) Simulated momentum ranges for the individual start counters and telescope #13. For the simulation horizontal emission angles of even up to 30° were permitted. The central arrow indicates the start counter which detects particles emitted at 0° at this setting of the beam energy and field strength in D2; the range of start-stop combinations accepted by the fast trigger is indicated by the horizontal bar. Also shown by the open squares are the mean ejectile momenta calculated from TOF spectra, see Section 3.1 for details.

originate from the target at angles less than $\sim 15°$ (see right column of Table 2), allows to exploit the different ranges and energy losses of ejectiles with different masses for the $K^+$-identification, see Section 3.1 for details.

Fig. 4b shows momentum distributions for telescope #13 and the individual start counters. It can be seen that particles which traverse start counters #10–21 have a small momentum spread, $\Delta p/p \approx 8\%$. The lowest counters also detect fast ejectiles which are emitted from the target at large angles $\vartheta \leqslant 30°$. Since they miss the well-defined field region of D2 they are only slightly deflected so that their momentum distributions smear out. Indicated in the figure is the range of valid start counters which are accepted by the on-line TOF

trigger. For these counters, corresponding to horizontal emission angles $|\vartheta| \leqslant 12°$, the imaging properties of D2 are sufficient to detect ejectiles with well defined momenta.

The telescopes consist of vertically oriented scintillators and copper degraders. The thicknesses of all components were determined with the help of GEANT simulations [17,18] for $K^+$-identification. The results of the simulations were verified for a sample telescope by test measurements with pion, kaon and proton beams from the 10 GeV proton synchrotron at ITEP, Moscow [4]. Table 2 shows the thicknesses of all components used during the measurements described here. The first counter in each telescope is the TOF-stop counter, see Fig. 5, followed by 5 cm thick lucite Cherenkov counters (in telescopes #9–15 only) for the suppression of fast pionic and leptonic background. During data analysis it turned out that these counters provide no additional background suppression. Thus they were not used in the current analysis for kaon identification.

The function of degrader I is twofold: first, it stops protons originating from the target and prevents them from entering the $\Delta E$ counter. Second, it slows down kaons such that they are stopped at the far end of the $\Delta E$ counter or in the second degrader. This results in a large $K^+$ energy loss in the $\Delta E$ counter which helps to separate them from pions and scattered protons, see
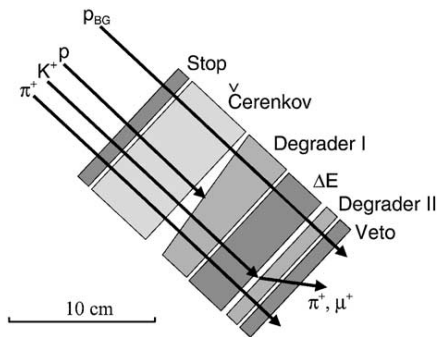


Fig. 5. Sketch of telescope #13. The ranges of pions, kaons and protons originating from the target as well as scattered protons ($p_{BG}$) with the same velocity (i.e. TOF) as kaons are indicated. See text for a detailed description of detector components.

Section 3.1. The tapered shape of degrader I accounts for the momentum dispersion along the focal surface of D2: From the left to the right edge of each telescope the degrader thickness increases in correspondence with the ejectile momentum. In order to minimize the range spread for kaons, each telescope is positioned such that the first degrader is located in the focal plane where the momentum spread of the ejectiles is smallest. Pions from the target pass through the counters and degraders almost unaffected due to their high velocity and result in small energy losses in all counters. The thicknesses of degrader I have carefully been fine tuned during calibration measurements (by adding thin copper sheets) at $T_p = 2.3$ GeV where the kaon rate is sufficiently high to identify them without the help of the energy-loss spectra in the $\Delta E$ counter, see Section 4.

Kaons which are stopped in the $\Delta E$ counter or in the second degrader decay with a lifetime of $\tau = 12.4$ ns. Their decay products, $\mu^+$ or $\pi^+$ emitted isotropically, can reach the veto counter and result in signals which are characteristically delayed with respect to $K^+$-signals in the stop or $\Delta E$ counters of the same telescope. This provides an additional criterion for $K^+$-identification which becomes particularly important for low beam energies. This method based on the detection of delayed decay muons was already applied previously in the measurement of total cross-sections at beam energies between 0.8 and 1.0 GeV [1].

The most problematic background is caused by secondary protons produced on the pole shoes of D2 or in the vacuum chamber. This contains a component with the same time-of-flight as the kaons and thus approximately twice their momenta. Such protons ($p_{BG}$), which are also indicated in Fig. 5, pass through all detectors of a telescope. The thicknesses of degrader II were chosen larger than necessary to prevent kaons from reaching the veto counter: they also slow down the background protons such that their energy loss in the veto counter significantly increases beyond that of the koan-decay products. Selection of events with small energy losses in the veto counters thus is an additional criterion for kaon identification since their decay muons and pions are minimum ionizing.

## 3. Data analysis

### 3.1. Examples of scintillator spectra

Examples of time-of-flight (TOF) distributions between the stop counter of telescope #13 and the different start counters are shown in Fig. 6. The data were taken during a calibration run with high field strength in D2 ($B = 1.57$ T). During data taking an open on-line TOF trigger was chosen such that pions, protons and scattered particles are visible in the spectra. Most of the spectra show two distinct peaks for pions and protons originating from the target which have well defined momenta,

$p \approx 430$–$460$ MeV/$c$, see Table 2 and Fig. 4. From the spectra an average time resolution of $\sim 650$ ps (FWHM) for target pions in the central region—start counters #10–21, corresponding to horizontal emission angles $|\vartheta| \leqslant 12°$—has been deduced. The shift of the proton peaks towards smaller flight times and the larger width ($\sim 1000$ ps) for the lower start-counter numbers is due to the momentum spread shown in Fig. 4b which causes a variation of the proton velocities. This is not the case for pions since, due to the low mass, their velocity is close to the speed of light. For start-counters with numbers below 5, the two peaks start to disappear and a broad TOF distribution
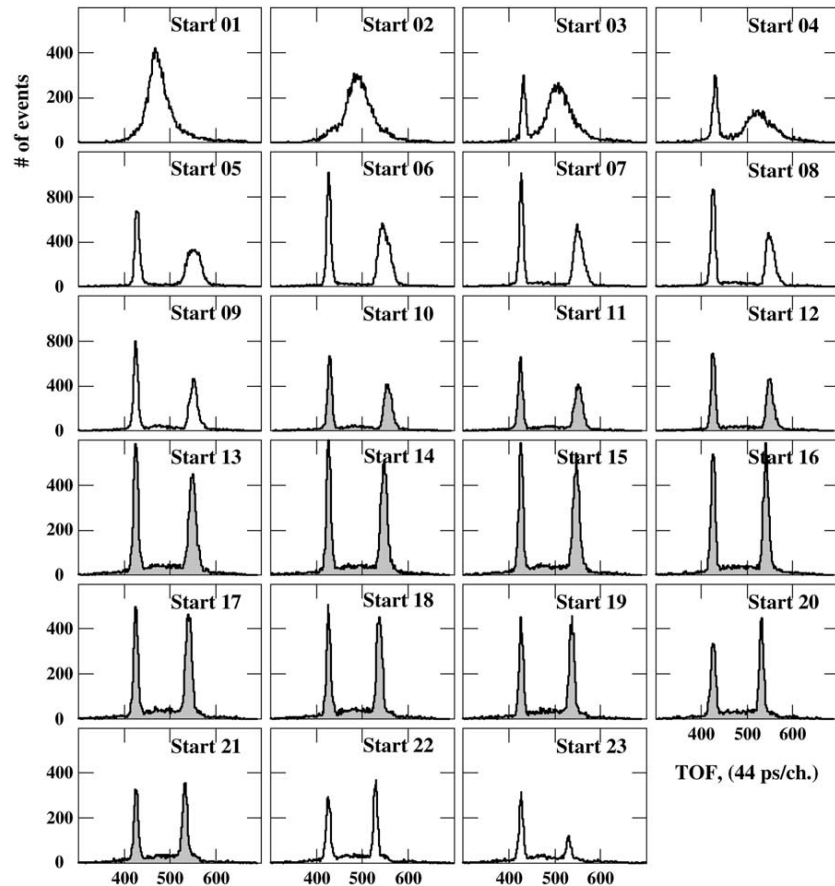


Fig. 6. Time-of-flight spectra at an incident proton energy $T_p = 1.5$ GeV between stop counter #13 and start counters # 1–23. The data presented in this figure were obtained during a dedicated calibration run with open trigger at $B = 1.57$ T with a carbon target. The range of "valid" start counters for this particular stop counter, see Fig. 4b, is indicated by the shaded histograms.

develops because of the high-momentum protons, see Fig. 4b. The pions are suppressed here because of inefficiencies of the first few start counters for high momentum pions. In start counter #23 the peak of protons from the target is reduced for the following reasons: the average ejectile momenta (and ranges) are smaller, see Fig. 4b, and the effective counter thickness is increased due to the smaller entrance angle into the telescope. This prevents part of the target protons from reaching the $\Delta E$ counter. Since a signal in this counter was required in the on-line trigger only the fastest protons can be detected and the proton rate is reduced. This effect also has an influence on the spectra of start counters #18–21. Here the width of the proton peak is reduced from 1000 ps down to 500 ps.

The separation of the pion- and proton-TOF peaks in Fig. 6 allows to calculate the average momentum of the ejectiles originating from the target. The deduced values for start counters #10–21 are presented as the open squares in Fig. 4b and agree with the momenta from ray-tracing calculations using GEANT. Remember that the TOF spectra from Fig. 6 were obtained at a field strength of $B = 1.57$ T in D2 (field setting used for the TOF calibrations) whereas the momentum ranges in Fig. 4 are given for $B = 1.30$ T (field setting used for the cross-section measurements). Thus the momenta from TOF were multiplied by the ratio of the field strengths 1.30/1.57 in order to allow a comparison with the GEANT simulations.

Fig. 7 shows the energy-loss spectra which were measured simultaneously with the TOF spectra of Fig. 6. They allow to determine the detection efficiencies for pions in the start counters assuming that the energy-loss distributions can be fitted by Landau distributions. Values of $\sim 95\%$ were obtained, except for the first two start counters which are only 0.5 mm thick. In this case the efficiencies are below 50%. For kaons the detection efficiencies are higher and very close to 100%. The efficiencies are taken into account when normalizing the number of identified kaons to known pion-production cross sections.

Fig. 8a shows the combined TOF distribution for the stop counter of telescope #13 and start counters #10–21 from Fig. 6. The time resolution for pions in Fig. 8a amounts to 650 ps (FWHM), as in case of the individual spectra from Fig. 6. Due to the different lengths of the flight paths for each start counter, the values of the TOF difference between pions and protons vary, which causes a smearing of the proton peak in the sum spectrum.

In principle, the observed time resolution should allow a clear separation of pions (protons) and kaons. The TOF difference between pions and kaons (peak-to-peak) amounts to $\sim 8\sigma$; assuming a pure gaussian distribution one would expect a pion suppression much better than the requested $10^6$. Such a huge suppression is, however, not achieved in the experiment due to background produced in secondary hadronic interactions. The flat background in Fig. 8 is mainly caused by fast protons emitted from the target at small angles. These protons can hit the pole shoes of D2 or structure material of the vacuum chamber and produce secondary particles which then can reach the telescopes. Such secondary particles are not focussed by D2 and, hence, do not have well defined momenta. Therefore, they result in a broad background distribution in the TOF spectra. Indicated by the shaded area in the sum spectra of Fig. 8 and the following ones are the regions where kaons are expected. This serves for illustration only since in the process of kaon identification, individual gates were used for each start-stop combination (i.e. spectra in Fig. 6). The same applies for *all other* scintillator time and amplitude spectra.

Fig. 8b shows the energy-loss distribution in stop counter #13 for ejectiles detected in coincidence with start counters #10–21. As for the TOF spectrum of Fig. 8a the raw spectrum shows two peaks from pions and protons from the target and a broad background distribution. The ratio of the energy losses of protons and pions is $\sim 4.5$ as expected from the Bethe-Bloch formula. Consequently, only a moderate separation of pions and kaons (expected energy-loss ratio $\sim 1.7$) can be achieved from the amplitude signals. Since the lower edge of the pion energy-loss distribution is clearly visible in Fig. 8b, the detection efficiency for pions is larger than
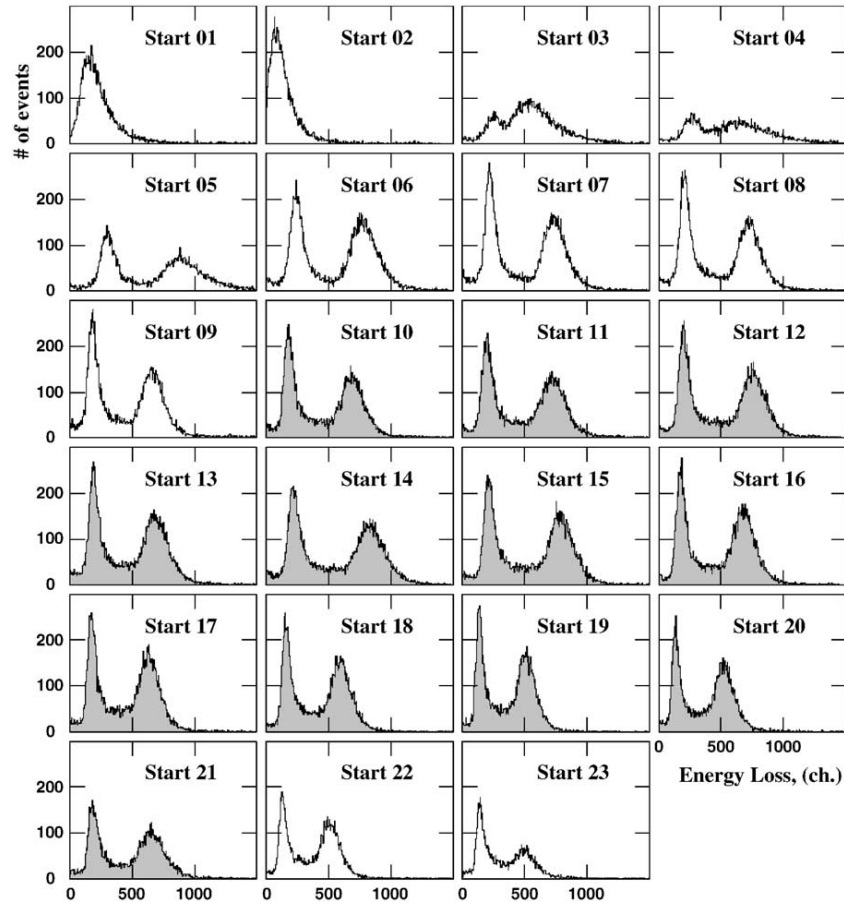
Fig. 7. Energy-loss spectra for the same start-stop combinations as in Fig. 6.

98%. The same high efficiency has been obtained for kaons since the gate indicated in the figure is rather wide.

Fig. 9a shows the energy-loss distribution in the $\Delta E$ counter of telescope #13. The data were obtained at $B = 1.30$ T. Since protons from the target are stopped in the Cherenkov counter or in the first degrader there is only one peak from target pions and a broad background distribution from secondary particles visible in the spectrum. As explained in Section 2.3.2, the first degraders are used to optimize the energy loss of kaons in the $\Delta E$ counters. The solid histogram in Fig. 9b shows the corresponding energy-loss spectrum for kaons

(identified as described later in Section 3.4). During the measurements it has been checked whether slight modifications of the degrader thicknesses can improve the kaon-to-background separation. For this purpose the kaon energy loss should be as large as possible (better separation from target pions), while keeping the width of the distributions small (optimization of the kaon to scattered-background ratio). It turned out that the optimization procedure for most telescopes resulted in thicknesses at which the kaons pass through the $\Delta E$ counter and are stopped in the second degrader. As an example the corresponding distribution is shown by the dashed histogram in

40
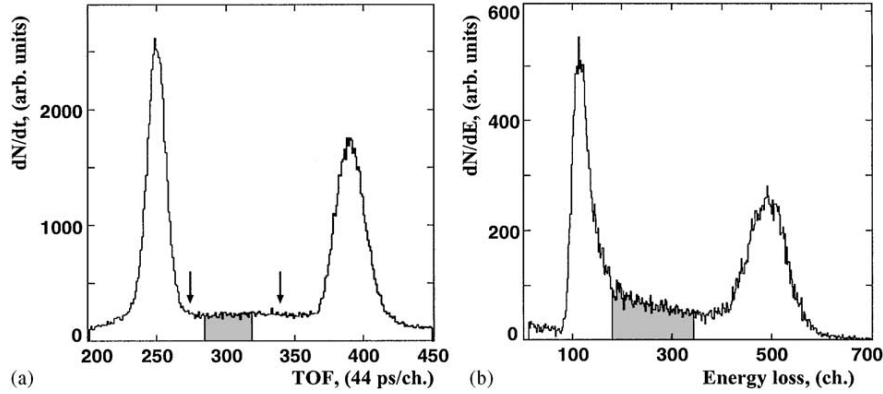
Fig. 8. (a) TOF and (b) amplitude spectra of stop counter #13 in coincidence with start counters #10–21. The approximate position of the gates for the off-line kaon identification are indicated by the shaded areas (see text). Arrows mark the narrowest TOF gates used for on-line event selection. The data were obtained at $B = 1.57$ T with a carbon target.
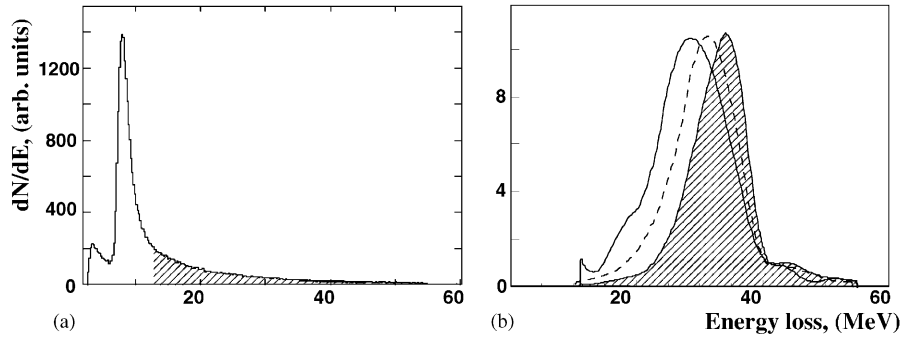


Fig. 9. Energy-loss spectra for $\Delta E$-counter #13 in coincidence with start counters #10–21. (a) Raw spectrum, the gate for kaons is located above $\Delta E \sim 13$ MeV. (b) Kaon spectra taken during optimization of degrader I. The values of the tapered degrader thickness are: (i) 2.76–3.69 cm (solid histogram, initial value from simulation calculations), (ii) 2.66–3.59 cm (dashed histogram), and (iii) 2.56–3.49 cm (shaded histogram, optimum thickness given in Table 2). All data were obtained at $T_p = 2.0$ GeV and $B = 1.30$ T with a carbon target.

Fig. 9b. As explained in Section 2.3.2, the time information from the veto counter is a particularly effective criterion for kaon identification. If the kaons are stopped in the second degrader one expects that only their decay muons and pions can reach the veto counter with a time delay characteristic for the $K^+$-lifetime of 12.4 ns. Fig. 10 shows the distribution of the time difference of particle detection in the veto and stop counters of telescope #13. One can clearly see a peak from particles directly passing through the second degrader (pions and secondary protons). In addition, there are delayed events visible which can be attributed to the decay products of $K^+$-mesons stopped in the second degrader, see Section 3.4. The on-line trigger for the accumulation of the $K^+$-data at low projectile energies rejected prompt events and admitted only those with a delay $> 1.3$ ns (channel 30). Off line a threshold of $> 2.3$ ns (channel 55) was set.
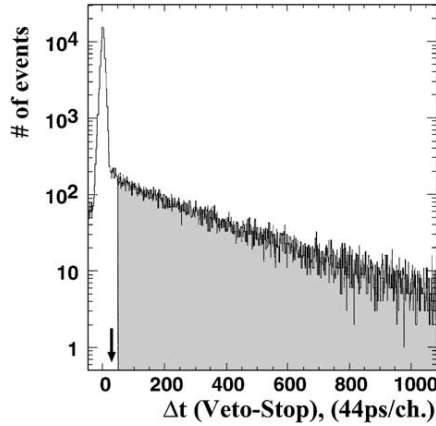
Fig. 10. Time difference between detection of particles in veto- and stop counter of telescope #13. To make the spectrum more illustrative, kaon gates were applied in the scintillator spectra described above and only particles were accepted which vertically come from the target plane (see next section). The arrow shows the location of the gates used during the measurements whereas the off-line cut is indicated by the shaded area, see text for details. The data were obtained at $T_\mathrm{p} = 2.3\,\mathrm{GeV}$ and $B = 1.30\,\mathrm{T}$ with a carbon target.



Fig. 11. Ejectiles from the target and scattered background in general have different vertical angles behind the spectrometer. See text for details.

The use of the full scintillator information (TOF, energy loss in start, stop, $\Delta E$ and veto counters plus selection of delayed events in the veto counter) allows for a clear separation of the kaons from pions and protons originating from the target even at the lowest beam energy $T_p = 1.0\,\mathrm{GeV}$. However, the background from secondary particles scattered at the pole shoes of D2 cannot sufficiently be suppressed. This is only possible by using the information from the wire chambers on the direction of the ejectiles as explained in the following section.

### 3.2. Background suppression using the MWPC information

As indicated in Fig. 11 by the dashed line, particles from the target within the angular acceptance passing through the first MWPC at some vertical coordinate $y$ are expected to have a certain vertical angle $\vartheta$ (which is measured with the second chamber). All ejectiles undergo multiple scattering in the vacuum foil of D2 and in detector

components. This causes some smearing $\Delta\vartheta$ of the expected vertical angular distributions of particles from the target, for example $\Delta\vartheta_\mathrm{K}^+$. In contrast to target ejectiles, scattered protons $p_\mathrm{BG}$ in general have larger angular differences $\Delta\vartheta p_\mathrm{BG}$. Thus the vertical MWPC information can very efficiently be used for the suppression of scattered particles.

Fig. 12 shows the vertical angular distributions $\Delta\vartheta$ for the remaining $\mathrm{K}^+$-candidates after applying all cuts in the scintillator spectra described above. At the highest beam energy shown in the figure, $T_\mathrm{p} = 2.0\,\mathrm{GeV}$, there is a clear peak around $\Delta\vartheta = 0$ corresponding to ejectiles from the target. These particles can be identified as kaons, see Section 3.4. Only very few events from background particles are still visible. With decreasing beam energy the background surviving the scintillator cuts becomes significantly more important. The broad bumps at both sides of the target peak are mainly from ejectiles scattered at the pole pieces of D2 whereas background events underneath the peak must originate from the same vertical plane in which the target is located. The spectra from Fig. 12 are, for illustration, summed over all valid start counters. However, for identification of the $\mathrm{K}^+$-mesons and for background suppression, the gates

42
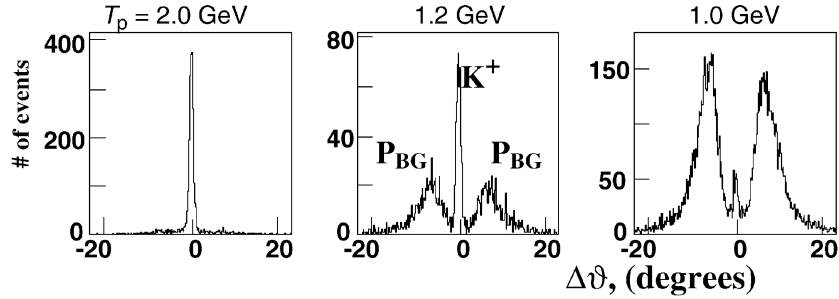
Fig. 12. Distribution of vertical angles measured with the two MWPC's after applying the $K^+$-cuts in the scintillator spectra of telescope #11. The spectra show a clear peak of kaons originating from the target. Background from scattered particles is also visible. The spectra were measured with a carbon target at three different beam energies.

Table 3
Effectiveness of the individual cuts for $T_p = 2.3\,\text{GeV}$. The numbers presented in columns "$K^+$" and "B.g." are the probabilities that $K^+$-mesons or background particles, accepted by the preceding criteria, are within the gate corresponding to the criterion described in the first two columns of the same line

| Criterion | Shown by | $K^+$ | B.g. |
|---|---|---|---|
| Valid start counters (on-line) | Shaded spectra in Fig. 6 | $1.0^a$ | 0.25 |
| TOF (on-line) | Arrows in Fig. 8a | 1.0 | 0.11 |
| TOF (off-line) | Shaded area in Fig. 8a | 0.99 | 0.29 |
| Vertical direction | Fig. 12 | 0.99 | 0.11 |
| Delayed veto | Shaded area in Fig. 10 | $0.2^b$ | $<10^{-3}$ |
| All | | 0.2 | $<3.5 \times 10^{-6}$ |

[a] For kaons with emission angles $|\vartheta| \leqslant 12°$.
[b] See Fig. 18 for efficiencies of the individual telescopes.

around the peak at $\Delta\vartheta = 0$ were optimized for each individual start-stop combination. It will be shown in Section 3.4 that for $Tp = 1.0\,\text{GeV}$ the remaining background underneath the peak is smooth and can be subtracted in order to determine the number of kaon events in each telescope. This is particularly important for measurements far below threshold.

In addition to the cuts on the vertical distributions from Fig. 12, in the horizontal direction (vertically oriented wires) events are only accepted if the responding wires are inside a corridor defined by trajectories connecting the edges of the individual start and stop counters. This criterion further helps to suppress scattered background, accidental coincidences and chamber noise. The width of these allowed corridors typically is 40–100 wires (10–25 cm).

3.3. Effectiveness of different criteria

In this section we briefly summarize the effectiveness of the most important cuts presented in Sections 3.1 and 3.2 for beam energies $T_p = 1.0$ and $2.3\,\text{GeV}$. At $2.3\,\text{GeV}$ an on-line trigger based only on the TOF information was used which reduces the background and, thus, the amount of data written to tape, by about one order of magnitude. All other criteria, including narrower TOF gates, were applied off-line. The efficiencies of these criteria are summarized in Table 3.

At $T_p = 1.0\,\text{GeV}$ the background-to-kaon ratio is much larger than at $2.3\,\text{GeV}$. Thus, a stronger on-line trigger, based on TOF measurements and the (delayed) time signal from the veto counters, was used which drastically reduces the amount of

data written to tape. During the off-line analysis subsequently stronger criteria were applied. In some cases two criteria were applied at the same time so that the combined efficiencies are shown in Table 4.

### 3.4. Identification of $K^+$-mesons

Fig. 13 shows the remaining events when analysis gates are set on (i) TOF between start- and stop counters (Fig. 6), (ii) amplitude information of all scintillation counters (e.g. Figs. 7, 8b, 9), (iii) time difference between veto- and stop counters of one telescope (Fig. 10) and (iv) MWPC

information (Fig. 12). Due to the moderately large cross-sections for kaon production at $T_p = 2.3$ GeV, clear peaks without background in the vertical-angle and TOF distributions are seen. The vertical-angle distribution (a) proves that the particles are directly coming from the target region and the TOF peak (b) is located at the position were kaons are expected. An exponential fit to the time distribution in the veto counters yields a value of $\tau = 12.0 \pm 0.3$ ns, consistent with the expected 12.4 ns.

Fig. 14 shows the same spectra as in Fig. 13 but now for the lowest beam energy, $T_p = 1.0$ GeV. Except for the beam energy, all other experimental

Table 4
Same as Table 3 for $T_p = 1.0$ GeV

| Criterion | Shown by | $K^+$ | B.g. |
|---|---|---|---|
| Valid start counters (on-line) | Shaded spectra in Fig. 6 | 1.0[a] | 0.25 |
| TOF | Arrows in Fig. 8a | | |
| and delayed veto (both on-line) | Arrow in Fig. 10 | 0.22 | 0.002 |
| TOF (off-line) | Shaded area in Fig. 8a | | |
| and vertical direction | Fig. 12 | 0.99 | 0.002 |
| Delayed veto (off-line) | Shaded area in Fig. 10 | 0.92 | 0.3 |
| Narrower TOF cuts | See Section 3.4 | | |
| and Amplitude in $\Delta E$ counters | Shaded area in Fig. 9a | 0.6[b] | 0.05 |
| All | | 0.12 | $6 \times 10^{-8}$ |

[a] For kaons with emission angles $|\vartheta| \leqslant 12°$.
[b] See Fig. 18 for efficiencies of the individual telescopes.



(a) $\Delta \vartheta$, (degrees)    (b) TOF, (44 ps/ch.)    (c) $\Delta t$ (Veto-Stop), (44 ps/ch.)
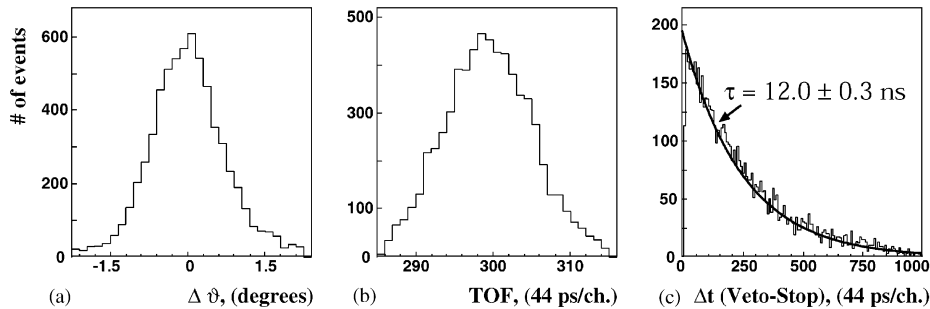
Fig. 13. (a) Vertical angular distribution of $K^+$-events (c.f. Fig. 12). (b) TOF distribution (c.f. Fig. 8a). (c) Time difference of detection in the veto and stop counters (c.f. Fig. 10); the spectrum has been shifted such that the gate for kaon detection is located at channel #0. All data were taken at $T_p = 2.3$ GeV with a carbon target. For illustration and in order to increase the number of events, the spectra shown in this section are summed over all valid start-stop combinations by properly shifting the distributions for each individual combination.

44
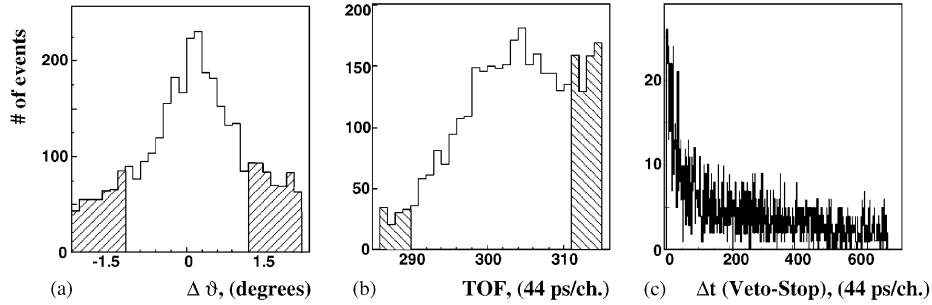
Fig. 14. Same as Fig. 13 but for $T_p = 1.0\,\text{GeV}$. Indicated in (a) and (b) by the shaded areas are the angular and TOF cuts on background events which were used to determine the shape of the background distributions in Fig. 15.
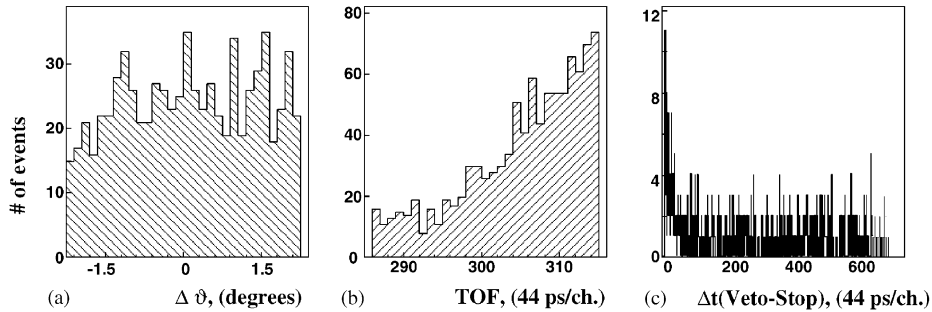


Fig. 15. (a) Same as Fig. 14a for background events within the outside gates of the $K^+$-TOF distribution from Fig. 14b. (b) Same as Fig. 14b for background events at the sides of the angular distribution from Fig. 14a. (c) Same as Fig. 14c for the events from (a).

conditions and software gates remain unchanged. Neglecting the now visible background, the location of the kaon distributions and, in the case of the vertical angle distributions, also the shape is the same as for the high energy where the production cross section is approx. $10^5$ times larger.

In order to determine the number of detected kaons one has to subtract the background underneath the kaon peaks. The analyses show that this background has a smooth behaviour. As an example, in Fig. 15 the distributions of background events in the vertical-angle, TOF and $\Delta t$(veto-stop) spectra is shown. In particular, the vertical-angle distribution is constant in the region of the kaon peak and, thus, the background subtraction can be done by assuming a linear shape of the background in Fig. 14a.

The remaining kaon distributions after background subtraction are shown in Fig. 16. Both the width of the TOF distribution as well as the exponential slope in the veto counter agree with the (clean) data at $T_p = 2.3\,\text{GeV}$.

## 4. $K^+$-momentum spectra

It has been shown in the previous sections that, after applying all criteria on TOF, energy losses and the MWPC information, $K^+$-mesons can be identified even at $T_p = 1.0\,\text{GeV}$. From the number of observed kaons in each telescope one can deduce momentum spectra, since the telescopes are placed along the focal surface of the spectrometer dipole. In order to obtain the double differential cross sections $d^2\sigma/d\Omega\,dp$ for $K^+$-

45
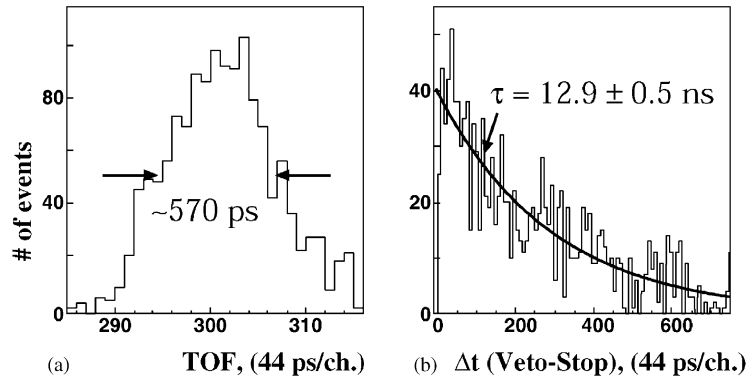
Fig. 16. Same as Fig. 14b and c after background subtraction.

mesons produced at $\vartheta \sim 0°$, the kaon-detection efficiencies in each telescope have to be corrected for. The cross-sections can then be obtained by normalizating to the number of identified $\pi^+$-mesons, which were measured in parallel, and to the known $\pi^+$-production cross-sections. Further corrections, like e.g. for the different solid angles covered by each telescope and the acceptance gaps between them, are not necessary since they are identical for pions and kaons.

At ANKE, we have the possibility to directly determine the $K^+$-detection efficiencies in the telescopes through measurements at high beam energy, $T_p = 2.3\,\text{GeV}$. Due to the rather large kaon-production cross-section, it is sufficient to use for $K^+$-identification the TOF and the MWPC information *only*. Under these conditions, the efficiencies for kaon (and pion) detection result from the efficiencies of the involved detectors (TOF-start and -stop, MWPC's) which are well known and close to 100%, see Section 3. The upper spectra of Fig. 17 show the vertical-angle and TOF distributions of the events fulfilling these criteria. In both cases a peak of kaon events can be seen on top of a flat background distribution. The shape of this background has been determined in independent analyses: (i) The data taken at 1.0 GeV were used where the cross sections are so small that, with the TOF/MWPC gates, "contaminations" from kaons can be neglected. (ii) Events from the sides of the kaon distributions

were used, see shaded areas of Fig. 14. In both cases the background distributions are almost linear. However, for background subtraction, different background shapes were taken into account and the uncertainties have been included into the errors for the detection efficiencies.

The lower spectra in Fig. 17 show the remaining $K^+$-events when *all criteria* (same as used in Section 3.4) for kaon identification are applied. In case of telescope #13, shown in the figure, approximately 10% of the kaons "survive" the cuts. The efficiencies—which are equal to the ratio of identified kaons with full gates and TOF/MWPC gates only—could be determined for telescopes 3–15. The corresponding numbers are shown in Fig. 18a (for the first two telescopes the high background level of scattered particles does not permit to identify kaons with the TOF/MWPC gates only). The detection efficiencies are in range of $\sim 10$–30%. The main kaon losses are due to a probability of only about 30% that a decay muon or pion enters the veto counter (limited solid angle), to kaon-scattering out of the telescopes in the first degrader and to hadronic interactions in the telescopes. The decreasing efficiency from telescopes #6 to #15 is caused by increasing thicknesses of the detectors and degraders. The step between #8 and #9 is due to the Cherenkov counters installed in telescopes #9–15; between telescopes #12 and #13 there is, for technical reasons, a significant increase of the distance
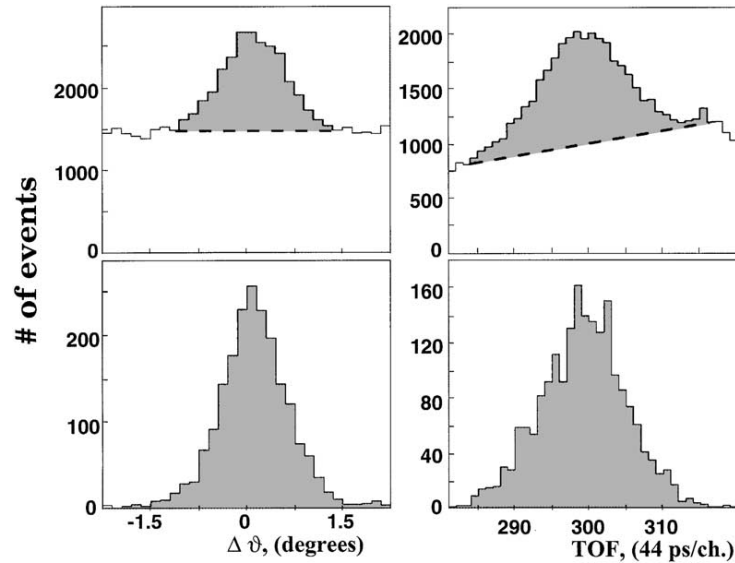
Fig. 17. Same as Fig. 13a and b but for telescope #13 only. Upper spectra: gates on TOF and vertical angles only (the gate widths correspond to the ranges of the two histograms). The background is indicated by the dashed lines. Lower spectra: all criteria for K$^+$-identification applied (as in Fig. 13). The number of entries in the histograms cannot directly be compared to Fig. 13 since a different data set was used.
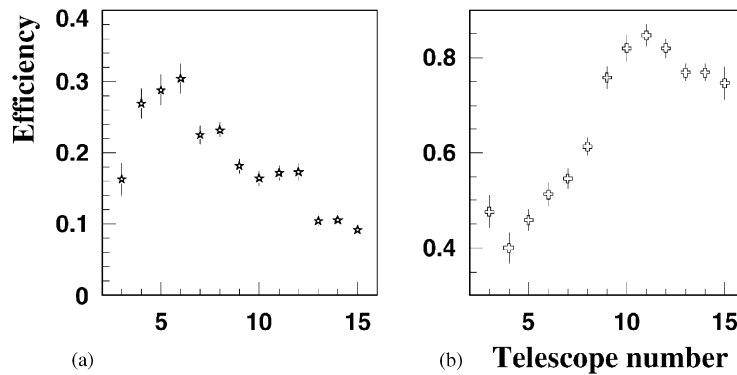


Fig. 18. (a) Measured K$^+$-detection efficiencies in the individual telescopes. (b) Correction factors which take into account the losses of K$^+$-counts due to the narrow TOF and energy-loss gates used in the off-line analysis at 1.0 GeV.

between the $\Delta E$ and veto counters. In the lowest telescopes higher thresholds in the $\Delta E$ counters had to be used for kaon identification in order to suppress scattered background which leads to decreasing efficiencies.

The cuts set on the spectra in the analysis of the data obtained at the lowest projectile energies were narrower than those for $T_p = 2.3$ GeV in order to suppress background as efficiently as possible. This leads to an additional loss of kaon events. Consequently, the obtained numbers of kaons at low energies also have to be corrected for the efficiencies shown in Fig. 18b which were determined through a comparison of the numbers of
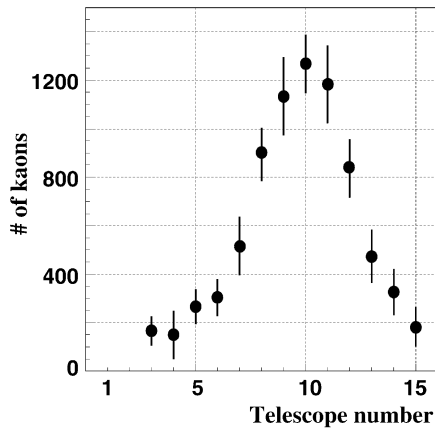
Fig. 19. Momentum distribution of $K^+$-mesons produced in a carbon target at $T_p = 1.0$ GeV. The numbers are not corrected for losses from decay-in-flight between target and stop counters and the different momentum bites of the telescopes (see Table 2). The error bars include the statistical uncertainties as well as the ones from the telescope-efficiency calibration.

identified $K^+$-mesons at 2.3 GeV with wide and narrow TOF and energy-loss gates.

Fig. 19 shows the number of identified $K^+$-mesons in each telescope corrected for the efficiencies from Fig. 18. Except for the above mentioned corrections for decay-in-flight and the different momentum bites and solid angles covered by the individual telescopes, the spectrum shown in the figure is proportional to the double-differential cross section $d^2\sigma/d\Omega\,dp$ for kaons produced in $p(1.0\,\text{GeV}) + {}^{12}C \rightarrow K^+X$ reactions and emitted into forward angles $\vartheta \leqslant 12°$.

## 5. Outlook

First measurements of $K^+$-momentum distributions in pA collisions at emission angles around 0° have been performed with the ANKE spectrometer at beam energies in the range $T_p = 1.0 - 2.3$ GeV. It has been shown that ANKE and its $K^+$-detection system allow to identify the kaons out of a $10^6$ times higher background of pions, protons and scattered particles. In order to extract double differential cross-sections from the number of identified kaons shown in Fig. 19, one

still has to correct for decay-in-flight between target and stop counters (30% to 36% of the kaons reach the counters) and the different momentum bites covered by the telescopes. Absolute normalization of the cross sections will be obtained from a comparison of $\pi^+$-data taken at ANKE with known $\pi^+$-production cross-sections [19,20]. The results of the corresponding analysis procedures will be presented in forthcoming publications.

## References

[1] V.P. Koptev, et al., JETP 67 (1988) 2177.
[2] S. Schnetzer, et al., Phys. Rev. C 40 (1989) 640.A. Shor, et al., Nucl. Phys. A 514 (1990) 717;
W. Cassing, et al., Phys. Lett. B 238 (1990) 25;
H. Müller, K. Sistemich, Z. Phys. A 344 (1992) 197;
A.A. Sibirtsev, M. Büscher, Z. Phys. A 347 (1994) 91;
W. Cassing, et al., Z. Phys. A 349 (1994) 77;
A.A. Sibirtsev, Phys. Lett. B 359 (1995) 29;
M. Büscher, et al., Z. Phys. A 355 (1996) 93;
M. Debowski, et al., Z. Phys. A 356 (1996) 313;
A.A. Sibirtsev, et al., Z. Phys. A 358 (1997) 357;
A. Badala, et al., Phys. Rev. Lett. 80 (1998) 4863;
Yu.T. Kiselev, et al., J. Phys. B 25 (1999) 381.
[3] E.Ya. Paryev, Eur. Phys. J. A 5 (1999) 307.
[4] M. Büscher, et al., Z. Phys. A 351 (1995) 333.

[5] W. Borgs, et al., COSY Proposal no. 18, 1991, unpublished.

[6] M. Büscher, Ph.D. Thesis, Universität zu Köln 1992.

[7] M. Büscher, et al., in: M.K. Khankhasayev, Z.B. Kurmanov (Eds.), Proceedings of the International Conference on Mesons and Nuclei at Intermediate Energies, Dubna, Russia, May 3–7, 1994, World Scientific, Singapore, 1994, p. 446, ISBN 981-02-1787-0.

[8] O.W.B. Schult, et al., Nucl. Phys. A 583 (1995) 629.

[9] S. Barsov, et al., Nucl. Instr. and Meth. A 462 (2001) 364.

[10] S. Barsov, et al., Proceedings of the 16th International Conference on Magnetic Technology, September 26–October 2, 1999, Ponte Vedra Beach, USA, Trans. Appl. Supercond. 10 (2000) 1; H.J. Stein, et al., Rev. Sci. Instr., 72 (2001) 2003.

[11] H. Müller, Z. Phys. A 339 (1991) 409.

[12] R. Schleichert, Ph.D. Thesis, Technische Hochschule Aachen, 1996.

[13] L. von Horn, Ph.D. Thesis, Universität zu Köln, 1996.

[14] H. Junghans, Ph.D. Thesis, Universität zu Köln, 1999.

[15] M. French, et al., Nucl. Instr. and Meth. A 343 (1994) 222.

[16] W. Erven, et al., IEEE Trans. Nucl. Sci. 45 (1998) 852.

[17] A. Schneider, Ph.D. Thesis, Universität zu Köln, 1998.

[18] A. Franzen, Ph.D. Thesis, Universität zu Köln, 1996.

[19] V.V. Abaev, et al., J. Phys. G 14 (1988) 903.

[20] J. Papp, et al., Phys. Rev. Lett. 34 (1975) 601.

# MONTE CARLO SIMULATIONS
# FOR ANKE EXPERIMENTS*

IZABELLA ZYCHOR

for the ANKE Collaboration†
(COSY–Jülich)

The Andrzej Sołtan Institute for Nuclear Studies
05-400 Świerk, Poland

The Monte Carlo code ANKE-GEANT is used to simulate experiments with the ANKE spectrometer — an experimental facility for the spectroscopy of products from proton-induced reactions on internal targets, placed in the accelerator ring of the cooler synchrotron COSY of the Forschungszentrum Jülich, Germany. Monte Carlo simulations are needed to determine a detector acceptance, estimate background, understand measured particle spectra. Calculations are also necessary to identify particles and to obtain their energy losses. The Monte Carlo simulations are the *only* method to reconstruct, without free parameters, momenta of ejectiles using information from scintillation counters and hit wire numbers in multi-wire proportional chambers.

PACS numbers: 24.10.Lx, 29.30.–h, 29.85.+c

## 1. ANKE spectrometer

The Apparatus for studies of Nucleon and Kaon Ejectiles ( ANKE ) is a new experimental facility [1] for the spectroscopy of products from proton-induced reactions on internal targets, placed in the accelerator ring of the cooler synchrotron COSY of the Forschungszentrum Jülich, Germany. It is a magnetic spectrometer with a large acceptance $\sim$50 msr for ejectiles emitted under forward angles and COSY independent setting of the field strength in its dipole magnets and, thus, momentum range.

COSY provides both unpolarized and polarized proton beams with momenta varying from 0.294 GeV/$c$ to 3.450 GeV/$c$.

---

(521)

ANKE makes possible various hadron-physics experiments like meson production in elementary proton–nucleon processes, studies of medium modifications of heavy meson production in proton–nucleus reactions [2,3], investigation of nucleon–nucleon final state interaction.

The device consists of three dipole magnets, various target installations and dedicated detection systems (see Fig. 1 ).
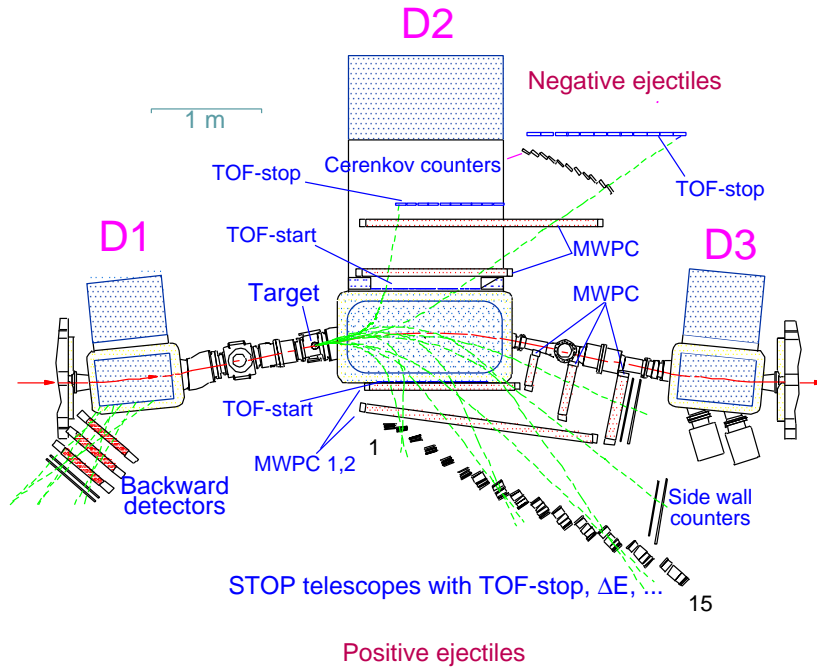


Fig. 1. ANKE spectrometer and detectors [1].

Three magnets (D1, D2 and D3) are used to deflect the circulating COSY beam off its straight path, to analyze momenta of reaction products and to deflect the beam back to the nominal orbit, respectively. The momentum range covered by the individual detection system depends on the field strength in the spectrometer dipole D2. For example, at the maximum field strength of 1.57 T kaons with momenta of 130 up to 635 MeV/$c$ are detected.

The target can be a thin strip ($\leq 1.5$ mg/cm$^2$ ) made of any solid material, a cluster jet, a frozen pellet or a polarized storage cell gas.

Luminosities up to $3 \times 10^{32}$/(cm$^2$s) are achieved with solid targets and up to a few $10^{30}$/(cm$^2$s) for cluster-jet.

The horizontal acceptance of ANKE is approximately $\pm(12°\text{--}15°)$ for positively charged particles which are emitted in the forward direction. The vertical acceptance depends on the exit position at D2 and typically ranges between $\pm3°$ and $\pm5°$.

Detection systems allow to identify different ejectiles, positively and *negatively* charged: *e.g.* forward going fast $p$, $d$, ${}^3$H and ${}^3$He, charged mesons, slow spectator particles. A large side detector, optimized for the detection of $K^+$-mesons, is built of START scintillators, two Multi-Wire Proportional Chambers MWPC and STOP telescopes.

## 2. ANKE-GEANT package

One of the major parts of the ANKE-GEANT [4] program is the geometry package which has two main functions: (1) define, *during the initialization of the program*, the geometry in which the particles will be tracked, (2) communicate, *during the event processing phase*, to the tracking routines the information for the transport of the particles in the geometry which has been defined.

The ANKE-GEANT geometry package precisely describes the full spectrometer: magnets, vacuum chambers, target chambers, detector systems etc. The real setup is divided into parts easily converted into shapes supported by GEANT. Preparation of description of the ANKE geometry for the Monte Carlo code was a time consuming task which has started from measurements of dimensions and positions of all ANKE elements. Measured dimensions and positions of all elements of the ANKE setup are then used to calculate shape parameters and positions of volumes according to the GEANT convention.

For the description of the magnetic field in the space occupied by the ANKE facility, measured field maps are used in combination with three dimensional field calculations made with the MAFIA code. The MAFIA calculations were checked by comparison with floating wire measurements [5].

All physical phenomena (*e.g.* pair production, Compton scattering, photoelectric effect, Rayleigh scattering, bremsstrahlung, hadronic process, annihilation, $\delta$-rays, muon nuclear interaction, photofission, decay in flight, energy loss, multiple scattering, Čerenkov photon generation, Čerenkov light absorption, synchrotron radiation generation, different energy fluctuation models) can be switched on or off by the user.

Full information about events is written to output files. One event consists of several tracks and more than one particle can appear in it. Typical parameters of the particle track, like time of flight, energy loss in various counters and path length from the target to each detector, are stored.

Fig. 2 shows a dependence of the average ejectile momentum on the START detector obtained in ANKE-GEANT simulations. The difference between the expected and simulated values is observed for all STOP detectors and is caused by placing them not in the focal plane of D2.
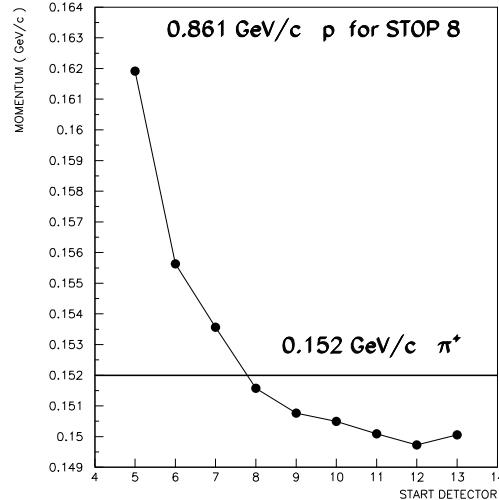


Fig. 2. Dependence of the average ejectile momentum on the number of the hit START detectors calculated for STOP #8. The momentum of 0.152 GeV/$c$ corresponds to the $\pi^+$ momentum from the two-body reaction 0.861 GeV/$c$ $pp \to d\pi^+$.

## 3. Reconstruction of ejectile momenta

Monte Carlo simulations are very useful to determine a detector acceptance, estimate background, understand measured particle spectra. These calculations are also necessary for identification of particles and calculations of their energy losses. The Monte Carlo simulations are the *only* method to reconstruct the momenta of ejectiles, without free parameters, from measured hits in MWPC's for the two body calibration reactions. Calculated and measured parameters are used to verify positions of setup elements, or even to find correct values (*e.g.* by comparing the simulated and experimental hit distributions in MWPC's).

The momentum calibration of ANKE is performed with pions emitted under forward angles from the two-body reaction $pp \to d\pi^+$ [6]. For emission angles $\leq 5°$ these pions are almost monoenergetic compared to the momentum resolution of ANKE. Calibrations have been done for the STOP telescopes with numbers from 6 to 15 and for low D2 magnetic field values

from 0.6493 to 0.8946 T. The COSY beam projectile momenta were in the range from 0.826 to 1.136 GeV/$c$. The corresponding $\pi^+$ momenta from the two-body reaction are then from 0.121 to 0.352 GeV/$c$, respectively. Information from START and STOP detectors and from hit wire numbers in two MWPC's is used in ANKE experiments for particle tracking to determine the ejectile momenta.

Typical distributions of hit wires from the 0.86 GeV/$c$ $p + p$ simulated reaction are shown in Fig. 3. Observed discrepancies in simulated and measured distributions are then used to find precise positions of the ANKE detectors.
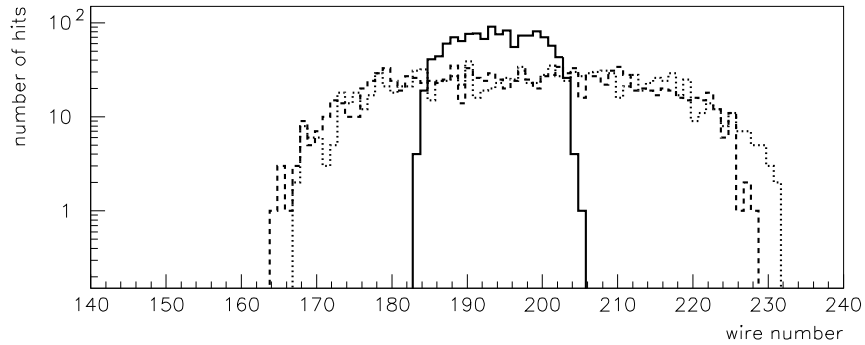


Fig. 3. Simulated distributions of hit wires in the 1$^{\text{st}}$ MWPC for START #8 and STOP #8. The most narrow distribution (solid line) corresponds to the vertical wires in the chamber, the broader distributions (dotted and dashed lines) to the inclined wires.

To obtain ejectile momenta measured in a certain STOP detector it is assumed that a unique dependence exists between momentum and 6 wires hit in the MWPC's. A 2$^{\text{nd}}$ order polynomial of 6 variables with 28 coefficients is fitted through a set of data points with the standard MINUIT program. Coefficients which are obtained from ANKE-GEANT simulations are then used to reconstruct momenta from measurements. The resolution of reconstructed momenta does not depend on the particle type.

Fig. 4 shows the reconstructed $\pi^+$ momenta, both for simulated and measured two-body events. It can be seen that the resolution for measured data is slightly worse than the value expected from the simulations. The difference is minimized by taking into account only events corresponding to a single START-STOP combination.
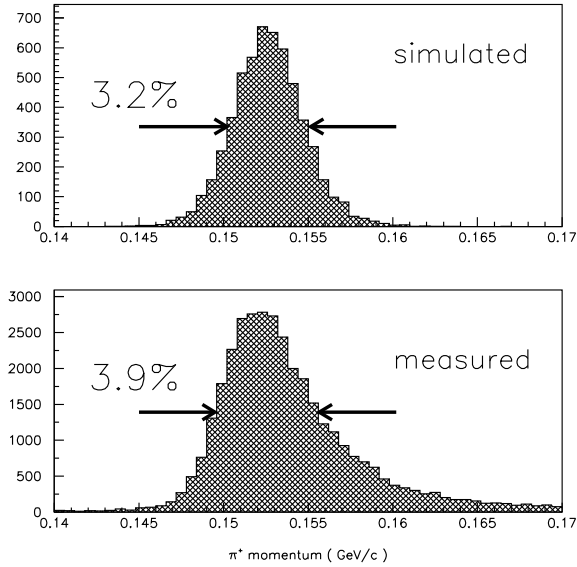
Fig. 4.   Simulated and measured (reconstructed) momenta of $\pi^+$ from the
0.861 GeV/$c$ $pp \to d\pi^+$ reaction. The coefficients were calculated for STOP #8
and START #7 and #8, then applied for all START's and STOP #8.

## REFERENCES

[1] S. Barsov *et al.*, *Nucl. Instrum. Methods Phys. Res.* **A462**, 364 (2001).

[2] M. Büscher *et al.*, *Nucl. Instrum. Methods Phys. Res.* **A**, in print.

[3] V. Koptev *et al.*, *Phys. Rev. Lett.* **87**, 022301 (2001).

[4] GEANT — Detector Description and Simulation Tool, CERN;
    ANKE-GEANT — http://www.fz-juelich.de/ikp/anke.

[5] H.J. Stein *et al.*, *Rev. Sci. Instrum.* **72**, 2003 (2001).

[6] S. Barsov *et al.*, *Acta Phys. Pol.* **B31**, 357 (2000).

# $a_0^+(980)$-Resonance Production in $pp \to dK^+\bar{K}^0$ Reactions Close to Threshold

V. Kleber,[1,*] M. Büscher,[1] V. Chernyshev,[2] S. Dymov,[1,3] P. Fedorets,[2] V. Grishina,[4] C. Hanhart,[1] M. Hartmann,[1]
V. Hejny,[1] A. Khoukaz,[5] H. R. Koch,[1] V. Komarov,[3] L. Kondratyuk,[2] V. Koptev,[6] N. Lang,[5] S. Merzliakov,[3]
S. Mikirtychiants,[6] M. Nekipelov,[1,6] H. Ohm,[1] A. Petrus,[3,†] D. Prasuhn,[1] R. Schleichert,[1] A. Sibirtsev,[1] H. J. Stein,[1]
H. Ströher,[1] K.–H. Watzlawik,[1] P. Wüstner,[7] S. Yaschenko,[3] B. Zalikhanov,[3] and I. Zychor[8]

[1]*Institut für Kernphysik, Forschungszentrum Jülich, 52425 Jülich, Germany*
[2]*Institute for Theoretical and Experimental Physics, Cheremushkinskaya 25, 117259 Moscow, Russia*
[3]*Laboratory of Nuclear Problems, Joint Institute for Nuclear Research, 141980 Dubna, Russia*
[4]*Institute for Nuclear Research, 60th October Anniversary Prospect 7A, 117312 Moscow, Russia*
[5]*Institut für Kernphysik, Universität Münster, W.-Klemm-Straße 9, 48149 Münster, Germany*
[6]*High Energy Physics Department, Petersburg Nuclear Physics Institute, 188350 Gatchina, Russia*
[7]*Zentralinstitut für Elektronik, Forschungszentrum Jülich, 52425 Jülich, Germany*
[8]*The Andrzej Soltan Institute for Nuclear Studies, 05400 Swierk, Poland*
(Received 6 May 2003; published 24 October 2003)

The reaction $pp \to dK^+\bar{K}^0$ has been investigated at an excess energy of $Q = 46$ MeV above the $K^+\bar{K}^0$ threshold with ANKE at the cooler synchrotron COSY-Jülich. From the detected coincident $dK^+$ pairs, about 1000 events with a missing $\bar{K}^0$ were identified, corresponding to a total cross section of $\sigma(pp \to dK^+\bar{K}^0) = [38 \pm 2(\text{stat}) \pm 14(\text{syst})]$ nb. Invariant-mass and angular distributions have been jointly analyzed and reveal $s$-wave dominance between the two kaons, accompanied by a $p$ wave between the deuteron and the kaon system. This is interpreted in terms of $a_0^+(980)$-resonance production.

One of the primary goals of hadronic physics is the description of the internal structure of mesons and baryons, their production and decays, in terms of quarks and gluons. However, the severe complications, related to nonperturbative contributions and confinement effects in QCD, mean that progress in understanding the structure of light hadrons has mainly been within models which use effective degrees of freedom. The constituent quark model is one of the most successful in this respect (see, e.g., [1]). This approach treats the lightest scalar resonances $a_0/f_0(980)$ as conventional $\bar{q}q$ states. However, the structure of these states seems to be more complicated and they have also been identified with $K\bar{K}$ molecules [2] or compact $qq$-$\bar{q}\bar{q}$ states [3]. It has even been suggested that at masses below 1.0 GeV a complete nonet of four-quark states might exist [4]. Possible deviations from the minimal quark model are also generating much interest in the baryon sector, where the recently discovered low-lying $\theta^+$ state in the $K^+n$ system [5] requires at least five quarks.

At the cooler synchrotron COSY-Jülich [6], an experimental program has been started, using the ANKE spectrometer [7], which aims at exclusive data on $a_0/f_0$ production from $pp$, $pn$, $pd$, and $dd$ interactions close to the $K\bar{K}$ threshold [8]. The final goal will be the extraction of the $a_0/f_0$ mixing amplitude to shed light on the nature of the light scalar resonances. Here, we report about the first exclusive study of the reaction $pp \to dK^+\bar{K}^0$, where some fraction of the kaon pairs is expected to stem from the decay of the $a_0^+$ resonance. The measurements were performed at a beam energy of $T_p =$

2.65 GeV ($p_p = 3.46$ GeV/$c$), corresponding to an excess energy of 46 MeV above the $K\bar{K}$ threshold.

The isovector $a_0(980)$ has been studied in $p\bar{p}$ annihilations [9], in $\pi^-p$ collisions [10], and $\gamma\gamma$ interactions [11]. Data on radiative $\phi$ decays [12,13] are interpreted in terms of $a_0/f_0$ production in the channels $\phi \to \gamma a_0/f_0 \to \gamma\pi^0\eta/\pi^0\pi^0$. In $pp$ reactions, the $a_0(980)$ has been seen at $T_p = 450$ GeV [14], and a resonant structure around 980 MeV/$c^2$ has been observed in inclusive $pp \to dX^+$ data at $p_p = 3.8$, 4.5, and 6.3 GeV/$c$ [15].

ANKE is located at an internal target position of COSY, which supplies stored proton beams with intensities up to $\sim 4 \times 10^{10}$. A $H_2$ cluster-jet target [16] has been used, providing areal densities of $\sim 5 \times 10^{14}$ cm$^{-2}$. The luminosity has been measured with the help of $pp$ elastic scattering events by detecting one fast proton concurrently recorded with the $dK^+$ data [17]. Protons in the angular range $\vartheta = 5.5°$–$9°$ have been selected, since the ANKE acceptance changes smoothly for these angles and the elastic peak in the momentum distribution is easily distinguished from the background. The average luminosity during the measurements has been determined to $L = [2.7 \pm 0.1(\text{stat}) \pm 0.7(\text{syst})] \times 10^{31}$ s$^{-1}$ cm$^{-2}$ corresponding to $L_{\text{int}} = 3.3$ pb$^{-1}$.

ANKE comprises three dipole magnets (D1-3), which guide the circulating COSY beam. The central C-shaped spectrometer dipole D2 downstream of the target separates the reaction products from the beam. The angular acceptance of D2 for kaons from $a_0^+$ decay is $|\vartheta_H| \leq 12°$ horizontally and $|\vartheta_V| \leq 3.5°$ vertically [18]. The angular acceptance for the fast deuterons ($p_d \sim 2100$ MeV/$c$) is

roughly $|\vartheta_H| \leq 10°$ and $|\vartheta_V| \leq 3.0°$ and depends on the momentum in the horizontal direction [19].

$K^+$ mesons are detected in range telescopes, located at the side of D2 along the focal surface, providing excellent kaon-versus-background discrimination, and were identified by means of time-of-flight (TOF) and energy-loss ($\Delta E$) measurements. Details of the procedure can be found in Ref. [18]. For our measurements, only some of the telescopes were used, covering the lower momentum range [$p_{K^+} = (390–625)$ MeV/$c$] of the $a_0^+$ decay $K^+$ mesons. Two multiwire proportional chambers (MWPCs) positioned in front of the telescopes allow one to deduce the ejectile momenta and to suppress scattered background [7,18]. Coincident fast particles and elastically scattered protons are detected in the ANKE forward-detection (FD) system consisting of two layers of scintillation counters for TOF and $\Delta E$ measurements as well as three MWPCs, each with two sensitive planes, for momentum reconstruction and background suppression [7,19].

Two bands from protons and deuterons are clearly seen in the time difference between the detection of a $K^+$ meson in one of the telescopes and a particle in the FD as a function of the FD particle momentum [see Fig. 1(a)]. The deuterons are selected with the criterion indicated by the dashed lines. In Fig. 1(b), the missing-mass distribution $m(pp, dK^+)$ for the selected $pp \rightarrow dK^+X$ events is presented. At $T_p = 2.65$ GeV, the missing particle $X$ must be a $\bar{K}^0$ due to charge and strangeness conservation. The measured $dK^+$ missing-mass distribution peaks at $m_{\bar{K}^0} = 498$ MeV/$c^2$, reflecting the clean particle identification. Approximately 1000 events within the gate indicated by the dashed arrows are accepted as $dK^+\bar{K}^0$ events for further analysis. The remaining background from misidentified particles is $(9 \pm 2)\%$.

The tracking efficiency for kaons in the side MWPCs has been determined by requiring TOF and $\Delta E$ of a kaon (and any particle in FD) and calculating the ratio of identified kaons (as peak in the TOF distribution) with and without demanding a reconstructed track. The effi-

ciency depends on the telescope number, i.e., $K^+$ momentum, and varies between 71% and 93%. The efficiency of the $\Delta E$ criterion for the $K^+$ mesons has been deduced with the help of simultaneously recorded $pp \rightarrow pK^+\Lambda$ events which, due to the significantly larger cross section, can be selected by TOF alone. This efficiency is independent of the telescope number and amounts to 52%. The FD MWPC efficiencies have been determined for each of the six sensitive planes individually from events with hits in all other five planes. The information from two horizontal (vertical) planes has been used to reconstruct the intersection point in the remaining plane and, subsequently, to determine the efficiency distribution across the chamber areas, i.e., the angular and momentum dependences. The average FD track efficiency for deuterons is 73%. The efficiency of the FD scintillators and all TOF criteria is larger than 99% [18]. The data have been corrected for all efficiencies on an event-by-event basis.

The differential acceptance of ANKE has been obtained with the Monte Carlo method described in Ref. [20], which allows one to determine the acceptance independently of the ejectile distributions at the production point. The acceptance is defined as a discrete function of the five relevant degrees of freedom in the three-body final state. For an unpolarized measurement, the acceptance can be expressed by a four-dimensional matrix with four independent kinematical variables. Two different matrices, each composed of 500 elements (see Table I) were used for the reconstruction of the invariant masses $m(K^+\bar{K}^0)$, $m(d\bar{K}^0)$, and the center-of-mass (cms) angular distributions $|\cos(pk)|$, $|\cos(pq)|$, and $\cos(kq)$ (for a definition see Fig. 2). Ninety million events following a phase-space distribution were simulated and tracked through ANKE, taking into account small angle scattering, decay in flight, and the MWPC resolutions. Subsequently, the mass and angular distributions have been corrected with the weights from the corresponding acceptance matrices on an event-by-event basis. The impact of the few acceptance holes has been investigated using distributions with different shapes in the masses and angles and is included in the systematic error of the differential distributions and the total cross section. The efficiency and acceptance corrected data are shown in Fig. 3 with statistical and systematic uncertainties.
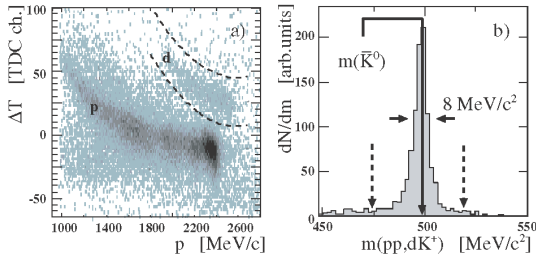


FIG. 1 (color online).   (a) Time difference between the fast forward going particles in layer 1 of the FD scintillators and the $K^+$ mesons versus the momentum of the forward particle. The dashed lines indicate the selection for deuteron identification. (b) Missing mass $m(pp, dK^+)$ distribution of the $pp \rightarrow dK^+X$ events.

TABLE I.   Variables (all in the overall cms) of acceptance matrices I (upper) and II (lower) and their number of bins. Matrices I and II are used for the correction of the mass and angular spectra, respectively. $\psi(K\bar{K})$ is the rotation angle of the decay plane around the direction of the deuteron momentum $\vec{k}$. The symmetry of the angular distributions around 90° with respect to the proton beam has been utilized.

| $m^2(K^+\bar{K}^0)$ | $m^2(d\bar{K}^0)$ | $|\cos(pk)|$ | $\psi(K\bar{K})$ |
|---|---|---|---|
| 5 | 5 | 5 | 4 |
| $|\cos(pk)|$ | $|\cos(pq)|$ | $\cos(kq)$ | $E(d)$ |
| 5 | 5 | 5 | 4 |

FIG. 2. Definition of the vectors $\vec{p}$, $\vec{k}$, and $\vec{q}$ in the cms of the reaction $pp \rightarrow dK^+\bar{K}^0$. Angular distributions with respect to the beam direction $\vec{p}$ have to be symmetric around 90° since the two protons in the entrance channel are indistinguishable.

The integrated acceptance of ANKE for the $dK^+\bar{K}^0$ events is 2.2%. Taking into account all correction factors, a total cross section of $\sigma(pp \rightarrow dK^+\bar{K}^0) = [38 \pm 2(\text{stat}) \pm 14(\text{syst})]$ nb has been derived.

The mass and angular resolutions for the spectra in Fig. 3 have been obtained from simulations and amount to $\delta m_{K^+\bar{K}^0} = (8-1)$ MeV/$c^2$ in the range (0.991–1.038) GeV/$c^2$, $\delta m_{d\bar{K}^0} \sim 3$ MeV/$c^2$ in the full mass range, and $\delta[\cos(\vartheta)] \sim 0.2$ for all angular spectra (FWHM values). The effect of these resolutions on the shape of the differential spectra is included in the systematic errors shown in Fig. 3. Because of the finite values of $\delta m$, some events lie outside the kinematical limits at $m(K^+\bar{K}^0) = 0.991$ and $m(d\bar{K}^0) = 2.420$ GeV/$c^2$ and have been excluded from the fit described below.

In the close-to-threshold regime, only a limited number of final states can contribute. If we restrict ourselves to the lowest partial waves, we need to consider either a $p$



FIG. 3. Angular and invariant mass distributions. The shaded areas correspond to the systematic uncertainties of the acceptance correction. The dashed (dotted) line corresponds to $K^+\bar{K}^0$ production in a relative $s$ ($p$) wave, and the solid line is the sum of both contributions. The overall errors from the luminosity determination are not included in the statistical and systematic uncertainties. The common fit with Eq. (1) to all spectra yields $\chi^2_{\text{ndf}} = 1.1$. The individual $\chi^2$ values are displayed in the corresponding panels.

wave in the $K\bar{K}$ system accompanied by an $s$ wave of the deuteron with respect to the meson pair or an $s$ wave $K\bar{K}$ with a $p$-wave deuteron. Selection rules do not allow for $s$ waves in both subsystems simultaneously. Under these assumptions, one may write for the square of the transition matrix element

$$|\bar{\mathcal{M}}|^2 = C_0^q q^2 + C_0^k k^2 + C_1(\hat{p} \cdot \vec{k})^2 + C_2(\hat{p} \cdot \vec{q})^2 \\ + C_3(\vec{k} \cdot \vec{q}) + C_4(\hat{p} \cdot \vec{k})(\hat{p} \cdot \vec{q}), \quad (1)$$

with $\hat{p} = \vec{p}/|\vec{p}|$. The parameters $C_i$ can be directly related to the eight allowed partial wave amplitudes, as was done, e.g., in Refs. [21–23]. Only $K\bar{K}$ $p$ waves contribute to $C_0^q$ and $C_2$, only $K\bar{K}$ $s$ waves to $C_0^k$ and $C_1$, and only $s$-$p$ interference terms to $C_3$ and $C_4$. Thus, a fit to the data supplies direct information on the relative strength of the different partial waves. The result of the fit is shown as the solid line in Fig. 3 and the corresponding parameters $C_i$ are displayed in Table II {note that from our spectra $C_3$ and $C_4$ cannot be extracted individually but only $[C_3 + (1/3)C_4]$}. The overall agreement between fit and data confirms the assumption that only the lowest partial waves contribute. The dashed lines in Fig. 3 depict the contributions from $K\bar{K}$ $s$ waves only ($C_0^q = C_2 = C_3 = C_4 = 0$) and the dotted line those from pure $K\bar{K}$ $p$ waves ($C_0^k = C_1 = C_3 = C_4 = 0$). Thus, we find that the reaction is dominated by the $K\bar{K}$ $s$ wave. The contribution from $K\bar{K}$ $p$ waves is less than 20%.

Since the $K\bar{K}$ $p$ waves prefer large masses, it is the slope at higher $K\bar{K}$ masses that sets an upper bound for the $p$-wave contribution. On the other hand, the slope of the $|\cos(pq)|$ distribution determines the minimum $p$-wave strength. Therefore, the contribution of $K\bar{K}$ $p$ waves is strongly constrained by the data. The deviation in $|\cos(pk)|$ might indicate a small contribution from a $d$ wave of the deuteron with respect to the $s$-wave meson pair. This $d$-wave contribution would have little influence on the shapes of the other measured distributions.

Since the excess energy is small and the nominal mass of the $a_0^+$ is very close to the $K\bar{K}$ threshold, the resonance cannot be seen as a clear structure in the invariant-mass spectra, but, in any case, the propagation of low energy $s$-wave $K\bar{K}$ pairs should be governed by the $a_0^+$ resonance due to the proximity of its pole to the $K\bar{K}$ threshold. This, together with the result of the fit, leads us to the conclusion that the reaction $pp \rightarrow dK^+\bar{K}^0$ at $T_p = 2.65$ GeV proceeds mainly via the $a_0^+$ resonance.

In Ref. [24], a model has been presented which describes both resonant, dominated by the direct $a_0$ production off a single nucleon, as well as nonresonant $K\bar{K}$

TABLE II. Result for the various coefficients of Eq. (1). All coefficients are given in units of GeV$^{-2}$.

| $C_0^q$ | $C_0^k$ | $C_1$ | $C_2$ | $C_3 + \frac{1}{3}C_4$ |
|---|---|---|---|---|
| $0 \pm 0.1$ | $0.89 \pm 0.03$ | $-0.5 \pm 0.1$ | $1.12 \pm 0.07$ | $-0.32 \pm 0.15$ |

FIG. 4. Predictions of the model of Ref. [24] in comparison to the experimental data. An overall scaling factor is included as described in the text.

production, driven by a $\pi$-$K^*$-$\pi$ exchange current. This current, due to $G$-parity conservation, generates the $K\bar{K}$ pair in a relative $p$ wave. The only free parameter of the model, an overall factor, was adjusted to higher energy data [15]. The predictions of this model for some of the spectra measured in this experiment are shown in Fig. 4. A scaling factor of 0.75 has been included in order to adjust the model results to the integrated cross section.

As can be seen from the figure, the model calculations agree with the data for $m(K^+\bar{K}^0)$ and $|\cos(pq)|$, the spectra which are most sensitive to the relative $s$- and $p$-wave contributions. The discrepancy in Fig. 4, left side, indicates that there might be another possible reaction mechanism involved. Here it is important to note that within the model from Ref. [24] the ratio of integrated resonant to nonresonant production cross section has very little sensitivity on the details of the $\cos(pk)$ distribution.

In summary, first, data on the reaction $pp \to dK^+\bar{K}^0$ close to the production threshold are presented. The total cross section for this reaction as well as differential distributions have been determined. Dominance of the $K\bar{K}$ $s$ wave ($>80\%$ of the total cross section) has been deduced based on a joint analysis of angular and invariant-mass spectra. This is clear evidence for a predominant resonant production via the $a_0^+(980)$. A comparison of the experimental data to model calculations [24] shows that the background ($K\bar{K}$ $p$ waves) can be understood in terms of a simple meson exchange current. Further theoretical investigations are necessary to identify the possible role of a strong $d\bar{K}$ interaction as proposed in Ref. [25]. Here both a measurement at higher energies and polarization experiments would be of great use. Our results demonstrate the feasibility of studying light scalar resonances in exclusive measurements close to the $K\bar{K}$ threshold with high mass resolution and low background using ANKE at COSY-Jülich.

*Present address: Institut für Kernphysik, Universität zu Köln, 50937 Köln, Germany.
Electronic address: v.kleber@fz-juelich.de
†Deceased.

[1] D. Morgan and M. R. Pennington, Phys. Rev. D **48**, 1185 (1993); A.V. Anisovich et al., Eur. Phys. J. A **12**, 103 (2001); S. Narison, hep-ph/0012235.
[2] J. Weinstein and N. Isgur, Phys. Rev. D **41**, 2236 (1990); G. Janssen et al., Phys. Rev. D **52**, 2690 (1995); J. A. Oller and E. Oset, Nucl. Phys. **A620**, 438 (1997); **652**, 407(E) (1999).
[3] N. N. Achasov, hep-ph/0201299; R. J. Jaffe, Phys. Rev. D **15**, 267 (1977); J. Vijande et al., in Proceedings of the International Workshop MESON 2002, Cracow, Poland (World Scientific, Singapore, 2002); hep-ph/0206263.
[4] F. E. Close and N. A. Törnqvist, J. Phys. G **28**, R249 (2002).
[5] T. Nakano et al., Phys. Rev. Lett. **91**, 012002 (2003).
[6] R. Maier, Nucl. Instrum. Methods Phys. Res., Sect. A **390**, 1 (1997).
[7] S. Barsov et al., Nucl. Instrum. Methods Phys. Res., Sect. A **462**, 364 (2001).
[8] M. Büscher et al., Proceedings of the International Workshop Physics at COSY, Jülich, 2002 (hep-ph/0301126).
[9] A. Abele et al., Phys. Lett. B **327**, 425 (1994); A. Abele et al., Phys. Rev. D **57**, 3860 (1998); A. Bertin et al., Phys. Lett. B **434**, 180 (1998).
[10] S. Teige et al., Phys. Rev. D **59**, 012001 (1999).
[11] P. Achard et al., Phys. Lett. B **526**, 269 (2002).
[12] N. N. Achasov et al., Phys. Lett. B **485**, 349 (2000); Phys. Lett. B **479**, 53 (2000).
[13] A. Aloisio et al., Phys. Lett. B **536**, 209 (2002); Phys. Lett. B **537**, 21 (2002).
[14] D. Baberis et al., Phys. Lett. B **440**, 225 (1998); Phys. Lett. B **488**, 225 (2000).
[15] M. A. Abolins et al., Phys. Rev. Lett. **25**, 469 (1970).
[16] A. Khoukaz et al., Eur. Phys. J. D **5**, 275 (1999).
[17] P. Fedorets and V. Kleber, Proceedings of the International Conference on Quarks and Nuclear Physics 2002, Jülich, Germany [Eur. Phys. J. (to be published)].
[18] M. Büscher et al., Nucl. Instrum. Methods Phys. Res., Sect. A **481**, 378 (2002).
[19] V. Komarov et al., Phys. Lett. B **553**, 179 (2003).
[20] F. Balestra et al., Phys. Rev. C **63**, 024004 (2001).
[21] V. Yu. Grishina et al., Phys. Lett. B **521**, 217 (2001).
[22] V. Chernyshev et al., nucl-th/0110069.
[23] A. E. Kudryavtsev et al., Phys. Rev. C **66**, 015207 (2002).
[24] V. Yu. Grishina et al., in Proceedings of the International Workshop MESON 2002, Cracow, Poland (Ref. [3], p. 465).
[25] E. Oset et al., Eur. Phys. J. A **12**, 435 (2001).

172304-4          172304-4

## ELEMENTARY PARTICLES AND FIELDS
### Theory

# $a_0^+(980)$-Resonance Production in the Reaction $pp \to d\pi^+\eta$ Close to the $K\bar{K}$ Threshold*

**P. V. Fedorets**[1),2)], **M. Büscher**[1)], **V. P. Chernyshev**[2)], **S. N. Dymov**[1),3)],
**V. Yu. Grishina**[4)], **C. Hanhart**[1)], **M. Hartmann**[1)], **V. Hejny**[1)], **V. Kleber**[5)],
**H. R. Koch**[1)], **L. A. Kondratyuk**[2)], **V. P. Koptev**[6)], **A. E. Kudryavtsev**[2)], **P. Kulessa**[1),7)],
**S. I. Merzliakov**[3)], **S. M. Mikirtychiants**[6)], **M. E. Nekipelov**[1),6)], **H. Ohm**[1)],
**R. Schleichert**[1)], **H. Ströher**[1)], **V. E. Tarasov**[2)], **K.-H. Watzlawik**[1)], and **I. Zychor**[8)]

**Abstract**—The reaction $pp \to d\pi^+\eta$ has been measured at a beam energy of $T_p = 2.65$ GeV ($p_p = 3.46$ GeV/$c$) using the ANKE spectrometer at COSY-Jülich. The missing-mass distribution of the detected $d\pi^+$ pairs exhibits a peak around the $\eta$ mass on top of a strong background of multipion $pp \to d\pi^+(n\pi)$ events. The differential cross section $d^4\sigma/d\Omega_d d\Omega_{\pi^+} dp_d dp_{\pi^+}$ for the reaction $pp \to d\pi^+\eta$ has been determined model independently for two regions of phase space. Employing a dynamical model for the $a_0^+$ production allows one then to deduce a total cross section of $\sigma(pp \to da_0^+ \to d\pi^+\eta) = 1.1 \pm 0.3_{\rm stat} \pm 0.7_{\rm syst}$ $\mu$b for the production of $\pi^+\eta$ via the scalar $a_0^+(980)$ resonance and $\sigma(pp \to d\pi^+\eta) = 3.5 \pm 0.3_{\rm stat} \pm 1.0_{\rm syst}$ $\mu$b for the nonresonant production. Using the same model as for the interpretation of recent results from ANKE for the reaction $pp \to dK^+\bar{K}^0$, the ratio of the total cross sections is $\sigma(pp \to d(K^+\bar{K}^0)_{L=0})/\sigma(pp \to da_0^+ \to d\pi^+\eta) = 0.029 \pm 0.008_{\rm stat} \pm 0.009_{\rm syst}$, which is in agreement with branching ratios in the literature.

PACS numbers : `13.75.Cs, 25.40.Ve`
**DOI:** `10.1134/S1063778806020153`

## 1. INTRODUCTION

One of the primary goals of hadronic physics is the understanding of the internal structure of mesons and baryons and their production and decay, in terms of quarks and gluons. The nonperturbative character of the underlying theory—quantum chromodynamics (QCD)—hinders straightforward calculations. QCD can be treated explicitly in the low-momentum-transfer regime using lattice techniques [1], which are, however, not yet in the position to make quantitative statements about the light scalar mesons. Alternatively, QCD-inspired models which employ effective degrees of freedom can be used. The constituent quark model is one of the most successful in this respect (see, e.g., [2]). This approach treats the lightest scalar resonances $a_0/f_0(980)$ as conventional $q\bar{q}$ states.

However, more states with quantum numbers $J^P = 0^+$ have been identified experimentally than would fit into a single $SU(3)$ scalar nonet: the $f_0(600)$ (or $\sigma$), $f_0(980)$, $f_0(1370)$, $f_0(1500)$, and $f_0(1710)$ with $I = 0$; the $\kappa(800)$ and $K^*(1430)$ with $I = 1/2$; and the $a_0(980)$ and $a_0(1450)$ with $I = 1$ [3]. Consequently, the $a_0/f_0(980)$ have also been associated with $K\bar{K}$ molecules [4] or compact $qq-\bar{q}\bar{q}$ states [5]. It has even been suggested that a complete nonet of four-quark states might exist with masses below $1.0$ GeV/$c^2$ [6].

The first clear observation of the isovector $a_0(980)$

---

*The text was submitted by the authors in English.

[1)]Institut für Kernphysik, Forschungszentrum Jülich, Germany.

[2)]Institute for Theoretical and Experimental Physics, Bol'shaya Cheremushkinskaya ul. 25, Moscow, 117218 Russia.

[3)]Joint Institute for Nuclear Research, Dubna, Moscow oblast, 141980 Russia.

[4)]Institute for Nuclear Research, Russian Academy of Sciences, pr. Shestidesyatiletiya Oktyabrya 7a, Moscow, 117312 Russia.

[5)]Institut für Kernphysik, Universität zu Köln, Germany.

[6)]Petersburg Nuclear Physics Institute, Gatchina, 188350 Russia.

[7)]The Henryk Niewodniczański Institute of Nuclear Physics, Cracow, Poland.

[8)]The Andrzej Soltan Institute for Nuclear Studies, Swierk, Poland.
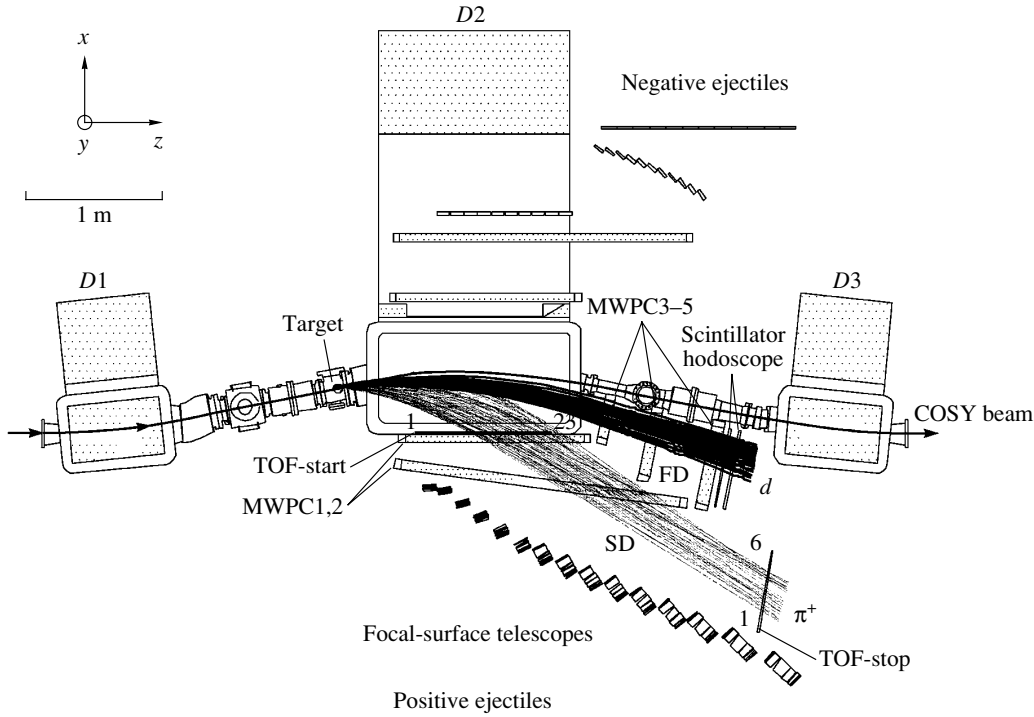
**Fig. 1.** Top view of the ANKE spectrometer and simulated tracks of pions and deuterons from $pp \to d\pi^+\eta$ events.

resonance was achieved in $K^-p$ interactions [7], and in subsequent experiments, it has also been seen in $p\bar{p}$ annihilations [8], in $\pi^-p$ collisions [9], and in $\gamma\gamma$ interactions [10]. Experiments on radiative $\phi$ decays [11, 12] have been analyzed in terms of the $a_0/f_0$ production in the decay chain $\phi \to \gamma a_0/f_0 \to \gamma\pi^0\eta/\pi^0\pi^0$. In $pp$ collisions, the $a_0(980)$ resonance has been measured at $p_p = 450$ GeV/$c$ via $f_1(1285) \to a_0^\pm\pi^\mp$ decays [13] and in inclusive measurements of the $pp \to dX^+$ reaction at $p_p = 3.8$, 4.5, and 6.3 GeV/$c$ [14]. Despite these many experimental results, the properties of the $a_0(980)$ resonance are still far from being established. The Particle Data Group [3] gives a mass of $m_{a_0} = 984.7 \pm 1.2$ MeV/$c^2$ and a width of $\Gamma_{a_0} = 50-100$ MeV/$c^2$. The main decay channels, $\pi\eta$ and $K\bar{K}$, are quoted as "dominant" and "seen," respectively.

An experimental program has been started at the Cooler Synchrotron COSY, Jülich [15], aiming at exclusive data on the $a_0/f_0$ production from $pp$, $pn$, $pd$, and $dd$ interactions at energies close to the $K\bar{K}$ threshold [16]. The final goal of these investigations is the extraction of the $a_0/f_0$-mixing amplitude, a quantity which is believed to shed light on the nature of these resonances [17, 18]. As a first stage,

the reaction $pp \to dK^+\bar{K}^0$ has been measured at $T_p = 2.65$ GeV, corresponding to an excess energy of $Q = 46$ MeV above the $K^+\bar{K}^0$ threshold, using the ANKE spectrometer [19]. The data, which have been decomposed into partial waves, show that more than 80% of the kaons are produced in a relative $s$ wave, corresponding to the $a_0^+$ channel [20]. In this paper, we report on the analysis of the reaction $pp \to d\pi^+\eta$, which was measured in parallel.

## 2. THE ANKE SPECTROMETER AND DATA ANALYSIS

Figure 1 shows the layout of ANKE. It consists of three dipole magnets $D1-D3$, installed at an internal target position of COSY. $D1$ and $D3$ deflect the circulating COSY beam from and back into the nominal orbit. The $C$-shaped spectrometer dipole $D2$ separates forward-going reaction products from the COSY beam. The angular acceptance of ANKE covers $|\theta_h| \leq 10°$ horizontally and $|\theta_v| \leq 3°$ vertically for the detected deuterons ($p_d > 1300$ MeV/$c$) and $|\theta_h| \leq 12°$ and $|\theta_v| \leq 3.5°$ for the pions. An $H_2$ cluster-jet target [21] placed between $D1$ and $D2$ was used, providing areal densities of $\sim 5 \times 10^{14}$ cm$^{-2}$. The luminosity was measured using $pp$
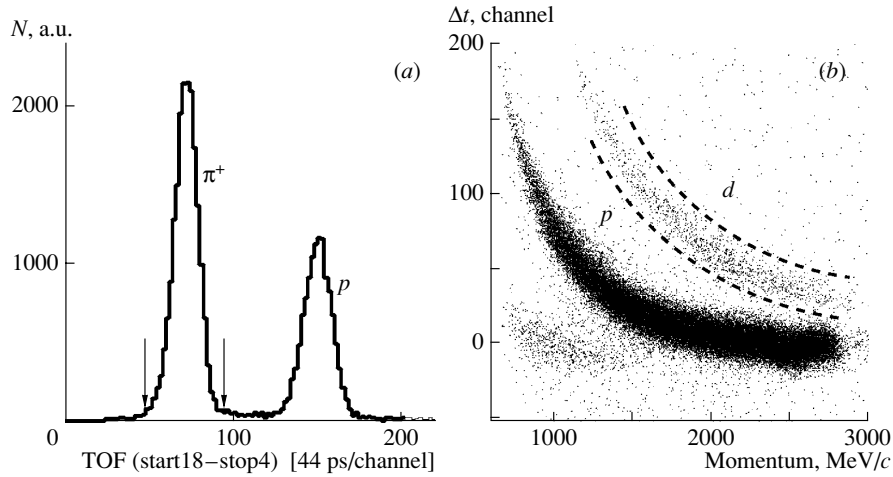
**Fig. 2.** (*a*) Time-of-flight of particles detected in TOF-start counter 18 and TOF-stop counter 4; (*b*) time difference $\Delta t$ between fast forward-going particles in the FD and $\pi^+$ mesons as a function of the momentum of the forward particle. The dashed curves indicate the criteria for deuteron identification.
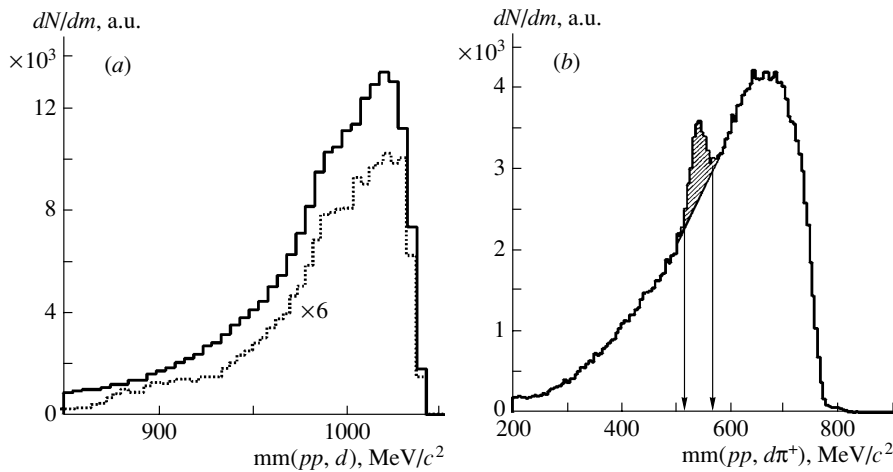


**Fig. 3.** Missing-mass distributions (*a*) mm($pp, d$) and (*b*) mm($pp, d\pi^+$) for the reaction $pp \rightarrow d\pi^+ X$. The dotted histogram in mm($pp, d$) (scaled by a factor of 6) corresponds to the selected area around the $\eta$ peak (530−560 MeV/$c^2$) in mm($pp, d\pi^+$) (indicated by arrows).

elastic scattering, recorded simultaneously with the $d\pi^+$ data. Protons in the angular range $\theta = 5.5°−9°$ were selected, since the ANKE acceptance changes smoothly in this region and the elastic peak is easily distinguished from the background in the momentum distribution. The average luminosity during the measurements was determined as $L = (2.7 \pm 0.1_{\text{stat}} \pm 0.7_{\text{syst}}) \times 10^{31}$ s$^{-1}$ cm$^{-2}$, corresponding to an integrated value of $L_{\text{int}} = 3.3$ pb$^{-1}$ at a proton beam intensity of up to $\sim 4 \times 10^{10}$.

Two charged particles, $\pi^+$ and $d$, were detected

in coincidence. Their trajectories, simulated with the ANKE-GEANT program package [22], are shown in Fig. 1. Positively charged pions in the momentum range $p_\pi = 600−1100$ MeV/$c$ were identified in the side detection system (SD) [19, 23], consisting of one layer of 23 start time-of-flight (TOF) scintillation counters, two multiwire proportional chambers (MWPCs), and one layer of six counters for TOF stop. These pions were selected by a TOF technique (Fig. 2*a*). The fast deuterons with momenta $p_d = 1300−2800$ MeV/$c$ (and elastically scattered protons

Differential production cross sections for the reaction $pp \to d\pi^+\eta$; for both regions of phase space, where $a_0^+$ and nonresonant $\pi^+\eta$ production contribute (for the momentum range $p_d = 1.4-1.6$ GeV/$c$, the nonresonant $\pi^+\eta$ production should be dominant, because this momentum range corresponds to low masses of the $\pi^+\eta$ system, where the $a_0^+$ production is suppressed)

| $d^4\sigma/d\Omega_d d\Omega_{\pi^+} dp_d dp_{\pi^+}$, $\mu$b/(sr GeV/$c$)$^2$ | Variables, lab. system | | |
|---|---|---|---|
| | $\theta_y$, deg | $\theta_x$, deg | $p$, GeV/$c$ |
| | Deuteron | | |
| $71 \pm 6_{\text{stat}} \pm 20_{\text{syst}}$ | $(-3°, +3°)$ | $(-3.5°, +3.5°)$ | $(1.4, 1.6)$ |
| | Pion | | |
| | $(-4°, +4°)$ | $(-11°, -3°)$ | $(0.65, 0.95)$ |
| | Deuteron | | |
| $30 \pm 4_{\text{stat}} \pm 9_{\text{syst}}$ | $(-3°, +3°)$ | $(-6°, -2°)$ | $(1.8, 2.7)$ |
| | Pion | | |
| | $(-4°, +4°)$ | $(-11°, -3°)$ | $(0.65, 0.95)$ |

with $p_p \approx 3400$ MeV/$c$) hit the forward detection system (FD)[19, 24], which included three MWPCs and two layers of scintillation counters. Two-dimensional distributions $\Delta t$ vs. momenta of forward particles were used for the deuteron identification; $\Delta t$ was calculated as the time difference between the detection of a pion in the TOF-stop counter and a fast forward-going particle in the first layer of the FD scintillators. Two distinct bands corresponding to protons and deuterons are seen in this distribution (Fig. 2$b$). The selection of deuterons was achieved by cutting along the deuteron band.

The tracking efficiency for pions in the SD MWPCs was calculated as the ratio of particles in the proper TOF range with and without requiring a reconstructed track. The efficiency depended on the SD stop-counter number (i.e., $\pi^+$ momentum) and varied between 53 and 76%. For the FD MWPCs, the efficiency was determined for each of the six sensitive planes (two per chamber). At least two vertical and horizontal planes were demanded for track reconstruction and for the calculation of the intersection point with the remaining plane. Each plane was divided in $20 \times 20$ subcells, and the efficiency of each cell was calculated from the presence and absence of a hit in the reconstructed intersection. The average FD MWPC track efficiency for deuterons was 73%. The efficiencies of the scintillators and TOF criteria were larger than 99% [23]. The efficiency correction is done on an event-by-event basis.

## 3. RESULTS FOR THE REACTION $pp \to d\pi^+\eta$

The missing-mass distributions mm$(pp, d)$ and mm$(pp, d\pi^+)$ for the selected $d\pi^+$ pairs are presented in Fig. 3. In the $(pp, d\pi^+)$ missing-mass distribution, a clear peak is observed around $m(\eta) = 547$ MeV/$c^2$

with about 6200 events. The peak sits on top of a smooth background from multipion production $pp \to d\pi^+(n\pi)$ $(n \geq 2)$. After selecting the mass range $530-560$ MeV/$c^2$ around the $\eta$ peak, the missing-mass spectrum mm$(pp, d)$ exhibits a shoulder at 980 MeV/$c^2$ (Fig. 3$a$, dotted histogram), where the peak from the $a_0^+(980)$ resonance is expected.

The table presents the differential cross sections for $pp \to d\pi^+\eta$ for two regions of phase space where the acceptance of ANKE is essentially 100% for this reaction. Six variables in the laboratory system have been chosen to describe these rectangular areas: the vertical ($\theta_y$) and horizontal ($\theta_x$) angles and momenta of the two detected particles, deuteron and $\pi^+$. These angles are defined as $\tan(\theta_y) = p_y/p_z$, $\tan(\theta_x) = p_x/p_z$.

Unfortunately, owing to the limited phase-space coverage of ANKE, a partial-wave decomposition of the type performed in [20] is not possible in this case. Thus, in order to interpret the data in terms of $a_0^+$ and nonresonant $\pi^+\eta$ production, we need to employ a model. This investigation will be described in the next section.

## 4. INTERPRETATION OF THE RESULTS

The $d\pi^+\eta$ final state can be produced via the $a_0^+$ resonance, $pp \to da_0^+ \to d\pi^+\eta$ (resonant production), or through the direct reaction $pp \to d\pi^+\eta$ (nonresonant production). The production mechanism for the $a_0^+$ has been studied theoretically in [25–29]. According to [25, 26], the cross section for $a_0^+$ production at $T_p = 2.65$ GeV is expected to be $\sim 1$ $\mu$b, while,
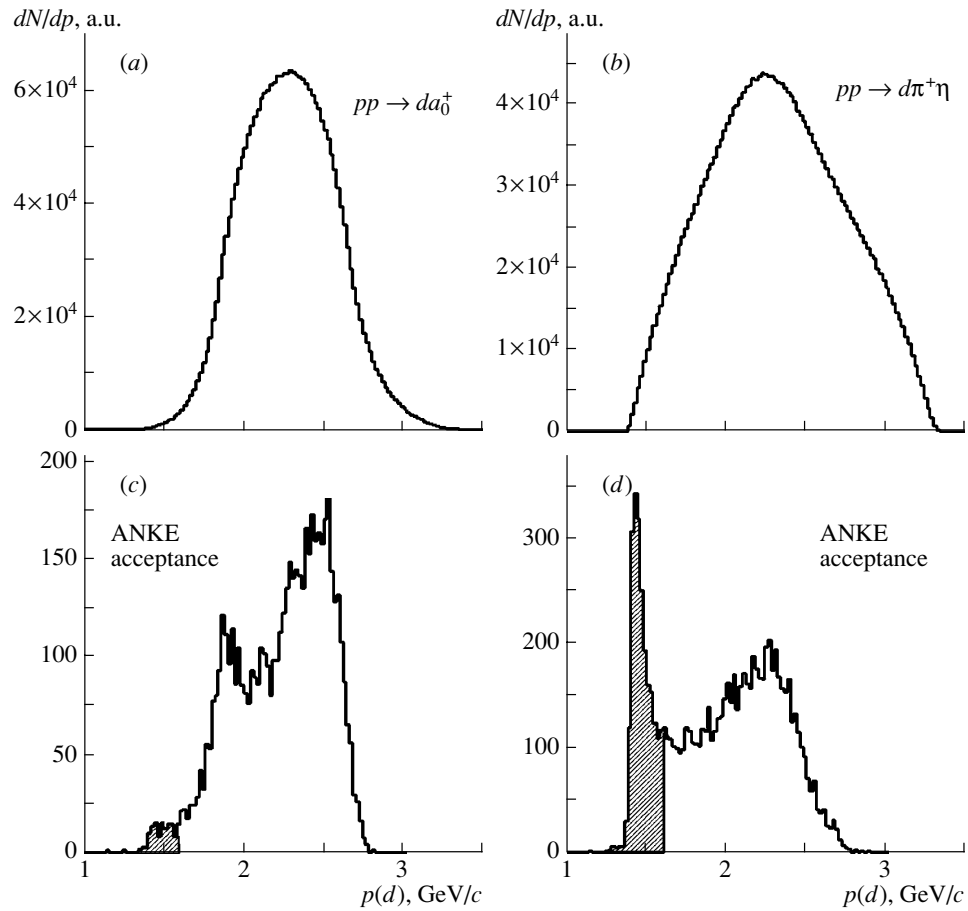
**Fig. 4.** Simulated acceptance for the deuteron momentum for the (*a*, *c*) resonant and (*b*, *d*) nonresonant $\pi^+\eta$ production. Upper row: the initial model distributions [29, 31−33]; lower row: momentum distributions within the ANKE acceptance.
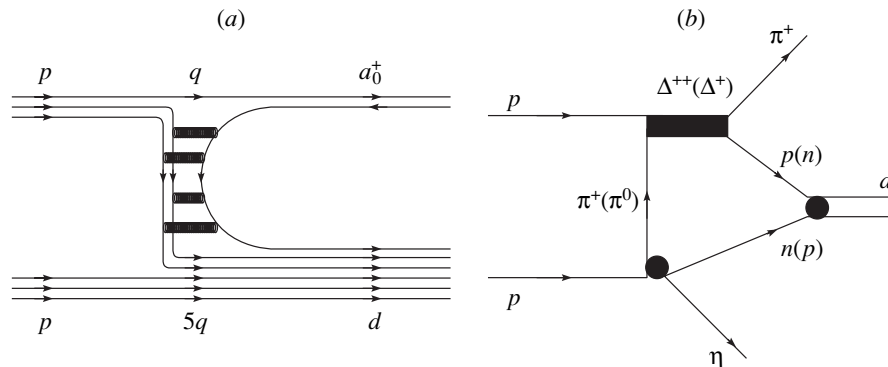


**Fig. 5.** Diagrams describing the (*a*) resonant $\pi^+\eta$ production within the QGSM [32] and (*b*) nonresonant production via $N^*$ and $\Delta$ excitations [29, 31, 33].
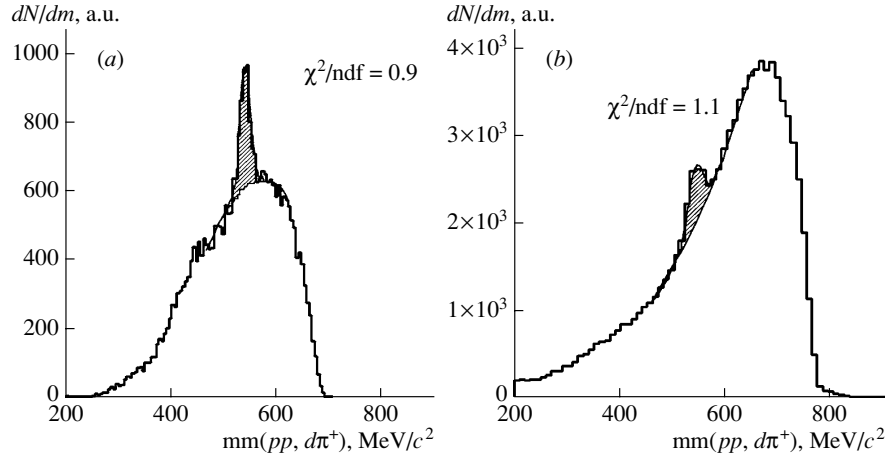
**Fig. 6.** Missing-mass distribution $mm(pp, d\pi^+)$ for the momentum ranges (a) $p_d = 1.4-1.6$ GeV/$c$ and (b) $p_d = 1.6-2.8$ GeV/$c$.
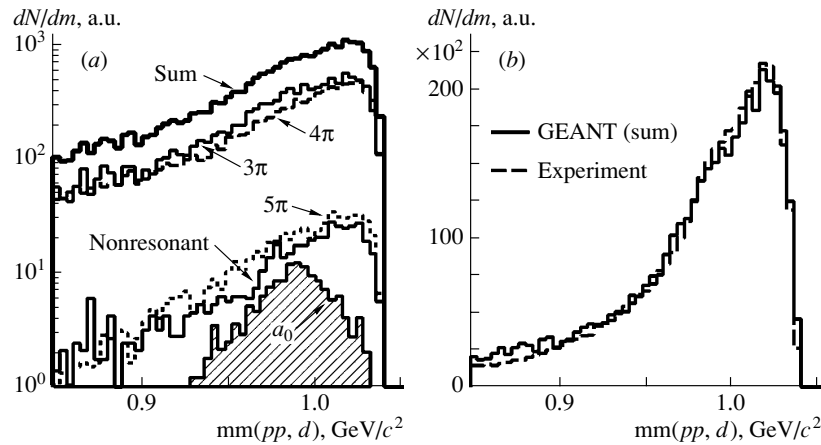


**Fig. 7.** (a) GEANT simulations for multipion background ($pp \to d\pi^+(n\pi)$ ($n \geq 2$)) and for resonant and nonresonant production of the $d\pi^+\eta$ final state in the ANKE acceptance; (b) comparison between the simulated missing-mass distribution $mm(pp, d)$ and experimental data.

for the nonresonant $\pi^+\eta$ production, different predictions exist, ranging from 0.6–1.4 $\mu$b [30] and 1.6–3.3 $\mu$b [31] up to one order of magnitude more [26].

The differential cross sections from the table contain contributions from both the resonant and the nonresonant reactions. We have performed a model-dependent analysis using the calculated momentum distributions of the produced deuterons (see Figs. 4a, 4b). The calculations are based on models describing the resonant process within the quark–gluon string model (QGSM) (Fig. 5a) [32] and the nonresonant (Fig. 5b) production via $N^*$- and $\Delta$-resonance excitation [29, 31, 33]. The momentum distribution for the resonant reaction is narrower, because low ($\pi^+\eta$)

masses are suppressed for $a_0^+$ production. The momentum distributions within the ANKE acceptance are shown in Figs. 4c and 4d.

Within the models, the nonresonant background has a negligible $\pi\eta$ $s$-wave contribution and thus does not interfere with the resonant amplitude. As a consequence, in the range $p_d = 1.4-1.6$ GeV/$c$, the contribution of the nonresonant process dominates, whereas the resonant part is negligibly small (see shaded areas in Figs. 4c, 4d). Thus, the cross section of the nonresonant contribution in this momentum range can be defined by fitting the $\eta$ peak in $mm(pp, d\pi^+)$ (Fig. 6a) and extracting the number
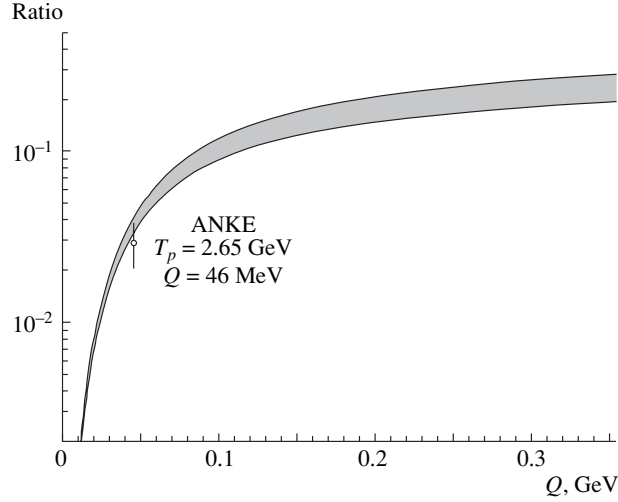
Ratio



**Fig. 8.** Ratio of the total cross sections $\sigma(a_0^+ \to K^+\bar{K}^0)/\sigma(a_0^+ \to \pi^+\eta)$ as function of $Q$. The error bar shows the statistical error only.

of $d\pi^+\eta$ events. The missing-mass spectra have been described by the sum of a Gaussian distribution and a fourth-order polynomial.

In the momentum range $p_d = 1.6{-}2.8$ GeV/$c$, where both the resonant and nonresonant reactions contribute, it is possible to calculate the number of events from the nonresonant production taking into account the different acceptances. Then the number of $a_0^+$ events is the difference between the total number of events under the $\eta$ peak (Fig. 6$b$) and the calculated number of nonresonant $\pi^+\eta$ events.

Including all corrections, total cross sections $\sigma_{a_0} = 1.1 \pm 0.3_{\mathrm{stat}} \pm 0.7_{\mathrm{syst}}$ $\mu$b for the $a_0^+$ production and $\sigma_{\mathrm{nr}} = 3.5 \pm 0.3_{\mathrm{stat}} \pm 1.0_{\mathrm{syst}}$ $\mu$b for the nonresonant $\pi^+\eta$ production have been obtained. It is obvious that these numbers could change if different assumptions were made on the partial-wave decomposition of the (non)resonant contributions. However, here, we refrain from investigating further the uncertainty induced by the model assumptions.

Figure 7$a$ presents the results of GEANT simulations of the ANKE acceptance for multipion background $(pp \to d\pi^+(n\pi)$ $(n \geq 2))$ and for resonant and nonresonant production of the $d\pi^+\eta$ final state. The number of initial events for each reaction is proportional to the known cross sections for multipion production [34] and the values of the total cross sections for the resonant and nonresonant $\pi^+\eta$ production given above. The shape of the simulated missing-mass distribution mm$(pp, d)$ including all channels is in good agreement with the experimental data (Fig. 7$b$).

Data for the second $a_0^+$-decay channel, $a_0^+ \to K^+\bar{K}^0$, have been obtained at ANKE in the reaction $pp \to da_0^+ \to dK^+\bar{K}^0$, simultaneously with the $\pi^+\eta$ data. The measured total cross section is $\sigma(pp \to dK^+\bar{K}^0) = 38 \pm 2_{\mathrm{stat}} \pm 14_{\mathrm{syst}}$ nb and the contribution of the $(K^+\bar{K}^0)_{L=0}$ channel is $\sim$83% [20]. Assuming that $s$-wave $K^+\bar{K}^0$ production proceeds fully via the $a_0^+(980)$ resonance, in accordance with the predictions of the models discussed above, the ratio of the total cross sections is $R = \sigma(a_0^+ \to (K^+\bar{K}^0)_{L=0})/\sigma(a_0^+ \to \pi^+\eta) = 0.029 \pm 0.008_{\mathrm{stat}} \pm 0.009_{\mathrm{syst}}$.

For measurements at an excess energy $Q \gg \Gamma_{a_0} \sim 50{-}100$ MeV, the ratio of the total cross sections $R = \sigma(a_0^+ \to K^+\bar{K}^0)/\sigma(a_0^+ \to \pi^+\eta)$ should not depend upon $Q$. However, when $Q$ is of the order of $\Gamma_{a_0}$, the contribution from the $a_0^+ \to K^+\bar{K}^0$ decay channel decreases more strongly owing to the proximity of the $K^+\bar{K}^0$ threshold and the consequently limited available phase space. The calculated ratio of the two cross sections as a function of $Q$ is presented in Fig. 8. The calculation is normalized to $R((K\bar{K})/(\pi\eta)) = 0.23 \pm 0.05$, which has been measured at Crystal Barrel in the reaction $p\bar{p} \to a_0\pi$ at $Q = 768$ MeV [35]. The parameters of the Flatté distribution [36] $m_0 = 999 \pm 2$ MeV/$c^2$, $g_{\pi\eta} = 324 \pm 15$ MeV, and $r = g_{KK}^2/g_{\pi\eta}^2 = 1.03 \pm 0.14$ are also taken from [35]. The errors of the Flatté parameters define the range of possible $R$ values (shaded area in Fig. 8). Our result is in agreement with the calculated value.

## 5. CONCLUSIONS

To summarize, data on the reaction $pp \rightarrow d\pi^+\eta$ at $T_p = 2.65$ GeV are presented. Differential cross sections for limited regions of phase space corresponding to forward emission of the $d$ and $\pi^+$ in the laboratory system have been extracted. Dynamical models for the reaction were employed to obtain the total cross sections for the resonant $\pi^+\eta$ production via the $a_0^+(980)$ and for the nonresonant $\pi^+\eta$ channel. For $a_0^+$ production, the value for the total cross section $pp \rightarrow da_0^+ \rightarrow d\pi^+\eta$ is in agreement with theoretical predictions based on the value for the $pp \rightarrow d(K^+\bar{K}^0)_{L=0}$ reaction recently measured at ANKE [20] and the branching ratio $\mathrm{BR}(K\bar{K}/\pi\eta)$ from the literature.

Our results, together with those from ANKE on the decay channel $a_0^+ \rightarrow K^+\bar{K}^0$, are the first evidence for $a_0^+$ production in $pp$ collisions, obtained in a simultaneous exclusive measurement of both $a_0^+$ decay channels.

## REFERENCES

1. T. Kunihiro *et al.* (SCALAR Collab.), hep-ph/0308291.
2. D. Morgan, Phys. Lett. B **51**, 71 (1974); K. L. Au, D. Morgan, and M. R. Pennington, Phys. Rev. D **35**, 1633 (1987); D. Morgan and M. R. Pennington, Phys. Lett. B **258**, 444 (1991); Phys. Rev. D **48**, 1185 (1993); A. V. Anisovich *et al.*, Eur. Phys. J. A **12**, 103 (2001); S. Narison, hep-ph/0012235.
3. Review of Particle Physics (S. Eidelman *et al.*), Phys. Lett. B **592**, 1 (2004).
4. J. Weinstein and N. Isgur, Phys. Rev. Lett. **48**, 659 (1982); Phys. Rev. D **27**, 588 (1983); **41**, 2236 (1990); G. Janssen *et al.*, Phys. Rev. D **52**, 2690 (1995); J. A. Oller and E. Oset, Nucl. Phys. A **620**, 438 (1997); **652**, 407 (E) (1999).
5. N. N. Achasov, hep-ph/0201299; R. J. Jaffe, Phys. Rev. D **15**, 267 (1977); J. Vijande *et al.*, in *Proceedings of the 7th International Workshop "MESON 2002"* (World Sci., Cracow, 2002), p. 501; hep-ph/0206263.
6. F. E. Close and N. A. Törnqvist, J. Phys. G **28**, R249 (2002).
7. J. B. Gay *et al.*, Phys. Lett. B **63**, 220 (1976).
8. A. Abele *et al.*, Phys. Lett. B **327**, 425 (1994); Phys. Rev. D **57**, 3860 (1998); A. Bertin *et al.*, Phys. Lett. B **434**, 180 (1998).
9. S. Teige *et al.*, Phys. Rev. D **59**, 012001 (1999).
10. P. Achard *et al.*, Phys. Lett. B **526**, 269 (2002).
11. N. N. Achasov *et al.*, Phys. Lett. B **485**, 349 (2000); **479**, 53 (2000).
12. A. Aloisio *et al.*, Phys. Lett. B **536**, 209 (2002); **537**, 21 (2002).
13. D. Barberis *et al.*, Phys. Lett. B **440**, 225 (1998); **488**, 225 (2000).
14. M. A. Abolins *et al.*, Phys. Rev. Lett. **25**, 469 (1970).
15. R. Maier, Nucl. Instrum. Methods Phys. Res. A **390**, 1 (1997).
16. M. Büscher, Acta Phys. Pol. B **35**, 1055 (2004).
17. C. Hanhart, Phys. Rep. **397**, 155 (2004).
18. N. N. Achasov *et al.*, Phys. Lett. B **88**, 367 (1979).
19. S. Barsov *et al.*, Nucl. Instrum. Methods Phys. Res. A **462**, 364 (2001).
20. V. Kleber *et al.*, Phys. Rev. Lett. **91**, 172304 (2003).
21. R. Santo *et al.*, Nucl. Instrum. Methods Phys. Res. A **386**, 228 (1997); A. Khoukaz *et al.*, Eur. Phys. J. D **5**, 275 (1999).
22. I. Zychor, Acta Phys. Pol. B **33**, 521 (2002).
23. M. Büscher *et al.*, Nucl. Instrum. Methods Phys. Res. A **481**, 378 (2002).
24. V. Komarov *et al.*, Phys. Lett. B **553**, 179 (2003).
25. V. Y. Grishina *et al.*, Phys. Lett. B **521**, 217 (2001).
26. H. Müller, Eur. Phys. J. A **11**, 113 (2001).
27. E. Oset *et al.*, Eur. Phys. J. A **12**, 435 (2001).
28. E. L. Bratkovskaya *et al.*, J. Phys. G **28**, 2423 (2002).
29. L. A. Kondratyuk *et al.*, Yad. Fiz. **66**, 155 (2003) [Phys. At. Nucl. **66**, 152 (2003)].
30. V. E. Tarasov and A. E. Kudryavtsev, private communication.
31. V. Y. Grishina *et al.*, Annual Report 2000 of the IKP, FZ Jülich, p. 30.
32. V. Y. Grishina *et al.*, Eur. Phys. J. A **21**, 507 (2004).
33. A. E. Kudryavtsev *et al.*, Yad. Fiz. **66**, 1994 (2003) [Phys. At. Nucl. **66**, 1946 (2003)].
34. A. Baldini, *Landolt−Börnstein, New Series*, Ed. by H. Shopper (Springer-Verlag, Berlin, 1988), Vol. I/12, p. 97; reactions 71−73.
35. A. Abele *et al.*, Phys. Rev. D **57**, 3860 (1998).
36. S. Flatté, Phys. Lett. B **63**, 225 (1976).

# Scalar-isovector $K\bar{K}$ production close to threshold

A. Dzyuba[1,2], V. Kleber[3,a], M. Büscher[2,b], V.P. Chernyshev[4†], S. Dymov[5], P. Fedorets[2,4], V. Grishina[6],
C. Hanhart[2], M. Hartmann[2], V. Hejny[2], L. Kondratyuk[5], V. Koptev[1], P. Kulessa[7], Y. Maeda[2,3,c], T. Mersmann[8],
S. Mikirtychyants[1], M. Nekipelov[1,2], D. Prasuhn[2], R. Schleichert[2], A. Sibirtsev[2,9], H.J. Stein[2], H. Ströher[2], and
I. Zychor[10]

1 High Energy Physics Department, Petersburg Nuclear Physics Institute, 188350 Gatchina, Russia
2 Institut für Kernphysik, Forschungszentrum Jülich, 52425 Jülich, Germany
3 Institut für Kernphysik, Universität zu Köln, 50937 Köln, Germany
4 Institute for Theoretical and Experimental Physics, Bolshaya Cheremushkinskaya 25, 117218 Moscow, Russia
5 Laboratory of Nuclear Problems, Joint Institute for Nuclear Research, 141980 Dubna, Russia
6 Institute for Nuclear Research, 60th October Anniversary Prospect 7A, 117312 Moscow, Russia
7 Institute of Nuclear Physics, Radzikowskiego 152, 31342 Cracow, Poland
8 Institut für Kernphysik, Universität Münster, 48149 Münster, Germany
9 Helmholtz-Institut für Strahlen- und Kernphysik (Theorie), Universität Bonn, Nußallee 14-16, 53115 Bonn, Germany
10 The Andrzej Sołtan Institute for Nuclear Studies, 05400 Świerk, Poland

**Abstract.** The reaction $pp \to dK^+\bar{K}^0$ has been investigated at excess energies $Q = 47.4$ and $104.7\,\text{MeV}$ above the $K^+\bar{K}^0$ threshold at COSY Jülich. Coincident $dK^+$ pairs were detected with the ANKE spectrometer, and subsequently $\sim 2000$ events with a missing $\bar{K}^0$ invariant mass were identified, which fully populate the Dalitz plot. The joint analysis of invariant mass and angular distributions reveals $s$-wave dominance between the two kaons, in conjunction with a $p$-wave between the deuteron and the kaon pair, *i.e.* $K\bar{K}$ production via the $a_0^+(980)$ channel. Integration of the differential distributions yields total cross-sections of $\sigma(pp \to dK^+\bar{K}^0) = (38 \pm 2_{\text{stat}} \pm 14_{\text{syst}})\,\text{nb}$ and $(190 \pm 4_{\text{stat}} \pm 39_{\text{syst}})\,\text{nb}$ for the low and high $Q$ value, respectively.

**PACS.** 25.10.+s Nuclear reactions involving few-nucleon systems – 13.75.-n Hadron-induced low- and intermediate-energy reactions and scattering (energy $\leq 10\,\text{GeV}$)

## 1 Introduction

QCD is the fundamental theory of Strong Interactions. How quarks and gluons are bound into hadrons is as yet an unsolved strong-coupling problem. Though QCD can be treated explicitly in this regime using lattice techniques [1], these are not in a state to make quantitative statements about the light scalar mesons. Alternatively, QCD-inspired models, which employ effective degrees of freedom, can be used. The constituent quark model is one of the most successful in this respect (see, *e.g.*, ref. [2]).

a *Present address:* Physikalisches Institut, Universität Bonn, Nussallee 12, 53115 Bonn, Germany.
b e-mail: m.buescher@fz-juelich.de
c *Present address:* Research Center for Nuclear Physics, Osaka University, Ibaraki, Osaka 567-0047, Japan.
† Deceased.

This approach inherently treats the lightest scalar resonances $a_0/f_0(980)$ as conventional $q\bar{q}$ states.

Experimentally, more states with quantum numbers $J^P = 0^+$ have been identified than would fit into a single $SU(3)$ scalar nonet: the $f_0(600)$ (or $\sigma$), $f_0(980)$, $f_0(1370)$, $f_0(1500)$ and $f_0(1710)$ with $I = 0$, the putative $\kappa(800)$ and the $K^*(1430)$ ($I = 1/2$), as well as the $a_0(980)$ and $a_0(1450)$ ($I = 1$) [3]. Consequently, the $a_0/f_0(980)$ have been associated with crypto-exotic states like $K\bar{K}$ molecules [4] or compact $qq$-$\bar{q}\bar{q}$ states [5]. It has even been suggested that a complete nonet of four-quark states might exist with masses below $1.0\,\text{GeV}/c^2$ [6].

The first clear observation of the isovector $a_0(980)$ resonance was achieved in $K^-p$ interactions [7]. It has also been seen in $p\bar{p}$ annihilations [8], in $\pi^-p$ collisions [9], and in $\gamma\gamma$ interactions [10]. Experiments on radiative $\phi$-decays [11,12] have been analysed in terms of $a_0/f_0$ production in the decay chain $\phi \to \gamma a_0/f_0 \to \gamma\pi^0\eta/\pi^0\pi^0$. In

$pp$ collisions the $a_0(980)$ resonance has been measured at $p_p = 450 \, \text{GeV}/c$ via $f_1(1285) \rightarrow a_0^{\pm}\pi^{\mp}$ decays [13] and in inclusive measurements of the $pp \rightarrow dX^+$ reaction at $p_p = 3.8, 4.5$, and $6.3 \, \text{GeV}/c$ [14].

Despite these many experimental investigations, basic properties and even the nature of the $a_0(980)$ resonance are still far from being established (see, *e.g.*, refs. [15,16]). The Particle Data Group quotes a mass of $m_{a_0} = (984.7 \pm 1.2) \, \text{MeV}/c^2$ and a width of $\Gamma_{a_0} = (50\text{--}100) \, \text{MeV}/c^2$ [3]. The main decay channels, $\pi\eta$ and $K\bar{K}$, are denoted as "dominant" and "seen", respectively. The corresponding coupling constants $g_{\pi\eta}$ and $g_{K\bar{K}}$ differ significantly for the different data sets and analyses [16].

Therefore, an experimental programme has been started at the Cooler Synchrotron COSY Jülich [17] aiming at exclusive data on the $a_0/f_0(980)$ production from $pp$, $pn$, $pd$ and $dd$ interactions at energies close to the $K\bar{K}$ threshold [18]. The final goal of these investigations is the extraction of the $a_0/f_0$-mixing amplitude, a quantity which is believed to shed light on the nature of these resonances [19,20]. As a first step the reactions $pp \rightarrow dK^+\bar{K}^0$ [21] and $pp \rightarrow d\pi^+\eta$ [22] have been measured in parallel at the ANKE spectrometer [23] for $T_p = 2.65 \, \text{GeV}$, corresponding to an excess energy of $Q = 47.4 \, \text{MeV}$ with respect to the $K^+\bar{K}^0$ threshold. The data for the strangeness decay channel —which are almost background free— indicate that more than 80% of the kaon pairs are produced in a relative $s$-wave, corresponding to the $a_0^+$ channel [21]. On the other hand, the $\pi^+\eta$ signal sits on top of a strong but smooth background of multipion production which, together with the small acceptance of ANKE for this channel, makes the interpretation of the $a_0^+$ signal model dependent [22]. However, the obtained branching ratio $\sigma(pp \rightarrow d(K^+\bar{K}^0)_{s\text{-wave}})/\sigma(pp \rightarrow da_0^+ \rightarrow d\pi^+\eta) = 0.029 \pm 0.008_{\text{stat}} \pm 0.009_{\text{sys}}$ [22] is in line with values from the literature [3].

In this paper we report on a refined analysis of the $pp \rightarrow dK^+\bar{K}^0$ data at $T_p = 2.65 \, \text{GeV}$ as well as on new results from a second measurement at higher beam energy ($T_p = 2.83 \, \text{GeV}$, corresponding to $Q = 104.7 \, \text{MeV}$). The procedures for event identification and acceptance correction at the lower energy have been described in our previous publication [21].

# 2 Measurement of $pp \rightarrow dK^+\bar{K}^0$ events with ANKE

## 2.1 Experimental setup

ANKE is a magnetic spectrometer located in one of the straight sections of COSY and comprises three dipole magnets, D1–D3 [23]. D1 deflects the circulating COSY beam onto the target in front of D2, and D3 bends it back into the nominal orbit. The C-shaped spectrometer dipole D2 separates forward-going reaction products from the COSY beam and allows one to determine their emission angles and momenta. The angular acceptance of ANKE covers $|\vartheta_h| \leq 10°$ horizontally and $|\vartheta_v| \leq 3°$ vertically for the detected deuterons ($p_d > 1300 \, \text{MeV}/c$), and $|\vartheta_h| \leq 12°$ and $|\vartheta_v| \leq 3.5°$ for the $K^+$-mesons.

A cluster-jet target [24] of hydrogen molecules, placed between D1 and D2, has been used, providing areal densities of up to $\sim 5 \times 10^{14} \, \text{cm}^{-2}$. The luminosity has been measured with high statistical accuracy using $pp$ elastic scattering, recorded simultaneously with the $dK^+$ data. Protons with $\vartheta = 5.5° - 9°$ have been selected, since the ANKE acceptance changes smoothly in this angular range and the elastic peak is easily distinguished from background in the momentum distribution. The average luminosity during the measurements with up to $\sim 4 \times 10^{10}$ stored protons in the COSY ring has been determined as $L = (1.7 \pm 0.4_{\text{syst}}) \times 10^{31} \, \text{s}^{-1} \, \text{cm}^{-2}$, corresponding to an integrated value of $L_{\text{int}} = 7.5 \, \text{pb}^{-1}$.

## 2.2 Event selection for Q = 104.7 MeV

Two charged particles, $K^+$ and $d$, have been detected in coincidence. Positively charged kaons are identified in the side detection system (SD) [23,25] of ANKE by a time-of-flight (TOF) measurement. The TOF start counters, consisting of one layer of 23 scintillation counters, have been mounted next to the large exit window of the vacuum chamber in D2. Kaons from $a_0^+$ decay with momenta $p_{K^+} = 390\text{--}625 \, \text{MeV}/c$ have been stopped in range telescopes, located along the focal surface of D2. These telescopes comprise TOF stop counters and provide additional kaon-$vs.$-background discrimination by means of energy loss ($\Delta E$) measurements [25]. At $T_p = 2.83 \, \text{GeV}$, kaons with $p_{K^+} = (625\text{--}1000) \, \text{MeV}/c$ have been detected in a different part of the SD, consisting of one layer of 6 scintillation counters for TOF stop ("sidewall counters"). Two multi-wire proportional chambers (MWPCs) positioned between the TOF start and stop counters allow one to deduce the ejectile momenta and to suppress background from secondary scattering [21,22].

Fast particles produced in coincidence with the $K^+$-mesons as well as elastically scattered protons have been detected in the ANKE forward-detection system (FD) [26] containing two layers of scintillation counters for TOF and $\Delta E$ measurements. In addition there are three MWPCs, each with two sensitive planes, exploited for momentum reconstruction and background suppression [21,23]. Two bands of protons and deuterons are distinguished in the time difference between the detection of a $K^+$-meson in one of the TOF stop counters of the SD and a particle in the FD as a function of the FD particle momentum, see fig. 1a. The deuterons are selected with the cut indicated by the lines, plus the energy loss information from the FD scintillation counters. In fig. 1b the missing-mass distribution $m(pp, dK^+)$ for the selected $pp \rightarrow dK^+X$ events is presented. The missing particle $X$ must be a $\bar{K}^0$, due to charge and strangeness conservation. The measured $dK^+$ missing-mass distribution peaks around $m = m_{\bar{K}^0}$, reflecting the clean particle identification at ANKE.

About 2300 events are accepted as $dK^+\bar{K}^0$ candidates for further analysis (unshaded peak area of the histogram
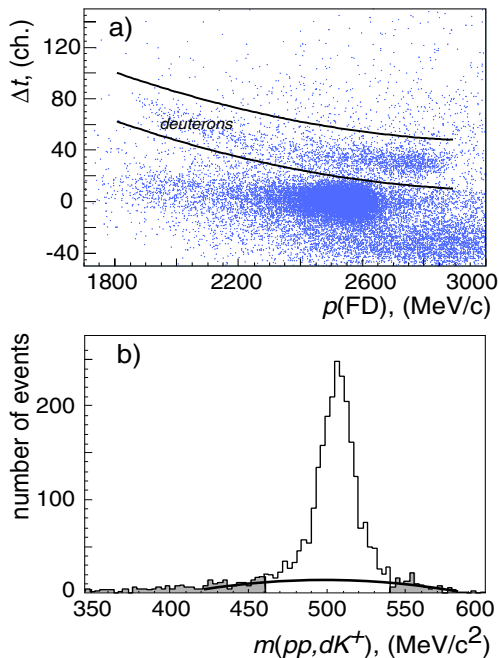
**Fig. 1.** a) Time difference between the fast forward-going particles in layer 1 of the FD scintillators and the $K^+$-mesons *vs.* the momentum of the forward particle. The lines indicate the selection for deuteron identification. b) Missing-mass $m(pp, dK^+)$ distribution of the $pp \to dK^+X$ events. The shaded areas indicate the events used for background subtraction, the solid line shows the background distribution under the $\bar{K}^0$ peak obtained from a polynomial fit.

in fig. 1b). The remaining background from misidentified particles is $(13\pm2)$%. The shape of this background in the differential spectra discussed below has been determined and subsequently subtracted by selecting events outside the $\bar{K}^0$ peak (shaded areas in fig. 1b).

The $K^+$ tracking efficiency in the side MWPCs and the efficiency of the $\Delta E$ cut have been determined using simultaneously recorded $pp \to pK^+\Lambda$ events, which, due to the significantly larger cross-section, can be identified by TOF criteria and a momentum cut for protons in the FD only. The efficiency of the track reconstruction varies from 96% for the telescopes to 76% for the sidewall counters. The efficiency of the $\Delta E$ cut has been determined for each telescope, with an average value of 53%, and for the sidewall counters, ranging from 87% to 74%. The efficiency of the FD $\Delta E$ criterion for deuterons has been deduced from the number of $\bar{K}^0$ events in the peak of fig. 1b before and after this cut. The efficiency of the FD scintillators and all TOF criteria is larger than 99%. The data have been corrected for all efficiencies on an event-by-event basis.

### 2.3 Kinematic fit

A kinematic fit has been carried out to improve the invariant mass and angular resolutions. This fit shifts the

measured $dK^+$ missing mass (fig. 1b) to the nominal value of $m_{\bar{K}^0} = 497.6\,\mathrm{MeV}/c^2$ on an event-by-event basis, varying the momentum components of the detected $K^+$ and $d$ within their resolutions. As a result of the fit, the deuteron missing-mass (*i.e.* the invariant $K^+\bar{K}^0$ mass) resolution improves from $\delta m_{K^+\bar{K}^0} = (35\text{–}3)\,\mathrm{MeV}/c^2$ over the range $(991\text{–}1096)\,\mathrm{MeV}/c^2$ to $\delta m_{K^+\bar{K}^0} < 10\,\mathrm{MeV}/c^2$ in the full range with minimum values of $\sim 3\,\mathrm{MeV}/c^2$ at the kinematic limits. Due to the fact that the $p_z$ resolution ($z$ being the beam direction) for deuterons is approximately a factor five worse than for all other variables, the fit procedure does not significantly improve the $K^+$ missing-mass and angular resolutions: $\delta m_{d\bar{K}^0} \sim 5\,\mathrm{MeV}/c^2$ in the full range, $\delta[\cos(\theta)] \sim 0.2$ for all angular spectra.

The same fit procedure has also been applied to the previously published data at $T_p = 2.65\,\mathrm{GeV}$ [21], and improves $\delta m_{K^+\bar{K}^0}$ from $(8\text{–}1)\,\mathrm{MeV}/c^2$ over the range $(991\text{–}1038)\,\mathrm{MeV}/c^2$ to $\delta m_{K^+\bar{K}^0} < 3\,\mathrm{MeV}/c^2$ in the full mass range.

### 2.4 Non-acceptance–corrected Dalitz plot

Figure 2 shows the distribution of the kinematically fitted $dK^+\bar{K}^0$ events in the Dalitz plot for both $Q$ values. It is observed that the kinematically allowed region is fully covered by the ANKE acceptance. For comparison the simulated population of the Dalitz plot is also shown for the case of phase-space–distributed events. The total ANKE acceptance for these $dK^+\bar{K}^0$ events is 2.1% at $Q = 47.4\,\mathrm{MeV}$ and 0.8% at 104.7 MeV. Due to the limited number of counts we present in the following only one-dimensional distributions. These also have the advantage of carrying additional information about the transition matrix, as shown in sect. 2.5.
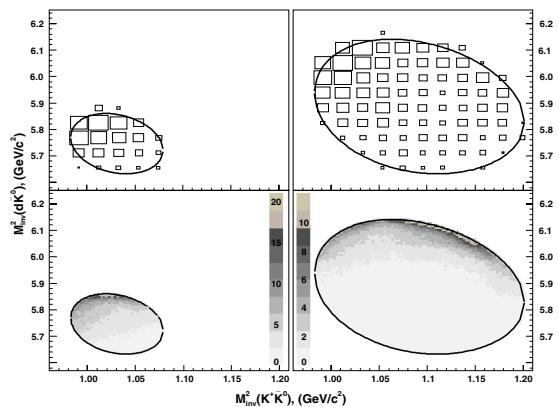


**Fig. 2.** Top: Dalitz plots of the events from the reaction $pp \to dK^+\bar{K}^0$ at $Q = 47.4$ (left) and 104.7 MeV (right). The data are not background subtracted and not corrected for the ANKE acceptance and the detection efficiencies, and are binned with cell size $21\,\mathrm{MeV}^2/c^4 \times 57\,\mathrm{MeV}^2/c^4$. The lines denote the kinematically allowed region. Bottom: simulated Dalitz plots inside the ANKE acceptance for phase-space–distributed events (*i.e.* configuration $[(K\bar{K})_s d]_s$, cf. sect. 2.5).

## 2.5 Acceptance correction

In comparison to the data at $T_p = 2.65\,\text{GeV}$ [21], the excess energy for the higher beam energy is approximitely twice as large. As a consequence, the method of model-independent acceptance correction (using a five-dimensional acceptance matrix) can no longer be used, since the number of zero elements in the acceptance matrix becomes too large. An alternative method has been developed which is described as follows.

In the close-to-threshold regime only a limited number of final states contribute. For the data analysis we have restricted ourselves to the lowest allowed partial waves, *i.e.* $s$-wave in the $K\bar{K}$ system accompanied by a $p$-wave of the deuteron with respect to the meson pair ($a_0^+(980)$-channel) and $p$-wave $K\bar{K}$ production with an $s$-wave deuteron (non-resonant channel). In the following we denote these two configurations by $[(K\bar{K})_s d]_p$ and $[(K\bar{K})_p d]_s$. It has been shown that the lower energy data can be described by this *ansatz* for the $dK^+\bar{K}^0$ final state [21], where the square of the spin-averaged transition matrix element can be written as

$$|\bar{\mathcal{M}}|^2 = C_0^q q^2 + C_0^k k^2 + C_1 (\hat{\mathbf{p}} \cdot \mathbf{k})^2$$
$$+ C_2 (\hat{\mathbf{p}} \cdot \mathbf{q})^2 + C_3 (\mathbf{k} \cdot \mathbf{q}) + C_4 (\hat{\mathbf{p}} \cdot \mathbf{k})(\hat{\mathbf{p}} \cdot \mathbf{q}). \quad (1)$$

Here $\mathbf{k}$ is the deuteron momentum in the overall CMS, $\mathbf{q}$ denotes the $K^+$ momentum in the $K\bar{K}$ system, and $\hat{\mathbf{p}}$ is the unit vector of the beam momentum. Only $K\bar{K}$ $p$-waves contribute to $C_0^q$ and $C_2$, only $K\bar{K}$ $s$-waves to $C_0^k$ and $C_1$, and only $s$-$p$ interference terms to $C_3$ and $C_4$. The coefficients $C_i$ can be determined from the data by fitting eq. (1) to the measured $d\sigma/dm_{K\bar{K}}$ and $d\sigma/dm_{dK}$ as well as to the angular distributions $d\sigma/d[\cos(\mathbf{pk})]$, $d\sigma/d[\cos(\mathbf{pq})]$, $d\sigma/d[\cos(\mathbf{kq})]$ and $d\sigma/d[\cos(\mathbf{pt})]$ [19] ($\mathbf{t}$ represents the $K^+$ momentum measured in the overall CMS). It should be noted that a fit to the two-dimensional Dalitz plot does not provide additional information about the transition matrix, but would only yield three linear combinations of two of the coefficients $C_i$ [19].

$|\bar{\mathcal{M}}|^2$ gives the production probability of an event with certain kinematic parameters $\mathbf{k}$ and $\mathbf{q}$ relative to $\hat{\mathbf{p}}$. The corresponding differential acceptance of the spectrometer $\alpha(\mathbf{k}, \mathbf{q}, \hat{\mathbf{p}})$ does not depend on the values of $C_i$, and can be determined using a large sample of simulated events, covering full phase space, which are tracked through a GEANT model of the setup [27]. Using the coefficients from ref. [21] as starting parameters, the simulations were carried out for different sets of the $C_i$, leading to differential distributions convoluted with the acceptance. For each choice of the $C_i$, the $\chi^2$ values have been calculated for the difference between simulated and measured distributions. Subsequently, the coefficients which describe the experimental data best have been determined by minimizing $\chi^2$ with the MINUIT package [28]. The best fit result of this procedure is shown in fig. 3 for two invariant-mass and four angular distributions (cf. table 1 in sect. 3.1 for numerical values).
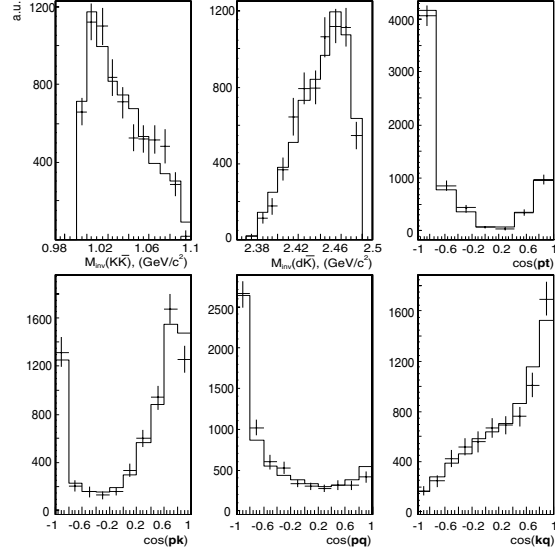


**Fig. 3.** Best fit to non-acceptance–corrected data at $T_p = 2.83\,\text{GeV}$.

## 3 Cross-sections of the reaction pp → dK⁺K̄⁰ at Q = 47.4 and 104.7 MeV

### 3.1 Differential spectra

With the best-fit coefficients $C_i$ one can simulate corresponding differential distributions at the target, track the events through the setup, and thus determine one-dimensional differential acceptances for, *e.g.*, the two invariant masses and four angles of fig. 3. Using these acceptances, differential cross-sections can be extracted from the data, and these are shown in fig. 4.

In order to verify the validity of the acceptance correction method using the coefficients $C_i$, the same procedure has been applied to the lower energy data. The results are shown in fig. 5 as solid dots and are compared to our results published previously [21], analyzed using the acceptance matrix method (open circles). For a $pp$ initial state all distributions must be forward-backward symmetric relative to the beam momentum; this feature has been exploited in ref. [21], where differential cross-sections as functions of $|\cos(\mathbf{pq})|$ and $|\cos(\mathbf{pk})|$ are presented. These are shown in the lower-left spectra of fig. 5 together with the mirrored distributions from the coefficient method (squares), each scaled by 0.25 for better distinction. In all cases good agreement between the model-independent matrix method [21] and the *ansatz* discussed here is observed. Note that the matrix method did not allow us to extract the $\cos(\mathbf{pt})$ distribution (upper right in the figure) from the 2.65 GeV data which is now possible with the coefficient *ansatz*.

The best-fit coefficients $C_i$ are presented in table 1 for both beam energies. All coefficients are given in units

**Table 1.** Quality and results of the fit using eq. (1). For the definition of $N$ see eq. (2).

| $Q$, MeV | $C_0^k$ | $C_0^q$ | $C_1$ | $C_2$ | $C_3$ | $C_4$ | $\chi^2$/ndf | $N$, $\mu$b MeV$^{-2}$ |
|---|---|---|---|---|---|---|---|---|
| 47.4 | 1 | $-0.34^{+0.26}_{-0.21}$ | $-0.14^{+0.14}_{-0.13}$ | $1.23^{+0.32}_{-0.32}$ | $-0.44^{+0.16}_{-0.16}$ | $-0.76^{+0.30}_{-0.33}$ | 1.38 | $26.6 \pm 10.9$ |
| 104.7 | 1 | $-0.07^{+0.14}_{-0.24}$ | $-0.22^{+0.12}_{-0.11}$ | $1.04^{+0.36}_{-0.19}$ | $-1.45^{+0.20}_{-0.12}$ | $0.09^{+0.25}_{-0.55}$ | 1.10 | $13.5 \pm 3.0$ |
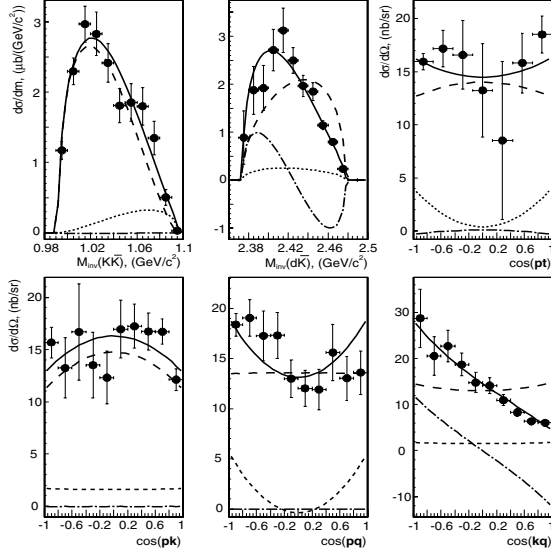


**Fig. 4.** Angular and invariant mass distributions for $T_p = 2.83$ GeV. The dashed (dotted) line corresponds to $K\bar{K}$ production in a relative *s*- (*p*-)wave, the dash-dotted to the interference term, and the solid line is the sum of these contributions. The error bars show the statistical uncertainties only. The systematic uncertainty for each bin is smaller than 10%; the overall uncertainty from the luminosity determination is given in sect. 2.1.

**Fig. 5.** Same as fig. 4 for $T_p = 2.65$ GeV but omitting the fitted partial-wave contributions. Full symbols denote the differential cross-sections obtained by the method described in this paper; open symbols are the previously published model-independent results [21] where the error bars include statistical and systematic uncertainties. The cos(**pt**) spectrum has not been presented in ref. [21]. See text for further details.

of $C_0^k$. This is due to the fact that $|\bar{\mathcal{M}}|^2$ from eq. (1) is proportional to the differential cross-sections, thus leaving one parameter undetermined in the fit. The errors of the $C_i$ are obtained by varying each coefficient (allowing the others to change) such that the total $\chi^2$ increases by one.

The parameters $C_i$ from eq. (1) can be directly related to the different partial waves [21]. Their contributions to the various observables are shown in fig. 4. The occurrence of interference terms in the $\bar{K}^0 d$ invariant mass distribution is due to the choice of the kinematic variables, *i.e.* relative momentum of the kaons and that of the deuteron with respect to the kaon pair. Consequently, there is no interference term in the $K^+\bar{K}^0$ mass distribution. To get a distribution for the other invariant mass that is free of interferences one needs to switch to the $\bar{K}^0 d$ relative momentum and the $K^+$ momentum. Then, however, there will be an interference term in the $K^+\bar{K}^0$ mass distribu-

tion. The method how to construct the variable transformation is described in detail in ref. [29].

Our fit reveals a strong dominance of the $K\bar{K}$ *s*-wave production rate (*i.e.* via the $a_0^+(980)$ channel) for both beam energies: $(95 \pm 4)\%$ and $(89 \pm 4)\%$ at $T_p = 2.65$ GeV and 2.83 GeV, respectively.

The quality of the fit clearly supports the *ansatz* to include only the lowest partial waves in the data analysis. It should be noted that the growth of the amplitudes due to the centrifugal-barrier factor is taken care off by eq. (1). An essential question is to understand the variation in the parameters $C_3$ and $C_4$, see table 1. As outlined above, these parameters emerge solely from an interference of the $[(K\bar{K})_s d]_p$ with the $[(K\bar{K})_p d]_s$ partial waves. Therefore, if there were a significant phase motion in one of these groups (*e.g.*, due to the strong final-state interaction in the $a_0$ channel), a variation with energy especially of $C_3$ and $C_4$ is expected. This point clearly calls for more theoretical investigations.

## 3.2 Total cross-sections

Knowing the coefficients $C_i$, and thus the initial differential distributions (figs. 4 and 5), the total acceptance and the total cross-sections can be evaluated. For the higher energy, a value of $\sigma(pp \to dK^+\bar{K}^0) = (190 \pm 4_{\mathrm{stat}} \pm 39_{\mathrm{syst}})$ nb is obtained. At the lower energy the extracted total cross-section is in agreement with the previously published value of $(38 \pm 2_{\mathrm{stat}} \pm 14_{\mathrm{syst}})$ nb [21]. In both cases the errors include the statistical and systematic uncertainty from the luminosity determination.

Figure 6 shows the measured total cross-sections in comparison with the expected $Q$-dependence of the cross-section calculated with the transition matrix element of eq. (1). After an angular integration the total $pp \to dK^+\bar{K}^0$ cross-section is given by

$$\sigma = \frac{N}{2^6\pi^3\sqrt{s^2 - 4sm_p^2}} \int\limits_{4m_K^2}^{(\sqrt{s}-m_d)^2} \frac{k\,q}{\sqrt{s\,s_{KK}}}\,|\tilde{\mathcal{M}}|^2\,\mathrm{d}s_{KK},$$

(2)

where $s$ and $s_{KK}$ are the squared invariant energies of the initial $pp$ and final $K^+\bar{K}^0$ systems, respectively. Here, $k$ and $q$ are defined as before and are given explicitly as

$$k^2 = \frac{(s - s_{KK} - m_d^2)^2 - 4s_{KK}m_d^2}{4s},$$

$$q^2 = \frac{s_{KK} - 4m_K^2}{4},$$

where $m_d$ and $m_K$ are the deuteron and kaon masses, *i.e.* we neglect the $K^+$ and $\bar{K}^0$ mass difference. The angular-integrated squared transition amplitude $|\tilde{\mathcal{M}}|^2$ is given as

$$|\tilde{\mathcal{M}}|^2 = \left(C_0^q + \frac{1}{3}C_2\right)q^2 + \left(C_0^k + \frac{1}{3}C_1\right)k^2. \quad (3)$$
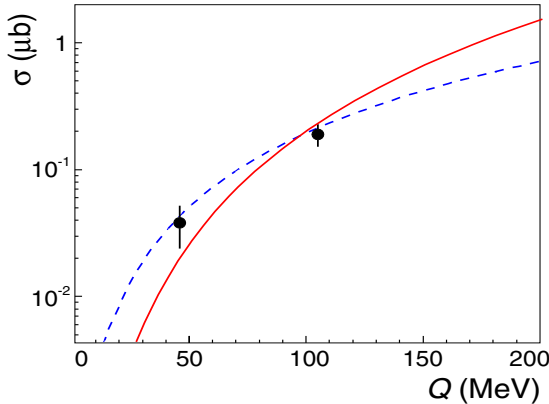


**Fig. 6.** Total cross-section of the $pp \to dK^+\bar{K}^0$ reaction as a function of the excess energy $Q$. The solid line is the result from eq. (2) with the squared transition amplitude given by eq. (3) and with $N = 18\,\mu$b MeV$^{-2}$. The dashed line shows the energy dependence for three-body phase space. Note that the latter is forbidden by selection rules.

The normalization factor $N$ has been determined for both energies and is quoted in table 1. The errors of $N$ include the systematic uncertainties of the total cross-sections. Note that the lines in figs. 4 and 5 have been properly scaled to the individual total cross-sections.

For illustration we show by the dashed line in fig. 6 the result of eq. (2) with a constant matrix element. This is a classical example when data can be well reproduced by a simple phase-space consideration although such a description is invalid for this particular reaction since selection rules do not allow for a pure $s$-wave.

## 4 Summary and conclusions

Using the ANKE spectrometer at an internal target position of COSY Jülich, we have searched for scalar $K\bar{K}$ production in the reaction $pp \to dK^+\bar{K}^0$ at two excess energies $Q = 47.4$ and $104.7$ MeV. Due to the excellent $K^+$ identification at ANKE, the detected events with coincident $K^+d$ pairs exhibit little background. This can be subtracted using events outside the $\bar{K}^0$ missing-mass peak. After a kinematic fit to the $\bar{K}^0$ mass, the invariant $K^+\bar{K}^0$ mass distribution has been obtained with an unprecedented resolution of better than 3 (10) MeV/$c^2$ for 47.4 (104.7) MeV.

Mass and angular distributions have been extracted from the data using an *ansatz* for the transition matrix element that includes the lowest allowed partial waves, *i.e.* an $s$-wave in the $K\bar{K}$ system accompanied by a $p$-wave of the deuteron with respect to the meson pair and $p$-wave $K\bar{K}$ production with an $s$-wave deuteron. All six coefficients that enter the spin-averaged matrix element have been obtained by a fit to the differential spectra. This fit reveals the dominance of $K\bar{K}$ production in a relative $s$-wave, $(95 \pm 4)\%$ and $(89 \pm 4)\%$ at 47.4 and 104.7 MeV, *i.e.* dominance of kaon-pair production via the $a_0^+(980)$ channel.

The reaction $pp \to dK^+\bar{K}^0$ has been subject of several theoretical papers. For example, the authors of ref. [30] point out that this reaction (and also $pp \to d\pi^+\eta$) is expected to be an additional source of information about the scalar sector. They account for the interactions of the mesons by using chiral unitary techniques, which dynamically generate the $a_0^+(980)$ resonance. In ref. [31] total cross-sections and differential spectra are calculated using a model in which the reaction $pp \to dK^+\bar{K}^0$ is dominated by intermediate $a_0^+(980)$ production.

As discussed in sect. 3.1, there is an energy dependence of the parameters $C_3$ and $C_4$ in the transition matrix element (eq. (1)) that is not yet understood and needs further theoretical study since it might indicate a final-state interaction in the $a_0$ channel.

grateful to the COSY-accelerator crew for providing the proton beam above the nominal accelerator energy. Special thanks to C. Wilkin for carefully reading the manuscript and for conducting photomultiplier tests.

## References

1. SCALAR Collaboration (T. Kunihiro *et al.*), Phys. Rev. D **70**, 034504 (2004).
2. D. Morgan, Phys. Lett. B **51**, 71 (1974); K.L. Au, D. Morgan, M.R. Pennington, Phys. Rev. D **35**, 1633 (1987); D. Morgan, M.R. Pennington, Phys. Lett. B **258**, 444 (1991); Phys. Rev. D **48**, 1185 (1993); A.V. Anisovich *et al.*, Eur. Phys. J. A **12**, 103 (2001); S. Narison, hep-ph/0012235.
3. Particle Data Group (S. Eidelman *et al.*), Phys. Lett. B **592**, 1 (2004).
4. J. Weinstein, N. Isgur, Phys. Rev. Lett. **48**, 659 (1982); Phys. Rev. D **27**, 588 (1983); **41**, 2236 (1990); G. Janssen *et al.*, Phys. Rev. D **52**, 2690 (1995); J.A. Oller, E. Oset, Nucl. Phys. A **620**, 438 (1997) (Nucl. Phys. A **652**, 407 (1999)(E)).
5. N.N. Achasov, hep-ph/0201299; R.J. Jaffe, Phys. Rev. D **15**, 267 (1977); J. Vijande *et al.*, *Proceedings of the International Workshop MESON 2002, May 24–28, 2002, Cracow, Poland* (World Scientific Publishing, 2003) ISBN 981-238-160-0, p. 501, hep-ph/0206263.
6. F.E. Close, N.A. Törnqvist, J. Phys. G **28**, R249 (2002).
7. J.B. Gay *et al.*, Phys. Lett. B **63**, 220 (1976).
8. A. Abele *et al.*, Phys. Lett. B **327**, 425 (1994); A. Abele *et al.*, Phys. Rev. D **57**, 3860 (1998); A. Bertin *et al.*, Phys. Lett. B **434**, 180 (1998).
9. S. Teige *et al.*, Phys. Rev. D **59**, 012001 (1999).
10. P. Achard *et al.*, Phys. Lett. B **526**, 269 (2002).
11. N.N. Achasov *et al.*, Phys. Lett. B **485**, 349 (2000); **479**, 53 (2000).
12. A. Aloisio *et al.*, Phys. Lett. B **536**, 209 (2002); **537**, 21 (2002).
13. D. Barberis *et al.*, Phys. Lett. B **440**, 225 (1998); **488**, 225 (2000).
14. M.A. Abolins *et al.*, Phys. Rev. Lett. **25**, 469 (1970).
15. V. Baru *et al.*, Phys. Lett. B **586**, 53 (2004).
16. V. Baru *et al.*, Eur. Phys. J. A **23**, 523 (2005).
17. R. Maier, Nucl. Instrum. Methods Phys. Res. A **390**, 1 (1997).
18. M. Büscher, Acta Phys. Pol. B **35**, 1055 (2004).
19. C. Hanhart, Phys. Rep. **397**, 155 (2004).
20. N.N. Achasov *et al.*, Phys. Lett. B **88**, 367 (1979).
21. V. Kleber *et al.*, Phys. Rev. Lett. **91**, 172304 (2003).
22. P. Fedorets *et al.*, Phys. At. Nucl. (Yad. Fiz.) **69**, 306 (2006).
23. S. Barsov *et al.*, Nucl. Instrum. Methods Phys. Res. A **462**, 364 (2001).
24. R. Santo *et al.*, Nucl. Instrum. Methods Phys. Res. A **386**, 228 (1997); A. Khoukaz *et al.*, Eur. Phys. J. D **5**, 275 (1999).
25. M. Büscher *et al.*, Nucl. Instrum. Methods Phys. Res. A **481**, 378 (2002).
26. S. Dymov *et al.*, Phys. Lett. B **635**, 270 (2006).
27. I. Zychor, Acta Phys. Pol. B **33**, 521 (2002).
28. F. James, M. Roos, Comput. Phys. Commun. **10**, 343 (1975).
29. A. Sibirtsev, M. Büscher, V.Y. Grishina, C. Hanhart, L.A. Kondratyuk, S. Krewald, U.G. Meissner, Phys. Lett. B **601**, 132 (2004).
30. E. Oset, J.A. Oller, U.-G. Meissner, Eur. Phys. J. A **12**, 435 (2001).
31. V.Y. Grishina *et al.*, Eur. Phys. J. A **21**, 507 (2004).
32. The ANKE Collaboration: www.fz-juelich.de/ikp/anke.

P H Y S I C A L   R E V I E W   L E T T E R S

# Evidence for an Excited Hyperon State in $pp \rightarrow pK^+Y^{0*}$

I. Zychor,[1] V. Koptev,[2] M. Büscher,[3] A. Dzyuba,[2] I. Keshelashvili,[3,4] V. Kleber,[5,*] H. R. Koch,[3] S. Krewald,[3] Y. Maeda,[3] S. Mikirtichyants,[2] M. Nekipelov,[2,3] H. Ströher,[3] and C. Wilkin[6]

[1]*The Andrzej Sołtan Institute for Nuclear Studies, 05400 Świerk, Poland*
[2]*High Energy Physics Department, Petersburg Nuclear Physics Institute, 188350 Gatchina, Russia*
[3]*Institut für Kernphysik, Forschungszentrum Jülich, 52425 Jülich, Germany*
[4]*High Energy Physics Institute, Tbilisi State University, 0186 Tbilisi, Georgia*
[5]*Institut für Kernphysik, Universität zu Köln, 550937 Köln, Germany*
[6]*University College London, London WC1E 6BT, United Kingdom*
(Received 10 June 2005; published 9 January 2006)

Indications for the production of a neutral excited hyperon in the reaction $pp \rightarrow pK^+Y^{0*}$ are observed in an experiment performed with the ANKE spectrometer at COSY-Jülich at $p_{\text{beam}} = 3.65$ GeV/$c$. Two final states were investigated simultaneously, viz. $Y^{0*} \rightarrow \pi^+ X^-$ and $\pi^- X^+$, and consistent results were obtained in spite of the quite different experimental conditions. The parameters of the hyperon state are $M(Y^{0*}) = (1480 \pm 15)$ MeV/$c^2$ and $\Gamma(Y^{0*}) = (60 \pm 15)$ MeV/$c^2$. The production cross section for $Y^{0*}$ decaying through these channels is of the order of few hundred nanobarns. Since the isospin of the $Y^{0*}$ has not been determined here, it could either be an observation of the $\Sigma(1480)$, a one-star resonance of the Particle Data Group tables, or, alternatively, a $\Lambda$ hyperon. Relativistic quark models for the baryon spectrum do not predict any excited hyperon in this mass range and so the $Y^{0*}$ may be of exotic nature.

The question of how hadrons arise from QCD is central to a fundamental understanding of hadronic multiquark and gluon systems. There has been a recent renaissance of QCD spectroscopy, triggered by observations of new narrow resonances, enhancements near thresholds, and possibly exotic states. Taken in conjunction with lattice QCD, which is poised to provide the theoretical insight into strong QCD, the new data may pave the way to achieve this understanding.

The production of hyperons and their decay properties have been a focus of experimental investigations ever since their discovery, mostly in hadron-induced reactions, but recently also in photoproduction. In comparison to the excitation spectrum of the nucleon resonances ($N, \Delta$), the excited states of hyperons ($\Lambda, \Sigma$) are still much less well known. The nature of experimentally well established states, such as the $\Lambda(1405)$, is not at all understood yet. This hyperon may be a genuine three-quark system, a molecularlike meson-baryon bound state, or even of exotic type.

The $\Sigma(1480)$ hyperon is far from being an established resonance. In the most recent compilation of the Particle Data Group [1], it is described as a "bump," with unknown quantum numbers and given a mere one-star rating. Very recently ZEUS has reported indications for a structure in the invariant mass spectrum for $K_S^0 p$ and $K_S^0 \bar{p}$, which may correspond to the $\Sigma(1480)$ [2]. However, the structure appears on a steeply varying background and therefore its significance is difficult to estimate. The Crystal Ball investigation of the $K^- p \rightarrow \pi^0 \pi^0 \Lambda$ reaction showed no sign for the resonance in the $\pi^0 \Lambda$ invariant mass spectra, but it should be noted that these are dominated by the $\Sigma^0(1385)$ [3].

In view of this uncertainty, we have investigated whether additional information might be obtained from proton-proton interactions at low energies. In so doing, we have found evidence for a neutral hyperon resonance $Y^{0*}$ in data originally taken for scalar meson production studies [4,5].

The experiments have been performed at the Cooler Synchrotron COSY, a medium energy accelerator and storage ring for protons and deuterons, which is operated at the Research Center Jülich (Germany) [6]. COSY supplied stored proton beams with a momentum of 3.65 GeV/$c$ at a revolution frequency of $\sim 10^6$ s$^{-1}$. Using a hydrogen cluster-jet target (areal density $\sim 5 \times 10^{14}$ cm$^{-2}$) the average luminosity during the measurements was $L = (1.38 \pm 0.15) \times 10^{31}$ s$^{-1}$ cm$^{-2}$.

The ANKE spectrometer [7] used in the experiments consists of three dipole magnets, which guide the circulating COSY beam through a chicane. The central C-shaped spectrometer dipole D2, placed downstream of the target, separates the reaction products from the beam. The ANKE detection system, comprising range telescopes, scintillation counters and multiwire proportional chambers, simultaneously registers particles of either charge and measures their momenta [8].

A multibody final state, containing a proton, a positively charged kaon, and a charged pion, together with an unidentified residue $X$, was studied in the $pp \rightarrow pK^+ \pi^{\pm} X^{\mp}$ reaction. Positively charged kaons and pions could be measured in the momentum ranges 0.2–0.6 GeV/$c$ and 0.2–0.9 GeV/$c$, respectively, negative pions between 0.4 and 1.0 GeV/$c$, and protons from 0.75 GeV/$c$ up to the kinematic limit. The angular acceptance of D2 is $|\vartheta_{\text{H}}| \lesssim 12°$ horizontally and $|\vartheta_{\text{V}}| \lesssim 5°$ vertically for any ejectile. By measuring delayed signals from the decay of stopped

012002-1

kaons, $K^+$ mesons can be identified in a background of pions, protons, and scattered particles up to $10^6$ times more intense.

Events with three identified charged particles $(p, K^+, \pi^\pm)$ were retained for further analysis. In Fig. 1 the missing-mass distributions $MM(pK^+\pi)$ vs $MM(pK^+)$ are shown for the reaction channels $pp \to pK^+\pi^+X^-$ and $pp \to pK^+\pi^-X^+$. The triangular shape of the distributions is due to the combination of kinematics and ANKE acceptance. Since the probability for detecting three-particle coincidences $(pK^+\pi^+)$ is about an order of magnitude smaller than for $(pK^+\pi^-)$, the resulting numbers of events are also drastically different.

For the reaction $pp \to pK^+\pi^+X^-$ a clear enhancement, corresponding to $X^- = \Sigma^-(1197)$, is observed on a top of a low background (see projection of the upper part of Fig. 1 in the upper part of Fig. 2). In the charge-mirrored $pp \to pK^+\pi^-X^+$ case, the $\pi^-$ may originate from different sources, e.g., a reaction with $X^+ = \Sigma^+(1189)$ or a secondary decay of $\Lambda \to p\pi^-$, arising from the major background reaction $pp \to pK^+\Lambda \to pK^+\pi^-p$. Protons from the latter reaction have been rejected by cutting $MM(pK^+\pi^-)$ around the proton mass (lower part in Fig. 1). Nevertheless the missing-mass distribution for the $(\pi^-X^+)$-final state is more complicated and the $\Sigma^+(1189)$ band is almost hidden underneath a strong background of, e.g., $\pi^0p$, $\pi^0\gamma p$, $\pi^+n$ arising from the decay of heavier hyperons (see lower part of Fig. 2). For both final states, background due to misidentified particles of different type is experimentally estimated to be $<3\%$.

For further event selection, different cuts have been applied for the two final states: for $(\pi^+X^-)$ the $\Sigma^-$ has been selected (1175 and 1220 MeV/$c^2$), while for $(\pi^-X^+)$ the corresponding range is between 1175 and 1300 MeV/$c^2$ in order to include $\Sigma^+$ as well as $\Sigma^-$ with a $\pi^-$ in its decay.

This cut largely excludes neutral hyperons producing a final state with two protons. The missing-mass distributions $MM(pK^+)$ for such events are plotted in Fig. 3(a). For $\pi^+X^-$, a double-humped structure is observed, with peaks around 1390 MeV/$c^2$ and 1480 MeV/$c^2$ (upper left). In the $\pi^-X^+$ case, the distribution also peaks at 1480 MeV/$c^2$ (upper right). The different shapes and event numbers of the resulting spectra are due to the various sources of $\pi^+$ and $\pi^-$ (see above). An obvious question is whether these distributions can be explained by the production of well established hyperon resonances [$\Sigma(1385)$, $\Lambda(1405)$, and $\Lambda(1520)$] plus nonresonant contributions or whether an additional source needs to be invoked, e.g., $pp \to pK^+Y^{0*}$ with a further $Y^{0*}$ hyperon state.

In order to try to answer this question, Monte Carlo simulations have been performed for both final states, using a simulation package based on GEANT3 [9]. The following reactions with $(pK^+\pi^\pm)$ in the final state have been used as input for this, assuming phase-space distributions and applying any constraints due to isospin invariance:

(i) intermediate hyperon resonance production [1]

$$pp \to pK^+\Sigma(1385) \to pK^+\pi^0(\pi^-p)$$
$$\to pK^+\pi^\pm(\pi^\mp n)$$
$$\to pK^+\pi^-(\pi^0 p),$$

$$pp \to pK^+\Lambda(1405) \to pK^+\pi^0(\pi^-p)\gamma$$
$$\to pK^+\pi^\pm(\pi^\mp n)$$
$$\to pK^+\pi^-(\pi^0 p),$$



FIG. 1. Missing-mass $MM(pK^+\pi)$ vs $MM(pK^+)$ distributions for $\pi^+$ (upper) and $\pi^-$ (lower) obtained in the reaction $pp \to pK^+\pi^\pm X^\mp$.
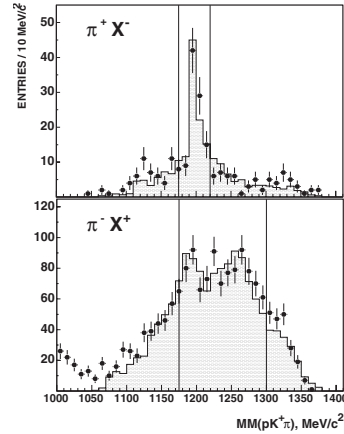


FIG. 2. Projections of Fig. 1 onto the three-particle missing mass $MM(pK^+\pi^\pm)$. Vertical lines show the $\Sigma$ bands used for event selection. The results of simulations for $MM(pK^+\pi^\pm) > 1050$ MeV/$c^2$, described in the text, are shown as a filled histogram.
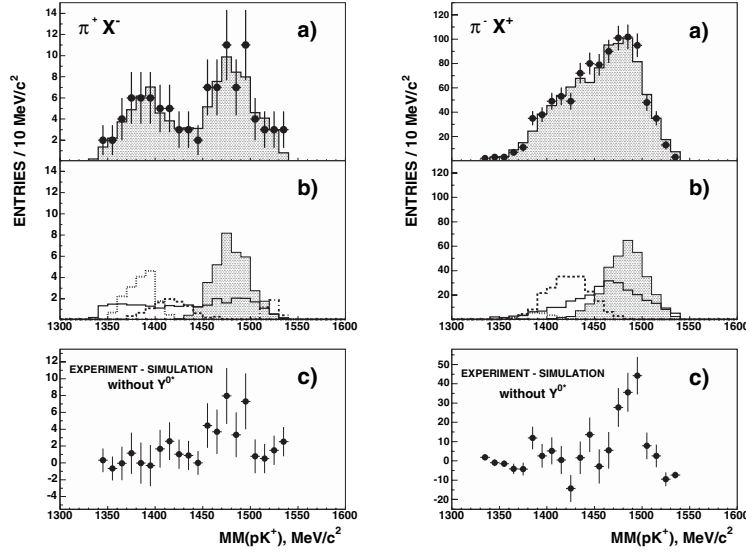
FIG. 3.   Missing-mass $MM(pK^+)$ spectra for the reaction $pp \to pK^+\pi^+X^-$ (left) and $pp \to pK^+\pi^-X^+$ (right). (a) Experimental points with statistical errors are compared to the shaded histograms of the fitted overall Monte Carlo simulations; (b) The simulation includes contributions from (i) resonances [$\Sigma(1385)$ (dotted), $\Lambda(1405)$ (dashed), $\Lambda(1520)$ (dotted-dashed)], (ii) nonresonant phase-space production (solid), and (iii) the $Y^{0*}$ resonance (shaded histogram), as described in the text; (c) Difference between the measured spectra and the sum of contributions (i) + (ii) fitted *without* $Y^{0*}$ production. Note that the contributions of the individual partial channels are different for (b) and (c).

$$pp \to pK^+\Lambda(1520) \to pK^+p(\pi^+\pi^-\pi^-)$$
$$\to pK^+p(\pi^-\pi^0\pi^0)$$
$$\to pK^+n(\pi^+\pi^-)$$
$$\to pK^+\pi^0(\pi^-p)\gamma$$
$$\to pK^+\pi^+\pi^-(\pi^-p)$$
$$\to pK^+\pi^+\pi^-(\pi^0n)$$
$$\to pK^+\pi^\pm(\pi^\mp n)$$
$$\to pK^+\pi^-(\pi^0p),$$

(ii) nonresonant production

$$pp \to NK^+X,$$

$$pp \to NK^+\pi X,$$

$$pp \to NK^+\pi\pi X,$$

with constraints for the relative contributions obtained on the basis of measured cross sections and phase-space considerations in the nonresonant cases [10,11].

The final state of $(\pi N)$ results from the decay of ground-state hyperons, while $(2\pi)$ and $(3\pi)$ are from $K^0$ and $K^-$ decays, respectively. $X$ represents any known $\Lambda$ or $\Sigma$ hyperon which could be produced in the experiment. When there are two particles of the same kind, both are further processed as in the analysis of experimental data.

In the lower parts of Fig. 3, the difference between the measured missing-mass distributions and the sum of fitted resonant and nonresonant production—contributions listed under (i) and (ii)—is shown. For both final states ($\pi^+X^-$ and $\pi^-X^+$) the shape of the measured distributions cannot be reproduced by the simulations and an excess of events is observed around the missing mass of 1480 MeV/$c^2$ in both cases. It is therefore suggested that another excited hyperon is produced and observed through the decay $pp \to pK^+Y^{0*} \to pK^+\pi^\pm X^\mp$.

The $Y^{0*}$ mass and width have been determined from a fit based on simulations that cover the range from 1460 to 1490 MeV/$c^2$ and from 45 to 75 MeV/$c^2$, respectively, both in steps of 5 MeV/$c^2$. From a minimization procedure the following parameters of the $Y^{0*}$, consistent for both final states, are obtained: $M(Y^{0*}) = (1480 \pm 15)$MeV/$c^2$ and $\Gamma(Y^{0*}) = (60 \pm 15)$MeV/$c^2$. Note that the experimental mass resolution is of the order of 10 MeV/$c^2$.

The fits to the data are shown in the two parts of Fig. 3(a), while the individual contributions are plotted in Fig. 3(b). These contributions are also used to obtain the three-particle missing-mass spectra for $MM(pK^+\pi^\pm) > 1050$ MeV/$c^2$ as shown in Fig. 2: in comparison with the experimental results a good agreement is achieved.

The numbers of events in the two peaks are $S(Y^{0*} \to \pi^+X^-) = 35 \pm 10$ and $S(Y^{0*} \to \pi^-X^+) = 330 \pm 60$. The statistical significance of the signal, assuming that this is due to the production of the $Y^{0*}$, is at least 4.5 standard deviations.

In order to estimate the production cross section for $Y^{0*}$ decaying through these channels, we used an overall detection efficiency of $\sim 7\%$ and an integrated luminosity of $\sim 6$ pb$^{-1}$. With acceptances obtained from simulations presented above, we arrive at cross section values of $(450 \pm 150 \pm 150)$ nb for $(\pi^+ X^-)$ and $(1200 \pm 250 \pm 500)$ nb for $(\pi^- X^+)$. The first error is statistical, while the second represents the systematic uncertainty. It can thus be concluded that the cross section estimates are consistent for both final states and are of the order of few hundred nanobarns.

Assuming that the $Y^{0*}(1480)$ hyperon exists, we briefly address the question of its possible theoretical description. In the constituent quark model, baryons are interpreted as bound states of three valence quarks where hyperons contain at least one strange quark. The baryon spectrum has been investigated systematically in a relativistic quark model with instanton-induced quark forces. No excited $\Lambda$ or $\Sigma$ resonances, in addition to the well known states, have been found for masses below $\approx 1600$ MeV/$c^2$ [12]. These findings are in agreement with results obtained in the relativized quark model of Capstick and Isgur [13]. Thus, it seems to be difficult to reconcile the low mass of the $Y^{0*}$ within the existing classification of $3q$ baryons.

In early papers, configurations of four quarks and an antiquark have been discussed for this mass range. Högaasen and Sorba have performed a group-theoretical classification of such states and arrived at an estimate of 1440 MeV/$c^2$ for the mass of an exotic $\Sigma$ [14]. Azimov *et al.* introduced a flavor octet and an antidecuplet of exotic baryons [15,16]. For the octet, a $\Sigma$ state with a mass of 1480 MeV/$c^2$ and a $\Lambda$ state at 1330 MeV/$c^2$ have been suggested in Ref. [16]. There were also attempts to mix octet and antidecuplet states, based on diquark correlations, as proposed by Jaffe and Wilczek [17]. A $\Sigma$ resonance with a mass of 1495 MeV/$c^2$ has been predicted as a member of the mixed multiplet [18].

In models, which couple nucleons with kaons and pions, quasibound states are generated with relatively low masses. In Ref. [19], a pole with the quantum numbers of the $\Sigma$, which might be identified with the $\Sigma(1480)$, is found at a mass of 1446 MeV/$c^2$, though a width of 343 MeV/$c^2$ is much larger.

Since a clear theoretical picture has not yet appeared, any conclusion about the nature of the $Y^{0*}$ would be premature.

In summary, we have observed indications in proton-proton collisions at 3.65 GeV/$c$ for a neutral hyperon resonance $Y^{0*}$ decaying into $\pi^+ X^-$ and $\pi^- X^+$ final states. Its parameters are $M(Y^{0*}) = (1480 \pm 15)$ MeV/$c^2$ and $\Gamma(Y^{0*}) = (60 \pm 15)$ MeV/$c^2$, though, since it is neutral, it can be either a $\Lambda$ or $\Sigma$ hyperon. The production cross section is of the order of few hundred nanobarns. On the basis of existing data we cannot decide whether it is a three-quark baryon or an exotic state, although some preference towards its exotic nature may be deduced from theoretical considerations.

Further studies are required to confirm the existence of the $Y^{0*}(1480)$ hyperon and to determine its quantum numbers. Such measurements, in particular, for $Y^*$ decays with photons in the final state, are foreseen with the WASA detector at COSY [20]. Searches for the charged $Y^{-*}$ hyperon in the reaction $pn \to pK^+ Y^{-*} \to pK^+ \pi^- X^0$, using a deuterium cluster-jet target and spectator proton tagging, are also conceivable.

---

*Present address: Physikalisches Institut, Universität Bonn, Nussallee 12, 53115 Bonn, Germany.

[1] S. Eidelman *et al.*, Phys. Lett. B **592**, 1 (2004).
[2] S. Chekanov *et al.*, Phys. Lett. B **591**, 7 (2004).
[3] S. Prakhov *et al.*, Phys. Rev. C **69**, 042202(R) (2004).
[4] M. Büscher, Acta Phys. Pol. B **35**, 1055 (2004).
[5] V. Kleber, Int. J. Mod. Phys. A **20**, 273 (2005).
[6] R. Maier, Nucl. Instrum. Methods Phys. Res., Sect. A **390**, 1 (1997).
[7] S. Barsov *et al.*, Nucl. Instrum. Methods Phys. Res., Sect. A **462**, 364 (2001).
[8] M. Büscher *et al.*, Nucl. Instrum. Methods Phys. Res., Sect. A **481**, 378 (2002).
[9] I. Zychor, Acta Phys. Pol. B **33**, 521 (2002).
[10] A. Baldini *et al.*, in *Numerical Data and Functional Relationships in Science and Technology, Total Cross-Sections for Reactions of High Energy Particles*, edited by H. Schopper, Landolt-Bornstein, New Series, Group 1, Vol. 12 (Springer-Verlag, Berlin, Heidelberg, 1988).
[11] E. Byckling and K. Kajantie, *Particle Kinematics* (John Wiley & Sons Ltd., New York, 1973).
[12] U. Löhring *et al.*, Eur. Phys. J. A **10**, 447 (2001).
[13] S. Capstick and N. Isgur, Phys. Rev. D **34**, 2809 (1986); S. Capstick and W. Roberts, Prog. Part. Nucl. Phys. **45**, S241 (2000).
[14] H. Högaasen and P. Sorba, Nucl. Phys. **B145**, 119 (1978).
[15] Ya. I. Azimov, Phys. Lett. B **32**, 499 (1970).
[16] Ya. I. Azimov *et al.*, Phys. Rev. C **68**, 045204 (2003).
[17] R. Jaffe and F. Wilczek, Phys. Rev. D **69**, 114017 (2004).
[18] Y. Oh, H. Kim, and S. H. Lee, Phys. Rev. D **69**, 094009 (2004).
[19] C. Garcia-Recio, M. F. M. Lutz, and J. Nieves, Phys. Lett. B **582**, 49 (2004).
[20] H. H. Adam *et al.* (WASA-at-COSY Collaboration), nucl-ex/0411038.

# Lineshape of the $\Lambda(1405)$ hyperon measured through its $\Sigma^0\pi^0$ decay

I. Zychor [a], M. Büscher [b], M. Hartmann [b], A. Kacharava [c,d], I. Keshelashvili [b,c], A. Khoukaz [e],
V. Kleber [f], V. Koptev [g], Y. Maeda [h], T. Mersmann [e], S. Mikirtychiants [g], R. Schleichert [b],
H. Ströher [b], Yu. Valdau [g], C. Wilkin [i,*]

[a] *The Andrzej Sołtan Institute for Nuclear Studies, 05-400 Świerk, Poland*
[b] *Institut für Kernphysik, Forschungszentrum Jülich, 52425 Jülich, Germany*
[c] *High Energy Physics Institute, Tbilisi State University, 0186 Tbilisi, Georgia*
[d] *Physikalisches Institut II, Universität Erlangen-Nürnberg, 91058 Erlangen, Germany*
[e] *Institut für Kernphysik, Universität Münster, 48149 Münster, Germany*
[f] *Physikalisches Institut, Universität Bonn, 53115 Bonn, Germany*
[g] *High Energy Physics Department, Petersburg Nuclear Physics Institute, 188350 Gatchina, Russia*
[h] *Research Center for Nuclear Physics, Osaka University, Ibaraki, Osaka 567-0047, Japan*
[i] *Physics and Astronomy Department, UCL, London, WC1E 6BT, UK*

**Abstract**

The $pp \to pK^+Y^0$ reaction has been studied for hyperon masses $m(Y^0) \leqslant 1540$ MeV/$c^2$ at COSY-Jülich by using a 3.65 GeV/$c$ circulating proton beam incident on an internal hydrogen target. Final states comprising two protons, one positively charged kaon and one negatively charged pion have been identified with the ANKE spectrometer. Such configurations are sensitive to the production of the ground state $\Lambda$ and $\Sigma^0$ hyperons as well as the $\Sigma^0(1385)$ and $\Lambda(1405)$ resonances. Applying invariant- and missing-mass techniques, the two overlapping excited states could be well separated, though with limited statistics. The shape and position of the $\Lambda(1405)$ distribution, reconstructed cleanly in the $\Sigma^0\pi^0$ channel, are similar to those found from other decay modes and there is no obvious mass shift. This finding constitutes a challenging test for models that predict $\Lambda(1405)$ to be a two-state resonance.
© 2008 Elsevier B.V. All rights reserved.

*PACS:* 14.20.Jn; 13.30.-a

*Keywords:* Hyperon resonances; Line shapes

The excited states of the nucleon are a topical field of research, since the full spectrum contains deep-rooted information about the underlying strong colour force acting between the quarks and gluons. In addition to searching for missing resonances predicted by quark models [1], it is important to understand the structure of certain well established states, such as the $\Lambda(1405)$ hyperon resonance.

Although a four-star resonance [2], and known already for many years, the dynamics of the $\Lambda(1405)$ are still not fully understood. Within the quark model it can be explained as a $P$-wave $q^3$ baryon [3]. It is also widely discussed as a candidate for a $\bar{K}N$ molecular state [4], or for one with a more intrinsic $q^4\bar{q}$ pentaquark structure [5]. If the $\Lambda(1405)$ is a dynamically generated resonance produced *via* $\bar{K}N$ rescattering within a coupled-channel formalism [6,7], it may consist of two overlapping $I = 0$ states [8–10]. Its decay spectrum would then depend upon the production reaction. Due to the opening of the $\bar{K}N$ channels, the $\Lambda(1405)$ lineshape is not represented satisfactorily by a Breit–Wigner resonance [4,11–13]. Nevertheless,

if the $\Lambda(1405)$ were a single quantum state, as in the quark model or molecular pictures, its lineshape should be independent of the production method.

Part of the difficulty in elucidating the nature of the $\Lambda(1405)$ is due to it overlapping the nearby $\Sigma^0(1385)$. The interference between these two states can distort significantly the $\Sigma^+\pi^-$ and $\Sigma^-\pi^+$ spectra [6], for which there are experimental indications [14]. This interference can be eliminated by taking the average of $\Sigma^+\pi^-$ and $\Sigma^-\pi^+$ data [11] but the cleanest approach is through the measurement of the $\Sigma^0\pi^0$ channel, since isospin forbids this for $\Sigma^0(1385)$ decay. This is the technique that we want to develop here and, although our statistics are rather poor, these are already sufficient to yield promising results.

We have used data obtained during high statistics $\phi$-production measurements with the ANKE spectrometer [15] to study the excitation and decay of low-lying hyperon resonances in $pp$ collisions at a beam momentum of 3.65 GeV/$c$ in an internal-ring experiment at COSY-Jülich. A dense hydrogen cluster-jet gas target was used and over a four-week period this yielded an integrated luminosity of $L = (69 \pm 10)$ pb$^{-1}$, as determined from elastic $pp$ scattering that was measured in parallel and compared with the SAID 2004 solution [16].

The detection systems of the magnetic three-dipole spectrometer ANKE simultaneously register and identify both negatively and positively charged particles [17]. Forward (Fd) and side-wall (Sd) counters were used for protons, telescopes and side-wall scintillators for $K^+$, and scintillators for $\pi^-$. Since the efficiencies of the detectors are constant to 2% ($\sigma$) across the momentum range of registered particles, any uncertainty in this can be neglected in the further analysis.

The basic principle of the experiment is the search for four-fold coincidences, comprising two protons, one positively charged kaon and one negatively charged pion, i.e., $pp \rightarrow pK^+p\pi^-X^0$. Such a configuration can correspond, e.g., to the following reaction chains involving the $\Sigma^0(1385)$ and $\Lambda(1405)$ as intermediate states:

$$pp \rightarrow pK^+\Sigma^0(1385) \rightarrow pK^+\Lambda\pi^0 \rightarrow pK^+p\pi^-\pi^0, \quad (1)$$

$$pp \rightarrow pK^+\Lambda(1405) \rightarrow pK^+\Sigma^0\pi^0 \rightarrow pK^+\Lambda\gamma\pi^0$$

$$\rightarrow pK^+p\pi^-\gamma\pi^0. \quad (2)$$

In the $\Sigma^0(1385)$ case, the residue is $X^0 = \pi^0$, while for the $\Lambda(1405)$, $X^0 = \pi^0\gamma$. The resonances overlap significantly because the widths of 36 MeV/$c^2$ for $\Sigma^0(1385)$ and 50 MeV/$c^2$ for $\Lambda(1405)$ are much larger than the mass difference [2]. The strategy to discriminate between them is to: (i) detect and identify four charged particles $p_{Fd}$, $p_{Sd}$, $K^+$ and $\pi^-$ in coincidence, thereby drastically reducing the accidental background at the expense of statistics, (ii) select those events for which the mass of a $(p_{Sd}\pi^-)$ pair corresponds to that of the $\Lambda$, (iii) select the mass of the residue $m(X^0)$ to be that of the $\pi^0$ to tag the $\Sigma^0(1385)$, and $m(X^0) > m(\pi^0) + 55$ MeV/$c^2$ for the $\Lambda(1405)$.

Fig. 1(a) shows the two-dimensional distribution of the four-particle missing mass $MM(pK^+\pi^-p)$ of the $p_{Sd}\pi^-$ pairs *versus* the invariant mass $M(p_{Sd}\pi^-)$. A vertical band corresponding to the $\Lambda$, is visible around a mass of 1116 MeV/$c^2$.
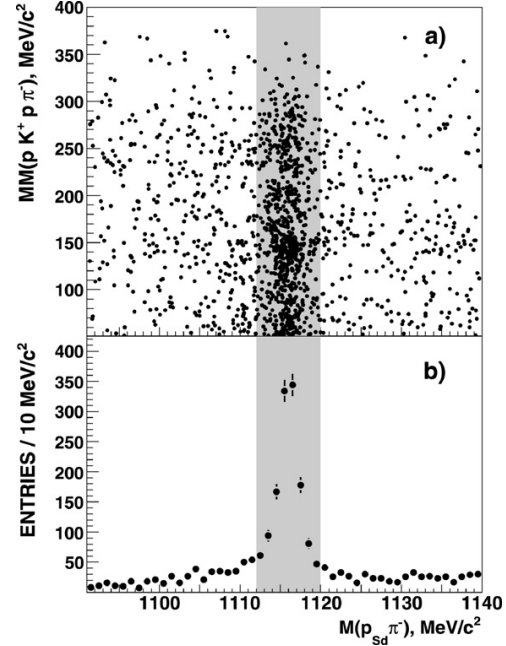


Fig. 1. (a) Missing mass $MM(pK^+p\pi^-)$ *versus* invariant mass $M(p_{Sd}\pi^-)$. The shaded vertical box shows the band used to select the $\Lambda$. (b) The projection of all the events from panel (a) onto the $M(p_{Sd}\pi^-)$ axis shows a clear $\Lambda$ peak with a FWHM projection of $\sim 5$ MeV/$c^2$ and a slowly varying background.

The features of this band are illustrated clearly in the projection onto the $M(p_{Sd}\pi^-)$ axis shown in Fig. 1(b). The $\Lambda$ peak, with a FWHM of $\sim 5$ MeV/$c^2$, sits on a slowly varying background, much of which arises from a false $p\pi^-$ association (the combinatorial background).

Data within the invariant-mass window 1112–1120 MeV/$c^2$ were retained for further analysis and, in Fig. 2, $MM(p_{Fd}K^+)$ is plotted against $MM(pK^+p\pi^-)$ for these events. The triangular-shaped domain arises from the constraint $MM(p_{Fd}K^+) \geqslant MM(pK^+p\pi^-) + m(\Lambda)$. Despite the lower limit of 50 MeV/$c^2$ on $MM(pK^+p\pi^-)$, there is a background from $\Sigma^0$ production at the bottom of the triangle, but this can be easily cut away. The enhancement for $MM(p_{Fd}K^+) \sim 1400$ MeV/$c^2$ corresponds to $\Sigma^0(1385)$ and $\Lambda(1405)$ production. The two vertical bands show the four-particle missing-mass $MM(pK^+p\pi^-)$ criteria used to separate the $\Sigma^0(1385)$ from the $\Lambda(1405)$. The left band is optimised to identify a $\pi^0$ whereas, in view of the missing-mass resolution, the right one selects masses significantly greater than $m(\pi^0)$.

Since the properties of the $\Sigma^0(1385)$ are undisputed [2], we first present and discuss results for this hyperon as a test case for the $\Lambda(1405)$ analysis. In Fig. 3 we show the experimental missing-mass $MM(p_{Fd}K^+)$ spectrum for events within the $\pi^0$-band of Fig. 2. When this is fit with a Breit–Wigner distribution plus a linear background, a mass of $M = (1384 \pm 10)$ MeV/$c^2$ and a width of $\Gamma \sim 40$ MeV/$c^2$ are obtained, in good agreement with the PDG values [2]. The resonance is located half way between the $\Sigma\pi$ and $\bar{K}N$ thresholds, indicated
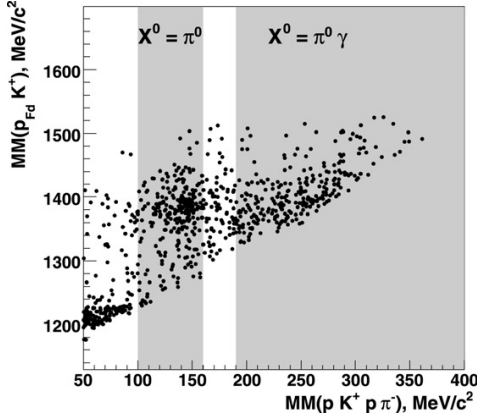
Fig. 2. Missing mass $MM(p_{Fd}K^+)$ versus $MM(pK^+p\pi^-)$. A clear concentration of $\pi^0$ events is seen, though with a central value of the mass $\sim 8$ MeV/$c^2$ too high, a deviation that is consistent with the resolution expected for a four-particle missing mass. The left shaded vertical box covers this $\pi^0$ region and the right one has $MM(pK^+p\pi^-) > 190$ MeV/$c^2$ originating, e.g., from $\pi^0\gamma$ and $\pi\pi$.

by arrows in Fig. 3, and no significant influence of either threshold is observed in the data.

To investigate possible contributions to the spectrum other than from the $\Sigma^0(1385)$ excitation, Monte Carlo simulations were performed for backgrounds from non-resonant and resonant production. The first group of reactions includes processes such as $pp \to NK^+\pi X(\gamma)$ and $pp \to NK^+\pi\pi X(\gamma)$, with $X$ representing any allowed $\Lambda$ or $\Sigma$ hyperon. The second group comprises $\Lambda(1405)$ and $\Lambda(1520)$ hyperon production. The simulations, based on the GEANT3 package, were performed in a similar manner to those in Ref. [18]. Events were generated according to phase space using relativistic Breit–Wigner parametrisations for the known hyperon resonances [2]. Their relative contributions were deduced by fitting the experimental data, giving the results shown by the histograms of Fig. 3. Also included is a small contribution from the $\Lambda(1405)$ channel, arising from the tail of the missing-mass events in Fig. 2 leaking into the $\pi^0$ region. As expected, the $\Sigma^0(1385)$ peak dominates over a small and smooth background.

In order to estimate the total $\Sigma^0(1385)$ production cross section we used the overall detector efficiency of $\sim 55\%$ and the cumulative branching ratio of 56% for the $\Sigma^0(1385)$ decay chain corresponding to reaction (1). With the calculated acceptance of $\sim 2 \times 10^{-6}$ and the number of $\Sigma^0(1385)$ events equal to $170 \pm 26$, we find

$$\sigma_{\text{tot}}\left(pp \to pK^+\Sigma^0(1385)\right) = (4.0 \pm 1.0_{\text{stat}} \pm 1.6_{\text{syst}}) \text{ μb}$$

at $p_{\text{beam}} = 3.65$ GeV/$c$. The systematic uncertainty in the fitting procedure and cross section evaluation was estimated by varying some of the event selection parameters, such as the width of the $MM(pK^+p\pi^-)$ bands or the range for the $\Lambda$ peak (see Fig. 1), or the non-resonant background in Fig. 3. The cross section is only a little lower than at 6 GeV/$c$, $(7 \pm 1)$ μb [19], whereas that for $pp \to pK^+\Lambda$ increases by a factor of four over a similar change in excess energy [20].
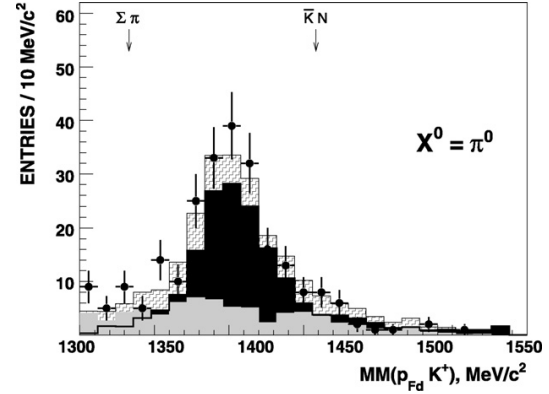


Fig. 3. Missing-mass $MM(p_{Fd}K^+)$ distribution for the $pp \to pK^+p\pi^-X^0$ reaction for events with $M(p_{Sd}\pi^-) \approx m(\Lambda)$ and for $MM(pK^+p\pi^-) \approx m(\pi^0)$. Experimental points with statistical errors are compared to the shaded histogram of the fitted overall Monte Carlo simulations. The simulation includes resonant contributions (solid-black) and non-resonant phase-space production (solid-grey). The structure in the latter arises from the various channels considered. Arrows indicate the $\Sigma\pi$ and $\bar{K}N$ thresholds.

Turning now to the $\Lambda(1405)$, simulations show that the $\Sigma^0(1385)$ does not contaminate the missing-mass $MM(pK^+p\pi^-)$ range above 190 MeV/$c^2$. This point is crucial since it allows us to obtain a clean separation of the $\Sigma^0(1385)$ and $\Lambda(1405)$. There is the possibility of some contamination from the $pK^+\Lambda(\pi\pi)^0$ channel but there is only a limited amount of the five-body phase space available near the maximum missing mass. Simulations also show that the ANKE acceptance varies only marginally in the mass range around 1400 MeV/$c^2$. The corresponding experimental missing-mass $MM(p_{Fd}K^+)$ spectrum is shown in Fig. 4(a). The asymmetric distribution, which peaks around 1400 MeV/$c^2$, has a long tail on the high missing-mass side that extends up to the kinematical limit.

In order to extract the $\Lambda(1405)$ distribution from the measured $\Sigma^0\pi^0$ decay, a different strategy has been applied, where we first fit the non-resonant contributions to the experimental data. The fit was performed for $1440 < MM(p_{Fd}K^+) < 1490$ MeV/$c^2$ to exclude heavier hyperon resonances, such as the $\Lambda(1520)$. The resulting non-resonant background is indicated by the shaded histogram in Fig. 4(a). When this is subtracted from the data we obtain the distribution shown as experimental points in Fig. 4(b).

Our background-subtracted data exhibit a prominent structure around 1400 MeV/$c^2$. There is no indication of a second near 1500 MeV/$c^2$, which might result from the production of the $\Lambda(1520)$ [11]. The excess of at most 20 events for $MM(p_{Fd}K^+) > 1490$ MeV/$c^2$ leads to an upper limit for the $\Lambda(1520)$ production cross section of $\sigma_{\text{tot}} < 0.2$ μb. The smallness of the signal in this case would be largely due to the low branching of only 9% into this channel. There is no evidence either for a significant contribution from the $Y^{0*}(1480)$ hyperon [18]. If this state were the same as the one-star $\Sigma^0(1480)$ of Ref. [2], the decay into $\Sigma^0\pi^0$ would be forbidden. However, this state is also not seen in the $K^-p \to \pi^0\pi^0\Lambda$ reaction [21].
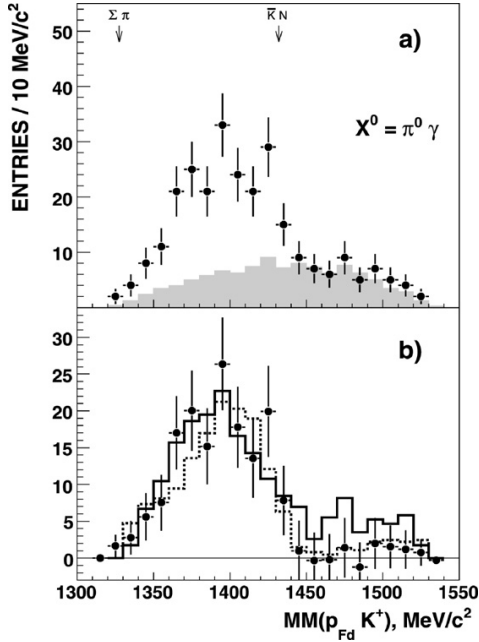
Fig. 4. (a) Missing-mass $MM(p_{Fd}K^+)$ distribution for the $pp \to pK^+p\pi^- X^0$ reaction for events with $M(p_{Sd}\pi^-) \approx m(\Lambda)$ and $MM(pK^+p\pi^-) > 190$ MeV/$c^2$. Experimental points with statistical errors are compared to the shaded histogram of the fitted non-resonant Monte Carlo simulation. (b) The background-subtracted lineshape of the $\Lambda(1405)$ decaying into $\Sigma^0\pi^0$ (points) compared to $\pi^- p \to K^0(\Sigma\pi)^0$ [13] (solid line) and $K^- p \to \pi^+\pi^-\Sigma^+\pi^-$ [11] (dotted line) data.

We finally turn to the contribution from lower missing masses. From the number of events with $1320 < MM(p_{Fd}K^+) < 1440$ MeV/$c^2$, equal to $156 \pm 23$, we find a total production cross section of

$$\sigma_{\text{tot}}\big(pp \to pK^+\Lambda(1405)\big) = (4.5 \pm 0.9_{\text{stat}} \pm 1.8_{\text{syst}}) \text{ μb}$$

at $p_{\text{beam}} = 3.65$ GeV/$c$. The cumulative branching ratio for the $\Lambda(1405)$ decay chain of reaction (2) of 21% and the acceptance of $\sim 4 \times 10^{-6}$ have been included, as well as the overall detection efficiency of $\sim 55\%$.

The $(\Sigma\pi)^0$ invariant-mass distributions have been studied in two hydrogen bubble chamber experiments. Thomas et al. [13] found $\sim 400$ $\Sigma^+\pi^-$ or $\Sigma^-\pi^+$ events corresponding to the $\pi^- p \to K^0\Lambda(1405) \to K^0(\Sigma\pi)^0$ reaction at a beam momentum of 1.69 GeV/$c$. Hemingway [11] used a 4.2 GeV/$c$ kaon beam to investigate $K^- p \to \Sigma^+(1660)\pi^- \to \Lambda(1405)\pi^+\pi^- \to (\Sigma^\pm\pi^\mp)\pi^+\pi^-$. For the $\Sigma^-\pi^-\pi^+\pi^+$ final state, the $\Sigma^-\pi^+$ mass spectrum is distorted by the confusion between the two positive pions. Thus, in the comparison with our data, we use only the $\Sigma^+\pi^-$ distribution, which contains 1106 events [11].

In Fig. 4(b) our experimental points are compared to the results of Thomas and Hemingway, which have been normalised by scaling their values down by factors of $\sim 3$ and $\sim 7$, respectively. The effect of the $\bar{K}N$ threshold is apparent in these published data, with the $\Lambda(1405)$ mass distribution being dis-

torted by the opening of this channel. Despite the very different production mechanisms, the three distributions have consistent shapes. A fit of one to either of the others leads to a $\chi^2/ndf$ of the order of unity though, as pointed out in Ref. [6], for $\Sigma^+\pi^-$ production [11] there is likely to be some residual distortion from $I = 1$ channels. The $K^- p \to \Lambda(1405)\pi^0 \to \Sigma^0\pi^0\pi^0$ data yield a somewhat different distribution [22] but, as noted in this reference, the uncertainty as to which $\pi^0$ originated from the $\Lambda(1405)$ *"smears the resonance signal in the spectra"*. The situation is therefore very similar to that of the Hemingway $\Sigma^-\pi^-\pi^+\pi^+$ data [11] and such results can only be interpreted within the context of a specific reaction model, such as that of Ref. [9].

Models based on unitary chiral perturbation theory find two poles in the neighborhood of the $\Lambda(1405)$ which evolve from a singlet and an octet in the exact SU(3) limit [8,9]. One has a mass of 1390 MeV/$c^2$ and a width of 130 MeV/$c^2$ and couples preferentially to $\Sigma\pi$. The narrower one, located at 1425 MeV/$c^2$, couples more strongly to $\bar{K}N$, whose threshold lies at $\sim 1432$ MeV/$c^2$. Both states may contribute to the experimental distributions, and it is their relative population, which depends upon the production mechanism, that will determine the observed lineshape. Our experimental findings show that the properties (mass, width, and shape) of the $\Lambda(1405)$ resonance are essentially identical for these three different production modes.

In summary, we have measured the excitation of the $\Sigma^0(1385)$ and $\Lambda(1405)$ hyperon resonances in proton–proton collisions at a beam momentum of 3.65 GeV/$c$. We have succeeded in unambiguously separating the two states through their $\Lambda\pi^0$ and $\Sigma^0\pi^0 \to \Lambda\gamma\pi^0$ decay modes. Cross sections of the order of a few μb have been deduced for both resonances. The $\Lambda(1405)$, as measured through its $\Sigma^0\pi^0$ decay, has a shape that is consistent with data on the charged decays [11,13], with a mass of $\sim 1400$ MeV/$c^2$ and width of $\sim 60$ MeV/$c^2$. This might suggest that, if there are two states present in this region, then the reaction mechanisms in the three cases are preferentially populating the same one. However, by identifying particular reaction mechanisms, proponents of the two-state solution can describe the shape of the distribution that we have found [10].

The $\Sigma^0\pi^0$ channel is by far the cleanest for the observation of the $\Lambda(1405)$ since it is not contaminated by the $\Sigma(1385)$ nor the confusion regarding the identification of the pion from its decay. However, although we have shown that the method works in practice, in view of our limited statistics, further data are clearly needed. The decay $\Lambda(1405) \to \Sigma^0\pi^0 \to \Lambda\gamma\pi^0$ can be detected directly in electromagnetic calorimeters. Corresponding measurements are under way in $\gamma p$ reactions (CB/TAPS at ELSA [23], SPring-8/LEPS [24]) and are also planned in $pp$ interactions with WASA at COSY [25].

## Supplementary material

The online version of this Letter contains additional supplementary material.

Please visit doi:10.1016/j.physletb.2008.01.002.

## References

[1] S. Capstick, W. Roberts, Prog. Part. Nucl. Phys. 45 (2000) S241.
[2] W.-M. Yao, et al., J. Phys. G 33 (2006) 1;
But see also the minireview in D.E. Groom, et al., Eur. Phys. J. C 15 (2000) 1.
[3] N. Isgur, G. Karl, Phys. Rev. D 18 (1978) 4187.
[4] R.H. Dalitz, S.F. Tuan, Ann. Phys. (N.Y.) 10 (1960) 307.
[5] T. Inoue, Nucl. Phys. A 790 (2007) 530.
[6] J.C. Nacher, et al., Phys. Lett. B 455 (1999) 55.
[7] J.A. Oller, U.-G. Meißner, Phys. Lett. B 500 (2001) 263.
[8] D. Jido, et al., Nucl. Phys. A 725 (2003) 181.
[9] V.K. Magas, E. Oset, A. Ramos, Phys. Rev. Lett. 95 (2005) 052301.
[10] L.S. Geng, E. Oset, arXiv: 0707.3343 [hep-ph].
[11] R.J. Hemingway, Nucl. Phys. B 253 (1984) 742.
[12] R.H. Dalitz, A. Deloff, J. Phys. G 17 (1991) 289.
[13] D.W. Thomas, et al., Nucl. Phys. B 56 (1973) 15.
[14] J.K. Ahn, Nucl. Phys. A 721 (2003) 715c.
[15] M. Hartmann, et al., COSY Proposal # 104, http://www.fz-juelich.de/ikp/anke/en/proposals.shtml, 2002.
[16] R.A. Arndt, I.I. Strakovsky, R.L. Workman, Phys. Rev. C 62 (2000) 034005;
http://gwadc.phys.gwu.edu, SAID solution SP04.
[17] S. Barsov, et al., Nucl. Instrum. Methods A 462 (2001) 364.
[18] I. Zychor, et al., Phys. Rev. Lett. 96 (2006) 012002.
[19] S. Klein, et al., Phys. Rev. D 1 (1970) 3019.
[20] A. Sibirtsev, et al., Eur. Phys. J. A 29 (2006) 363.
[21] S. Prakhov, et al., Phys. Rev. C 69 (2004) 042202(R).
[22] S. Prakhov, et al., Phys. Rev. C 70 (2004) 034605.
[23] H. Schmieden, ELSA Letter of Intent ELSA/4-2003.
[24] H. Fujimura, AIP Conf. Proc. 915 (2007) 737.
[25] H.-H. Adam, et al., nucl-ex/0411038.

World Scientific
www.worldscientific.com

# EXCITED HYPERONS PRODUCED IN PROTON-PROTON COLLISIONS WITH ANKE AT COSY

IZABELLA ZYCHOR

*Instytut Problemów Jądrowych, Pl-05-400 Świerk, Poland*
*i.zychor@fz-juelich.de*

Excited neutral hyperons $Y^{0*}$ produced in the $pp \to pK^+Y^{0*}$ reaction with a COSY beam momentum of 3.65 MeV/c have masses below 1540 MeV/c$^2$. The ANKE spectrometer allows the simultaneous observation of different decay modes: $Y^{0*} \to \pi^0\Sigma^0$, $\pi^\mp\Sigma^\pm$, $\pi^0\Lambda$, $K^-p$ by measuring kaons and pions of either charge in coincidence with protons.

We have found indications for a neutral excited hyperon resonance $Y^{0*}$ with a mass of $M(Y^{0*}) = (1480 \pm 15)$ MeV/c$^2$ and a width of $\Gamma(Y^{0*}) = (60 \pm 15)$ MeV/c$^2$. The cross section for $Y^{0*}$ is of the order of few hundred nanobarns. It can be either a $\Sigma^0$ or a $\Lambda$ hyperon and on the basis of existing data no conclusion could be made whether it is a three–quark baryon or an exotic state.

Missing- and invariant–mass techniques have been used to identify the $\Lambda(1405)$ resonance decaying via $\Sigma^0\pi^0$. The cross section for $\Lambda(1405)$ production is equal to $(4.5 \pm 0.9_{stat} \pm 1.8_{syst})$ $\mu$b. The shape and position of the $\Lambda(1405)$ distribution are similar to those found from other decay modes, so no support is given to the two-pole model.

## 1. Introduction

The production and properties of hyperons have been studied for more than 50 years, mostly in pion and kaon induced reactions. Hyperon production in *pp* collisions has been investigated close to threshold at SATURNE (Saclay, France) and COSY-Jülich. Reasonably complete information on $\Lambda(1116)$, $\Sigma^0(1192)$, $\Sigma^0(1385)$, $\Lambda(1405)$ and $\Lambda(1520)$ can be found in the Review of Particle Physics.[1]

For the $\Lambda(1405)$, in spite of rather high statistics achieved (the total world statistics is several thousand events), there are still open questions concerning the nature of this resonance: is it a singlet *qqq* state in the frame of SU(3) or a quark-gluon *(uds-q)* hybrid, or a KN bound state?[2−10]

On the contrary, the $\Sigma(1480)$ hyperon is not well established yet and it is described as a 'bump' with unknown quantum numbers.[1] The Crystal Ball experiment has not seen any indications for the resonance $\Sigma(1480)$ in the $\pi^0\Lambda$ invariant mass distribution measured in the reaction $K^-p \to \pi^0\pi^0\Lambda$, dominated by the $\Sigma(1385)$.[11]

The program to investigate hyperon production from *pp* interactions at low energies is very well suited for the ANKE spectrometer operated at COSY–Jülich.
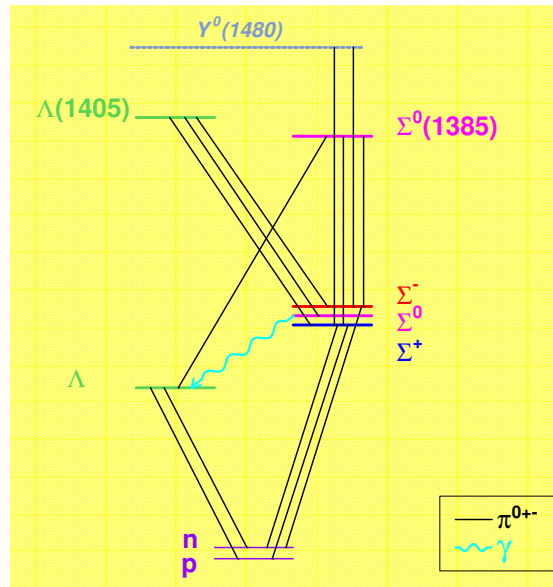
Fig. 1.   Simplified decay scheme of investigated hyperons.

In Fig. 1 a simplified decay scheme of hyperons investigated in our experiments is presented.

## 2.  Experiment and Particle Identification with ANKE

The experiments have been performed with the ANKE spectrometer[12] at the Cooler SYnchrotron COSY at the Research Center Jülich (Germany).[13]

COSY is a medium energy cooler synchrotron and storage ring for both polarized and unpolarized protons and deuterons. At COSY various targets can be used, e.g. solid or cluster–jet. COSY provides beams in the momentum range between 0.6 and 3.7 GeV/c.

ANKE (**A**pparatus for Studies of **N**ucleon and **K**aon **E**jectiles) is a magnetic spectrometer located at an internal target position of COSY. It consists of three dipole magnets, see Fig. 2. The central C–shaped spectrometer dipole D2, placed downstream of the target, separates the reaction products from the circulating COSY beam. The ANKE detection system, comprising range telescopes, scintillation counters and multi–wire proportional chambers, simultaneously registers both positively and negatively charged particles and measures their momenta.[14]

The ANKE telescopes are used to register positively charged particles. They discriminate pions, kaons and protons with the same momenta due to their different energy losses. Passive copper degraders in the telescopes between the scintillation counters enhance the discrimination efficiency. The $K^+$ mesons are stopped in the $\Delta E$ counters or in the second degrader of each telescope. Their decay, mainly into
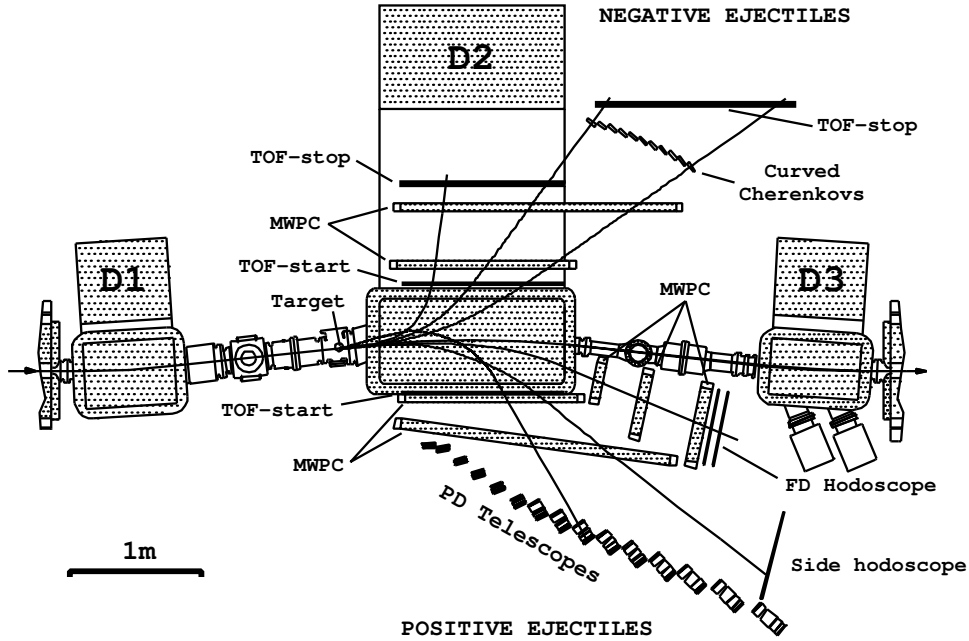
Fig. 2.   ANKE spectrometer and detectors.

Table 1.   Experimental details.

|  | 4 weeks in 2002 for $Y^{0*}(1480)$ | 4 weeks in 2005 for $\Lambda(1405)$ |
|---|---|---|
| integrated luminosity | 6 pb$^{-1}$ | 70 pb$^{-1}$ |
| coincidences | 3 particles (p, K$^+$, $\pi^+$ or $\pi^-$) | 4 particles (p, p, K$^+$, $\pi^+$) |
| $K^+/\pi^+$ momentum | 0.2–0.9 GeV/c | 0.2–0.9 GeV/c |
| p momentum | >0.75 GeV/c | >0.75 GeV/c |
| $\pi^-$ momentum | 0.4–1.0 GeV/c | 0.2–1.0 GeV/c |
| delayed veto for $K^+$ | yes | no |
| detection efficiency | 7% | 55% |
| mass resolution | ~10 MeV/c$^2$ | ~20 MeV/c$^2$ |

$\mu^+\nu_\mu$ and $\pi^+\pi^0$ with a lifetime of $\tau = 12.4$ ns, provides a very effective criterion for kaon identification via detection of delayed signals in a so-called veto counter (with respect to prompt signals from e.g. a $\pi^+$ produced in the target passing over all counters of a telescope). By measuring such delayed signals from the decay of stopped kaons, positively charged kaons can be identified at ANKE in a background of pions, protons and scattered particles up to $10^6$ times more intense.[15] The use of veto counters causes a decrease of particle identification efficiency, typically by factor of 6. The tracks of the ejectiles, measured with multi-wire proportional chambers (MWPCs), are used to reconstruct momenta of any registered particle.

Data originally taken for scalar meson[16] and $\phi$[17] production have been used to study the production of low-lying hyperon resonances in $pp$ collisions with ANKE@COSY. Experiments have been performed in 2002 and 2005, respectively.

In Table 1 details of the experimental conditions are given.

## 3. Excited Neutral Hyperon $Y^{0*}(1480)$

Final states comprising a proton, a positively charged kaon, a pion of either charge and an unidentified residue X were investigated in the reaction $pp \rightarrow pK^+Y \rightarrow pK^+\pi^\pm X^\mp$ at the beam momentum of 3.65 GeV/c. Kaons are identified by measuring delayed signals from the their decay, which, together with well-defined pions and protons, are used to determine the mass of X.

In the upper part of Fig. 3 the missing mass distributions $MM(pK^+\pi)$ *versus* $MM(pK^+)$ are shown for the reactions $pp \rightarrow pK^+\pi^+X^-$(left) and $pp \rightarrow pK^+\pi^-X^+$(right). Since the probability for detecting three–particle coincidences $(pK^+\pi^+)$ is about an order of magnitude smaller than for $(pK^+\pi^-)$, the resulting numbers of events are also drastically different. In the distribution for the reaction $pp \rightarrow pK^+\pi^+X^-$(left) an enhancement corresponding to $X^- = \Sigma^-(1197)$, is observed on a low background. In the charge–mirrored $pp \rightarrow pK^+\pi^-X^+$ case(right), the $\pi^-$ may originate from different sources, e.g. a decay with the $\Sigma^+(1189)$ or
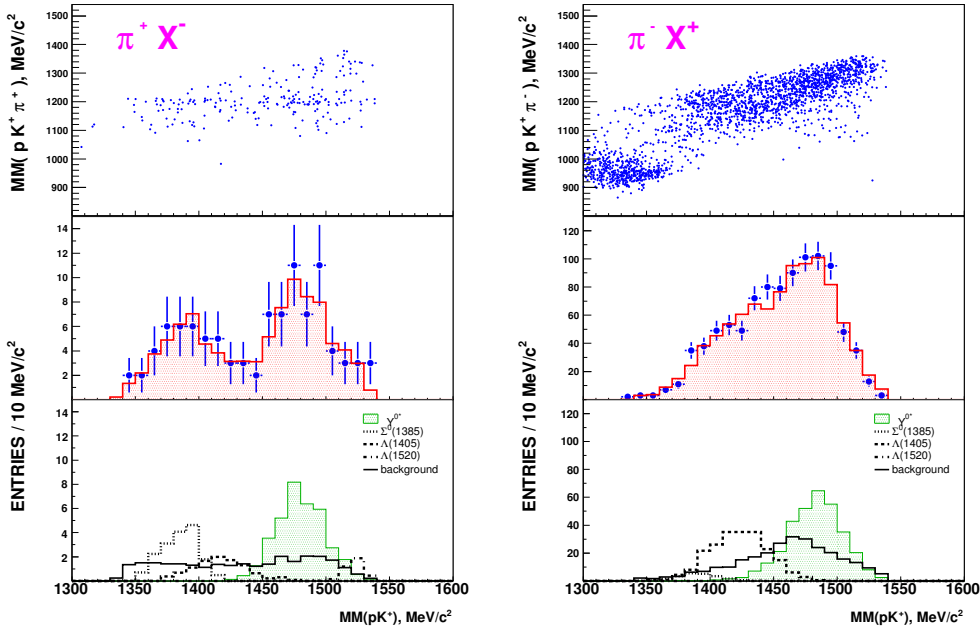


Fig. 3. Missing–mass $MM(pK^+)$ spectra for the reaction $pp \rightarrow pK^+\pi^+X^-$(left) and $pp \rightarrow pK^+\pi^-X^+$ (right). Upper parts: $MM(pK^+)$ *versus* $MM(pK^+\pi)$ for $\pi^+$ (right) and $\pi^-$ (left). Middle parts: Comparison of experimental (points) and simulated (shaded histograms) distributions. Lower parts: Non–resonant and resonant contributions to the overall simulated histograms.

a secondary decay of $\Lambda \rightarrow p\pi^-$, arising from the major background reaction $pp \rightarrow pK^+\Lambda \rightarrow pK^+\pi^-p$. Protons from this reaction are easily rejected by cutting the missing mass $MM(pK^+\pi^-)$ around the proton mass.

If only events around the $\Sigma$ mass are selected, then the missing mass spectrum $MM(pK^+)$ in the reaction $pp \rightarrow pK^+\pi^+X^-$ shows two peaks, see in the middle–left part in Fig. 3. One of them corresponds to the contribution of $\Sigma^0(1385)$ and $\Lambda(1405)$ hyperons. The second peak is located at a mass $\sim 1480$ MeV/c$^2$. In the $\pi^-X^+$ case, the distribution also peaks at 1480 MeV/c$^2$, see the right–middle part in Fig. 3.

We have assumed that the measured missing mass $MM(pK^+)$ spectra can be explained by the production of hyperon resonances and non-resonant contributions. Detailed Monte Carlo simulations have been performed including the production of well established excited hyperons ($\Sigma^0(1385)$, $\Lambda(1405)$, $\Lambda(1520)$) and non-resonant contributions like $pp \rightarrow NK^+\pi X$ and $pp \rightarrow NK^+\pi\pi X$; $X$ denotes any hyperon which could be produced in the experiment. For both final states the shape of the measured distributions cannot be reproduced by the simulations and an excess of events is observed around the missing mass of 1480 MeV/c$^2$. Thus, an the excited hyperon $Y^{0*}$ decaying via $\pi^\pm X^\mp$ was included into simulations. The best fit to the experimental data was obtained for the $Y^{0*}$ with a mass $M(Y^{0*}) = (1480 \pm 15)$ MeV/c$^2$ and a width $\Gamma(Y^{0*}) = (60\pm15)$ MeV/c$^2$, see lower parts in Fig. 3. There have been identified 100 and 1000 events for $\pi^+X^-$ and $\pi^-X^+$ case, respectively. The statistical significance of the signal, assuming that this is due to the production of the $Y^{0*}$, is between 4 and 6 $\sigma$ depending on a procedure. The production cross section is of the order of few hundred nanobarns.[18]

## 4. The $\Lambda(1405)$ Hyperon

The $pp \rightarrow pK^+p\pi^-X^0$ reaction is selected by a multiparticle final state, containing two protons, a positively charged kaon, a negatively charged pion and an unidentified residue $X^0$. In the $\Sigma^0(1385) \rightarrow \Lambda\pi^0$ decay the $X^0$ residue is a $\pi^0$ while, for the $\Lambda(1405) \rightarrow \Sigma^0\pi^0$ decay, $X^0 = \pi^0\gamma$ (see Fig. 1). In the upper part of Fig. 4 a distribution of $MM(p_{Fd}K^+)$ *versus* $MM(pK^+\pi^-p)$ is plotted for events with the invariant mass $M(p_{Sd}\pi^-)$ of the $p_{Sd}\pi^-$ pairs corresponding to the mass of the $\Lambda$, i.e. between 1112 and 1120 MeV/c$^2$. The two horizontal bands show the four–particle missing–mass $MM(pK^+\pi^-p)$ criteria used to separate the $\Sigma^0(1385)$ candidates from those of the $\Lambda(1405)$. The lower band is optimised to identify a $\pi^0$ whereas the upper one selects masses significantly greater than $m(\pi^0)$.

In order to extract the $\Lambda(1405)$ distribution from the measured $\Sigma^0\pi^0$ decay, the non–resonant contributions have been fitted to the experimental data. After subtracting them from the data, the distribution shown as experimental points in the lower panel of Fig. 4 was obtained. 156 events have been identified in this spectrum.[19]
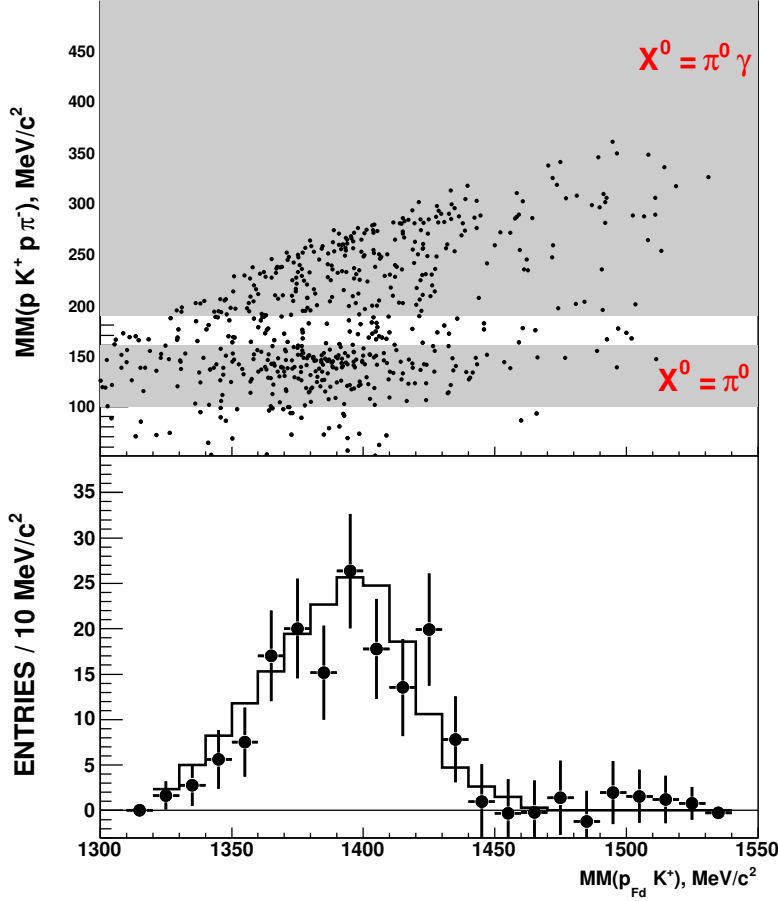
Fig. 4.    Upper panel: Missing mass $MM(pK^+\pi^-p)$ *versus* $MM(p_{Fd}K^+)$ with the shaded horizontal boxes showing the $MM(pK^+\pi^-p)$ bands used for event selection. The lower one is located around the $\pi^0$ mass and the upper one selects $MM(pK^+\pi^-p) > 190$ MeV/$c^2$, significantly greater than the $\pi^0$ mass. Lower panel: The background–subtracted line shape of the $\Lambda(1405)$ decaying into $\Sigma^0\pi^0$ (points) compared to the spectrum of the $\Lambda(1405)$ from the LEPS experiment for photon energy range of $1.5 < E_\gamma < 2.0$ GeV (solid line).

The $(\Sigma\pi)^0$ invariant–mass distributions have been previously studied in two hydrogen bubble chamber experiments. Thomas *et al.* found $\sim 400\ \Sigma^+\pi^-$ or $\Sigma^-\pi^+$ events corresponding to the $\pi^-p \to K^0\Lambda(1405) \to K^0(\Sigma\pi)^0$ reaction at a beam momentum of 1.69 GeV/c.[20] Hemingway used a 4.2 GeV/c kaon beam to investigate $K^-p \to \Sigma^+(1660)\pi^- \to \Lambda(1405)\pi^+\pi^- \to (\Sigma^+\pi^-)\pi^+\pi^-$ and measured 1106 events.[21] Recently, the LEPS experiment has investigated the $\Lambda(1405)$hyperon production in the $\gamma p \to K^+Y^*$ reaction.[22] The $\Lambda(1405)$hyperon was measured in the $(K^+\Sigma^\pm\pi^\mp)$ final state, where the contamination from $\Sigma^0(1385)$was estimated from the $(K^+\Lambda\pi^0)$ final state. In the lower panel in Fig. 4 our experimental points are compared to the results of the LEPS experiment (for comparison with data of

Thomas and Hemingway see Ref. 19). Despite the very different production mechanisms, all four distributions have similar shapes and positions. This might suggest that, if there are two states present in this region, then the reaction mechanisms in the four cases are preferentially populating the same one. It should, however, be noted that by identifying a particular reaction mechanism, the proponents of the two–state solution can describe the shape of the distribution that we have found.[23]

## 5. Outlook

The decay of excited hyperons $Y^{0*}$ *via* $\Lambda\pi^0$ and $\Sigma^0\pi^0 \to \Lambda\gamma\pi^0$ can be detected directly in electromagnetic calorimeters by registering neutral particles, i.e. $\gamma$ and/or $\pi^0$. Measurements of such channels are discussed for $\gamma p$ reactions with CB/TAPS at ELSA[24] and are also planned in *pp* collisions with WASA at COSY.[25]

## Acknowledgments

## References

1. C. Amsler *et al.* (Particle Data Group), *Phys. Lett. B* **667** (2008) 1.
2. U. Löring, B. C. Metsch and H. R. Petry, *Eur. Phys. J. A* **10** (2001) 395.
3. W. Melnitchouk *et al.*, *Phys. Rev. D* **67** (2003) 114506.
4. R. Arnold and J. Sakurai, *Phys. Rev.* **128** (1962) 2808.
5. R. Dalitz, T. Wong and G. Rajasekaran, *Phys. Rev.* **153** (1967) 1617.
6. M. Jones, R. H. Dalitz and R. R. Horgan, *Nucl. Phys. B* **129** (1977) 45.
7. E. Oset and A. Ramos, *Nucl. Phys. A* **635** (1998) 99).
8. J. A. Oller and U. G. Meissner, *Phys. Lett. B* **500** (2001) 263.
9. E. Oset, A. Ramos and C. Bennhold, *Phys. Lett. B* **527** (2002) 99 [Erratum-ibid. *B* **530** (2002) 260].
10. D. Jido *et al.*, *Nucl. Phys. A* **725** (2003) 181.
11. S. Prakhov *et al.*, *Phys. Rev. C* **69** (2004) 042202(R).
12. S. Barsov *et al.*, *Nucl. Instr. Methods Phys. Res., Sect. A* **462** (2001) 364.
13. R. Maier, *Nucl. Instr. Methods Phys. Res., Sect. A* **390** (1997) 1.
14. M. Büscher *et al.*, *Nucl. Instr. Methods Phys. Res., Sect. A* **481** (2002) 378.
15. M. Büscher *et al.*, *Eur. Phys. J. A* **22** (2004) 301.
16. M. Büscher *et al.*, COSY proposal #55 (2001), www.fz-juelich.de/ikp/anke/.
17. M. Hartmann *et al.*, COSY proposal #204 (2002), www.fz-juelich.de/ikp/anke/.
18. I. Zychor *et al.*, *Phys. Rev. Lett.* **96** (2006) 012002.
19. I. Zychor *et al.*, *Phys. Lett. B* **660** (2008) 167.
20. D. W. Thomas *et al.*, *Nucl. Phys. B* **56** (1973) 15.
21. R. J. Hemingway, *Nucl. Phys. B* **253** (1984) 742.
22. M. Niiyama *et al.*, *Phys. Rev. C* **78** (2008) 035202.
23. L. S. Geng and E. Oset, *Eur. Phys. J. A* **34** (2007) 405.
24. H. Schmieden, Letter of Intent ELSA/4-2003.
25. H.-H. Adam *et al.*, nucl-ex/0411038.

# 7 The ANKE Collaboration

ANKE Collaboration (January 2007)

S. Barsov[1], V.G. Baryshevsky[2], U. Bechstedt[3], M. Büscher[3], M. Capiluppi[4], V. Chernetsky[5], B. Chiladze[6], D. Chiladze[3,6], M. Chumakov[5], M. Contalbrigo[4], P.F. Dalpiaz[4], M. Drochner[7], S. Dymov[8], A. Dzyuba[3,1], R. Engels[3], W. Erven[7], P. Fedorets[5], A. Garishvili[3,6], A. Gasparyan[5], R. Gebel[3], A. Gerasimov[5], V. Glagolev[9], G. Giullo[4], V. Goryachev[5], O. Grebenyuk[1], K. Grigoriev[1], V. Grishina[10], D. Gussev[8], J. Haidenbauer[3], Ch. Hanhart[3], G. Hansen[11], M. Hartmann[3], V. Hejny[3], A. Kacharava[12,6], N. Kadagidze[8], B. Kamys[13], M. Karnadi[3], I. Keshelashvili[3,6], A. Khoukaz[14], St. Kistryn[13], V. Kleber[15], F. Klehr[11], H. Kleines[7], H.R. Koch[3], V.I. Komarov[8], L. Kondratyuk[5], V. Koptev[1], A. Kovalov[1], P. Kravchenko[1], P. Kravtsov[1], T. Krings[3], V. Kruglov[8], P. Kulessa[16], A. Kulikov[8,17], A. Kurba-tov[8], N. Lang[14], N. Langenhagen[18], I. Lehmann[19], A. Lehrach[3], P. Lenisa[4], V. Leontiev[8,17], H. Loevenich[7], B. Lorentz[3], G. Macharashvili[6,8], Y. Maeda[20], A. Magiera[13], R. Maier[3], I. Majewski[7,13], S. Martin[3], T. Mersmann[14], S. Merzlia-kov[3,8], M. Mikirtychiants[3,1], S. Mikirtychiants[1], M. Mielke[14], H. Müller[18], A. Mussgiller[3], M. Nekipelov[3,1], R. Nellen[3], V. Nelyubin[1], N. Nikolaev[3], M. Nio-radze[6], D. Oellers[3], H. Ohm[3], Z. Oragvelidze[6], M. Papenbrock[14], D. Prasuhn[3], D. Protic[3], K. Pysz[16], F. Rathmann[3], T. Rausmann[14], B. Rimarzig[18], A. Ruba[2], Z. Rudy[13], J. Sarkadi[7], H. Paetz gen.Schieck[20], R. Schleichert[3], H. Schneider[3], V. Serdyuk[3,8], H. Seyfarth[3], A. Sibirtsev[3], K. Sistemich[3], M. Smiechowicz[13], M. Stancari[4], M. Statera[4], E. Steffens[12], H.J. Stein[3], H. Ströher[3], M. Tabidze[6], A. Täschner[14], P. Engblom-Thörngren[19], S. Trusov[18,17], Yu. Uzikov[8], Yu. Valdau[3,1], A. Vassiliev[1], A. Volkov[8], M. Wang[4], J. Wessels[14], C. Wilkin[21], A. Wronska[13], P. Wüstner[7], S. Yaschenko[12,8], L. Yurev[8], B. Zalikhanov[8], N. Zhuravlev[8], K. Zwoll[7] und I. Zychor[22]

[1]High Energy Physics Department, Petersburg Nuclear Physics Institute, 188350 Gatchina, Russia
[2]Research Institute for Nuclear Problems, Belarusian State University, Minsk 220050, Belarus
[3]Institut für Kernphysik, Forschungszentrum Jülich, D-52425 Jülich
[4]University of Ferrara and INFN, 44100 Ferrara, Italy
[5]Institute for Theoretical and Experimental Physics, Cheremushkinskaya 25, 117259 Moscow, Russia
[6]Institute of High Energy Physics and Informatization, Tbilisi State University, University Str. 9, 380086 Tbilisi, Georgia
[7]Zentrallabor für Elektronik, Forschungszentrum Jülich, D-52425 Jülich
[8]Laboratory of Nuclear Problems, Joint Institute for Nuclear Research, Dubna, 141980 Dubna, Moscow Region, Russia
[9]Laboratory of High Energies, Joint Institute for Nuclear Research, Dubna, 141980 Dubna, Moscow Region, Russia
[10]Institute for Nuclear Research, Russian Academy of Sciences, Moscow 117312, Russia
[11]Zentralabteilung Technologie, Forschungszentrum Jülich, D-52425 Jülich
[12]Physikalisches Institut II, Universität Erlangen-Nürnberg, Erwin-Rommel-Str. 1, D-91058 Erlangen
[13]Institute of Physics, Jagellonian University, Reymonta 4, PL-30059 Cracow, Poland
[14]Institut für Kernphysik, Universität Münster, W.-Klemm-Str. 9, D-48149 Münster
[15]Physikalisches Institut, Universität Bonn, Nussallee 12, D-53115 Bonn
[16]Institute of Nuclear Physics, Radzikowskiego 152, PL-31342, Cracow, Poland
[17]Dubna Branch, Moscow State University, 141980 Dubna Moscow Region, Russia
[18]Institut für Hadronen- und Kernphysik, Forschungszentrum Rossendorf, D-01474 Dresden
[19]Department of Radiation Sciencies, Box 535, S-751 21, Uppsala, Sweden
[20]Institut für Kernphysik,Universität Köln, Zülpicher Str. 77, D-50937 Köln
[21]Physics Department, Univ. College London, Gower Street, London WC1 6BT, England
[22]The Andrzej Soltan Institute for Nuclear Studies, PL-05400 Swierk, Poland